

Review

# Advances in Three Dimensional Bioprinting for Wound Healing: A Comprehensive Review

Egemen Umur <sup>1,†</sup>, Emirhan Bayrak <sup>1,†</sup>, Fahriye Arslan <sup>1,†</sup>, Safiye Betül Bulut <sup>1,†</sup>, Engin Baysoy <sup>2,3</sup>, Gizem Kaleli-Can <sup>1,\*</sup> and Bugra Ayan <sup>4,\*</sup>

<sup>1</sup> Department of Biomedical Engineering, İzmir Democracy University, İzmir 35140, Türkiye

<sup>2</sup> Department of Electrical Engineering and Computer Sciences, University of California, Berkeley, CA 94720, USA

<sup>3</sup> Department of Biomedical Engineering, Bahçeşehir University, İstanbul 34353, Türkiye

<sup>4</sup> Department of Cardiothoracic Surgery, Stanford University, Stanford, CA 94305, USA

\* Correspondence: gizem.kalelican@idu.edu.tr (G.K.-C.); bugra@stanford.edu (B.A.)

† These authors contributed equally to this work.

**Abstract:** The vulnerability of skin wounds has made efficient wound dressing a challenging issue for decades, seeking to mimic the natural microenvironment of cells to facilitate cell binding, augmentation, and metamorphosis. Many three-dimensional (3D) bioprinted hydrogel-based configurations have been developed using high-tech devices to overcome the limitations of traditional dressing materials. Based on a material perspective, this review examines current state-of-the-art 3D bioprinting for hydrogel-based dressings, including both their advantages and limitations. Accordingly, their potential applications in terms of their performance in vitro and in vivo, as well as their adaptability to clinical settings, were investigated. Moreover, different configurations of 3D bioprinters are discussed. Finally, a roadmap for advancing wound dressings fabricated with 3D bioprinting is presented.

**Keywords:** three-dimensional bioprinting; wound dressing; hydrogel; biomaterial



**Citation:** Umur, E.; Bayrak, E.; Arslan, F.; Bulut, S.B.; Baysoy, E.; Kaleli-Can, G.; Ayan, B. Advances in Three Dimensional Bioprinting for Wound Healing: A Comprehensive Review. *Appl. Sci.* **2023**, *13*, 10269. <https://doi.org/10.3390/app131810269>

Academic Editor: David Mills

Received: 7 August 2023

Revised: 2 September 2023

Accepted: 8 September 2023

Published: 13 September 2023



**Copyright:** © 2023 by the authors. Licensee MDPI, Basel, Switzerland. This article is an open access article distributed under the terms and conditions of the Creative Commons Attribution (CC BY) license (<https://creativecommons.org/licenses/by/4.0/>).

## 1. Introduction

The skin provides protection against external physical and chemical harm as well as a defense against biological invasions. An external trauma disrupts the epithelial lining of the skin tissues, resulting in wound formation [1–3]. To restore damaged skin to regular functions, a complex interplay of varied factors is required, including cytokines, growth factors, blood, and the extracellular matrix (ECM) [4–6]. Cascade signaling initiates the healing of many superficial wounds naturally through overlapping phases including the coagulation and hemostasis phase, inflammation phase, and the proliferation and remodeling period [7].

Traditional wound dressings include products that provide economical and limited protection, such as gauze, plaster and cotton, which protect wounds from external influences and absorb excess fluid. One of the most important factors negatively affecting the healing process is the destruction of acute and chronic wounds during the removal of traditional dressings. Detachment of the traditional bandage from the surface can lead to secondary injuries. Traditional wound bandages are recommended for clean and dry wounds [8]. They function by absorbing fluid from the wound to maintain dryness. Modern wound dressings are therefore preferred to maintain the moist environment required by the wound. Unlike traditional products, 3D bioprinting products not only provide proper moisture and temperature to the wound, but also reduce the bacterial load of the wound with antibacterial materials or antibiotics. They also facilitate cell adhesion due to their similarity to cellular structure. Hydrogels made from hydrophilic polymers and similar structures have a high water content. Due to their high water content (up to 99.5%) and similarity to living tissues, these three-dimensional hydrogels can serve as an ideal

dressing candidate. In addition, active ingredients such as nutritional supplements, growth hormones, antibacterial agents and other drugs can be loaded into the wound dressing matrix, thereby releasing these active ingredients into the wound site. The 3D printing technology can be used to prepare wound condition-specific hydrogel dressings to meet patient requirements. Moreover, the simple printing principle, cost-effective bioprinting ink material and stable printing equipment make extrusion-based 3D printing suitable for the mass production of wound dressings. With modern dressings, compared to traditional dressings, removal of the dressing does not damage the site and bleeding does not occur.

Over the past few decades, the production of functional wound dressings involving solely hydrogels or hydrogels incorporated with growth factors, stem cells, antibiotics, and other therapeutic substances for wound management has been performed by advanced technologies to support and accelerate the healing process [9–12]. An optimal microenvironment for wounds could be obtained by enriching the material to acquire particular characteristics, like bacteria kill/inactivator, pH, moisture, oxygen, nutrients, cellular agents (calcium, hydrogen peroxide, copper, iron, etc.), and to exudate drainage regulators, regardless of skin damage severity [13]. Ultimately, they provide higher rates of wound closure, re-epithelization [14] and angiogenesis without exhibiting cytotoxicity [15]. Besides the importance of material characteristics for wound management, the selection of the production technique plays a crucial role in generating personalized hydrogels with high precision and speed, in the case of complex-shaped materials for the desired application. The use of 3D bioprinting enables the creation of wound dressings with micron-sized biomimetic structures. Traditional wound dressings use production techniques such as molding, casting, shaping, and processing, but these techniques are not suitable for complex and customized designs at high resolution. With the help of a 3D bioprinter, it is possible to create anatomically correct, patient-specific dressings containing antibacterial and bioactive molecules [16]. Three-dimensional bioprinting is an additive manufacturing process that incorporates various printing techniques (e.g., stereolithography, direct ink writing, digital light processing, etc.) through computer-aided design (CAD) for producing complex, patient-specific structures at high speed [17]. It is possible to create models using 3D CAD software, or by acquiring sliced images via computed tomography (CT) scans and magnetic resonance imaging (MRI). Due to their capacity for customization, these techniques enable the material to mimic the target wound area with high precision and resolution and create 3D structures containing living cells, therapeutic agents, and hydrogels [18,19].

In this review, first, we impart wound definitions and classifications, along with wound healing stages, so we can determine the type of dressing to use. Second, we consider recent developments in hydrogel-based dressings within the context of formulations and their manufacturing process through 3D bioprinting techniques such as laser-, droplet-, and extrusion-based bioprinting. As a final point, we discuss the effects of 3D-printed functional hydrogel dressings in terms of fluid handling, moisture vapor permeability, exudate absorption efficiency, rheological properties, biocompatibility, and healing process effects. Furthermore, the paper outlines the positives and negatives of future endeavors.

## 2. Structure and Function of Skin

Skin consists of three layers: the epidermis, the dermis, and the hypodermis (Figure 1A). These layers protect the skin from various stresses such as injuries, thermal trauma, surgical wounds, or medical conditions such as HIV/AIDS, sickle cell anemia, Raynaud syndrome, rheumatologic disease, anemia, Ehlers–Danlos, Cutis Laxa syndrome, ischemia, or diabetes mellitus [20,21]. The outermost layer, the epidermis is composed of the stratum basale, the stratum spinosum, the stratum granulosum, and the stratum corneum layers, which are epithelial cell layers up to a depth of 75 to 150  $\mu\text{m}$ . The corneocytes in the epidermis layer are embedded in a multilayer organized lipid matrix. Through this mechanism, the outer layer of the skin can stretch and move. This layer is at risk from pathogens and physical activities on a regular basis.

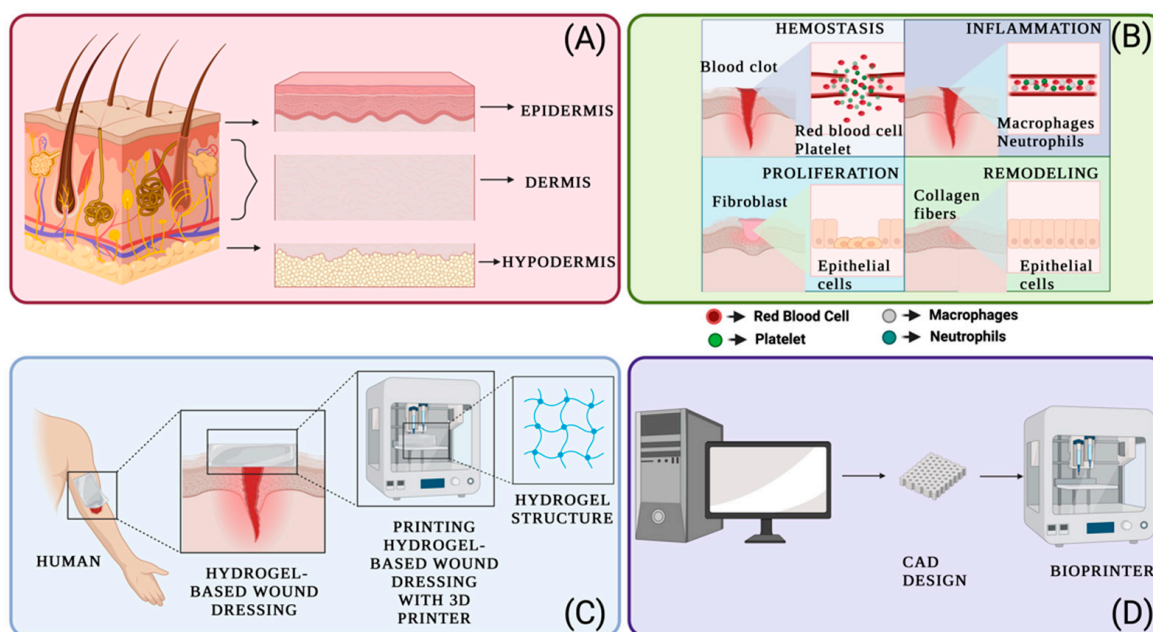


**Figure 1.** Schematic representation of wound treatment with 3D bioprinted hydrogel-based dressings. (A) The first diagram illustrates the cross-section of human skin, including the epidermis, dermis, and subcutaneous tissue layers. The epidermis is the outermost layer of the skin that protects from environmental damage, whereas the dermis is the layer that provides structural support and contains the hair follicles, sweat glands, and blood vessels. Fat and connective tissues are found in the subcutaneous tissue layer. (B) The second schematic illustrates the wound healing process, composed of four stages: hemostasis, inflammation, proliferation, and remodeling. As part of the initial stage of wound healing, hemostasis involves the formation of blood clots to stop the bleeding. During the second stage of the process, immune cells are responsible for cleaning the wound and preventing infection. Following that proliferation occurs, in which new tissue forms and blood vessels grow to restore the damaged area. Re-organization and strengthening of the new tissue constitute the final stage of remodeling. (C) An example of a solution to wound healing using hydrogel-based 3D bioprinting can be seen in the third schematic. The technology allows the precise placement of cells and biomaterials to create wound dressings that closely mimic natural tissue. The biocompatibility of hydrogel-based bioinks, their ability to respond to external stimuli, and their similarity to natural tissue make them an ideal choice for wound healing. (D) The fourth schematic depicts the components of the 3D bioprinting process, including the 3D printer and computer-aided design software (CAD). The CAD software enables the design of the bioink cartridge using hydrogel-based bioink deposited layer by layer onto the printing bed. These 3D printers provide a high level of precision in the creation of wound dressings, ensuring their perfect fit. This figure was created using <https://app.biorender.com/> (accessed on 1 August 2023).

The second layer of the skin, the dermis, is composed of the papillary dermis and the reticular dermis [22–25]. The papillary layer consists of a loose network of collagen and elastin fibers. It contains fibroblasts, a small number of fat cells, capillaries, lymphatic capillaries, nerve fibers, and touch receptors called Meissner bodies. The reticular layer lies beneath the papillary layer densely vascularized, composed of irregular connective tissue with the abundance of sensory and sympathetic nerves. While the elastin fibers in the layer provide some flexibility to the skin and allow movement, the collagen fibers extend to both the papillary layer and the hypodermis. Elastin fibers also provide tensile strength and keep the skin moist by facilitating water transmission [26]. The mechanical behavior of the skin is determined by collagen and elastic fibers. Collagen fibers make up 75% of the fat-free dry mass, while elastic fibers make up 4%. Collagen fibers are also more abundant in the dermis, making up 18–30% of its constitution, while elastic fibers

make up only 1% [27]. When the tension is at 0.3%, elastic fibers show low resistance, and the skin exhibits isotropic behavior. In addition, the collagen fibers remain branched with Young's Modulus values of 0.1–2 MPa. As the tension increases, the collagen fibers begin to stretch and resist the impact. The collagen fibers are linearly aligned between 0.6% and 0.7% tension, and when the tension is greater than 0.7%, the fibers break [28].

A hypodermis layer lies beneath the dermis layer to isolate the skin from internal organs and bones. The microvacuolar located in the hypodermis layer acts as a reservoir for interstitial fluid that changes the structural stiffness of the tissue. It contains proteoglycans and glycosaminoglycans, which attract ions and water molecules in the tissues. In addition, there are fibroblasts, adipose cells, and macrophages that have important tasks such as remodeling the hypodermis tissue, as well as stimulating the thermogenesis of fat in the cold and during exercise [25,26,29–33].

The multi-layered and complex structure of the skin protects and maintains internal hemostasis against external forces such as mechanical, chemical, and thermal factors. However, these forces may lead to structural non-uniformity [34], in the case of skin damage [35]. Hence, the wound area must be kept clean and protected until structural integrity is achieved during the healing phases.

### 3. Overview of Wound Pathophysiology and Wound Healing Process

Wounds can be classified as acute or chronic according to the recovery period. Acute wounds can usually be recovered within an acceptable period; however, certain factors may delay the healing process. Chronic wounds can be healed very slowly or not be healed due to several factors such as varied diseases, environmental conditions, nutrition, and increased bacterial loads leading to a weakening of the immune system. The physical signs of chronic wounds include exudation, persistent infection, and necrosis, all of which contribute to the complexity of managing and caring for these wounds [34,36–38].

The process of healing consists of four main phases: hemostasis, inflammation, proliferation, and remodeling (Figure 1B) [8,34,39]. The first step of the healing process starts with the contraction of the vessels, which slows the blood flow to the wound area. In the hemostasis phase, platelet receptors in the blood interact with ECM proteins and attach to the walls of blood vessels. Once attached, the platelet becomes activated, causing a conformational change and the release of bioactive molecules that enhance coagulation. With coagulation, a clot formation containing fibrin, fibronectin, vitronectin, and thrombospondin prevents bleeding and protects the blood environment from external pathogens [40]. Once the wound is hemostasized, the inflammatory process begins. During the process, immune system agents try to prevent infection by targeting pathogens in the region. Vascular permeability increases with vasodilation, allowing neutrophils and monocytes to accumulate in the wound area. About three days after wound formation, the proliferative phase initiates the accumulation of keratinocytes, fibroblasts, macrophages, and endothelial cells to regulate wound closure, matrix deposition, and angiogenesis. The activation of keratinocytes is triggered by changes in mechanical tension, electrical gradients, hydrogen peroxide, pathogens, growth factors, and cytokines. The endothelial cells enter a rapid growth phase and angiogenesis occurs within the granulation tissue [41]. The last and longest phase of wound healing is the formation of the ECM, which may take several years to remodel. This stage ends with the formation of granulation tissue through either fibroblast death by apoptosis, or their differentiation into myofibroblasts.

Parameters affecting wound healing are divided into systemic and local factors. Systemic factors are related to the person's age, diseases and their lifestyle. Local factors include temperature, pH, water content, microbial content, oxygen (O<sub>2</sub>), carbon dioxide (CO<sub>2</sub>), infection, foreign body and venous insufficiency. However, depending on the type of wound, local factors may differ. Particularly, O<sub>2</sub> is a crucial element providing the energy needed by the cells. By supporting the immune system, O<sub>2</sub> protects the wound from infection and induces angiogenesis. In addition, O<sub>2</sub> increases keratinocyte differentiation, migration, re-epithelialization, fibroblast proliferation, and collagen synthesis. A disruption

in the structural integrity of the skin results in direct exposure to external factors. Since microorganisms cause infection due to the contamination of the wound, it is essential to isolate the wound from the external environment [7,42,43].

The success of the wound healing process depends on growth factors, cytokines and chemokines, as they are involved in the integration of signals in cellular processes in the wound. However, the wound healing process may be delayed by the diseases a patient might have, which can reduce the amount of vascularity in the wound area. In such cases, it is necessary to use wound dressings containing active substances [44–46].

Even though all wounds follow similar healing stages, their components, microenvironments, and recovery time may vary depending on the type of the wound. Therefore, a patient-specific wound dressing needs to be produced, considering the wound type, to reduce the wound healing period.

### 3.1. Wound Dressings

The conventional healing process includes the covering of the wound with traditional dressings such as gauze [47], plasters [48] and cotton [49]—products that protect the wound area from external factors and absorb excess exudate. One of the most important factors that negatively affects the healing process is the disruption of acute and chronic wounds during the detachment of traditional dressings. Separating the traditional dressing from the wound may result in damage to the tissue and even bleeding. It may also cause serious complications, including fatal infections in time. Traditional wound dressings are only recommended for clean and dry wounds. In essence, they function by absorbing the exudate from the wound and maintaining its dryness. Unfortunately, traditional wound dressings are insufficient compared to modern wound dressings, which are competent in maintaining the moist environment the wound requires [8]. In contrast to traditional ones, modern wound dressings provide appropriate humidity and temperature for the wound site, as well as reducing the bacterial load of the wound with antibacterial materials or antibiotics. Due to their similarity to the ECM structure, they facilitate cell adhesion as well. In addition, active substances such as nutritional supplements, growth hormones, antibacterial agents, and other drugs may be loaded into the matrix of wound dressing to ensure the release of active components to the wound area. Unlike traditional dressings, modern ones do not cause any damage to the area or bleeding during dressing removal.

The functional effectiveness of a wound dressing is directly correlated with its chemical and physical properties, as well as therapeutic ingredients and production method. Appropriate dressings should be chosen considering the corresponding wound type and requirements for healing such as drug administration, cells, nutrient addition, and antibacterial elements [50]. In the next section, types of 3D-bioprinted dressings utilized in wound healing, specifically hydrogel-based dressings, will be discussed.

### 3.2. 3D Bioprinted Wound Dressings

Traditional wound dressings physically protect the wound and absorb exudate. Modern wound dressings created with 3D bioprinters offer additional contributions to wound healing compared to traditional ones [16]. Optimum wound dressings should provide the ideal temperature and a moist environment for the wound, increase epidermal migration, angiogenesis and connective tissue synthesis, allow gas exchange, protect against bacteria, provide ideal adhesion to the wound, enhance the debridement effect and weep enzyme accumulation, and be biocompatible [8]. For these features, it is possible to print composite wound dressings with a 3D bioprinting method.

Several studies have examined the efficacy of different types of bioinks (including natural, synthetic, or composite materials) for restoring skin integrity and accelerating wound healing. Among them, hydrogel-based bioinks dominate the field of 3D-bioprinted wound dressings due to their similarities to natural tissues (Figure 1C). A 3D hydrophilic polymer network of hydrogel composed of homopolymers, or copolymers, gives these materials significant swelling properties, while also making them insoluble in water [51].

Their water content may vary from 10–20% [52] up to several thousand times of their dry weight. Even though hydrogels present similar characteristics to other polymers in their dry state, they differ from other polymers once swollen. Hydrogels have both solid-like structural integrity and fluid-like diffusion transport properties, which makes them act as a natural tissue and enhances their biocompatibility in the swollen state [53]. Furthermore, chemical and/or physical linkages between individual polymer chains determine the structural integrity of hydrogels and their characteristic responses to various external stimuli, such as changes in pH, temperature, salt concentration, exposure to light, electromagnetic fields, and biomolecules [54,55]. Several techniques are available to produce hydrogel-based wound dressings, including wet chemistry; mechanical rupture, incorporating trypsin/EDTA processes or hypertonic/hypotonic solutions; electrospinning, and 3D bioprinting [56–63]. Wet chemistry involves cross-linking polymer chains in a solution to form a hydrogel, whereas mechanical rupture involves breaking apart preformed hydrogels. Hypertonic and hypotonic solutions may be used to induce hydrogel swelling or shrinkage. The trypsin/EDTA process creates porous structures by using enzymes to treat hydrogels. Electrospinning is an electrohydrodynamic process controlled by viscosity, and involves creating ultrafine fibers from a polymer solution, which can also be assembled into a hydrogel dressing production. As a different method, 3D bioprinting uses a computer-controlled printing process to produce a hydrogel structure with the desired shape and properties. These techniques offer a range of options for producing hydrogel-based wound dressings with different properties and functions.

Hydrogels can absorb from 10% to thousands of times their weight in water. As a result, they maintain the wound's moisture, contribute to the removal of necrotic tissue, and are transparent. Moreover, their degradation time can be adjusted for controlling drug delivery. Based on these characteristics, they are recommended for pressure ulcers, surgical wounds, burns, radiation dermatitis, and wounds with low to moderate exudate levels [50].

Hydrogel wound dressings have low mechanical strength due to their high water retention capacity, which might necessitate a second wound covering. Additionally, their liquid retention capability can promote bacterial growth. To mitigate this, a composite structure is formed with antimicrobial agents. In cases of injuries related to illnesses causing a weakened immune system, active antimicrobial pharmaceutical components are typically employed, while ensuring this does not disrupt the wound environment [64].

Besides all the advantages, negative impacts on matrix structure and unwanted residues have been observed with the use of high doses of detergent and enzymes during decellularization. Furthermore, a limitation has also been observed during the production of electrospun dressings with electrospinning techniques at large quantities. In contrast, 3D bioprinting offers unprecedented control over mechanical strength, the gelation process, chemical manipulation, composition, architecture, structure, and dynamics of bioinks. These advantages make it a promising technology for producing wound dressings designed to meet the specific needs of each patient [65].

Since 3D-bioprinted wound dressings with hydrogel-based bioink offer many advantages due to their similarity to natural tissues, excellent biocompatibility, and ability to respond to external stimuli, they are leading the field of 3D-bioprinted wound dressings.

### 3.2.1. Bioinks for Wound Dressings

In recent years, 3D bioprinting has become one of the most efficient technologies for producing wound dressings, as it can print cells and biomaterials on the exact print path [66,67]. The functionality of bioink depends on three factors: printability, shape accuracy, and biocompatibility [68]. These aspects not only determine the efficacy of the bioink but also influence the subsequent tissue development process [69]. For instance, during the degradation of a material scaffold, incorporated cells release proteases, initiating a cascade of events that ultimately leads to the synthesis of ECM proteins. These proteins play a crucial role in shaping the intricate architecture of the emerging tissue structure. Additionally, the material's suitability for use as a bioink relies on its rheological

characteristics, such as its ability to be extruded at low pressures and to maintain the desired shape. If 3D bioprinting involves the use of cells or bioactive agents, the rheological behavior should also support cell viability due to clinical and regulatory concerns [70,71]. According to the Food and Drug Administration's (FDA) regulations, antimicrobial wound dressings are classified as unclassified products with the code FRO (dressing, wound, drug). However interactive wound and burn dressings that promote or accelerate wound healing are classified as Class III devices. There are 24 types of polysaccharide-based hydrogel wound dressings registered by the FDA. These products are composed of materials such as alginate (ALG), cellulose, chitosan (CH), and hyaluronic acid (HA). Specifically, ALG-based hydrogels have dominated approximately 70% of the wound dressing market. These dressings provide a moist wound environment and facilitate autolysis, which is the natural breakdown of dead tissue. For instance, Algicell™ Algicell® is a hydrogel dressing that contains silver ions. The antibacterial properties of silver ions make them useful for preventing infections [72]. Various other examples of wound dressings (\*US FDA-approved indications) include 2nd Skin® by Spenco Medical, Ltd. (Waco, TX, USA), Carrasyn® developed by Carrington Laboratories (Irving, TX, USA), Clearsite® from ConMed Corporation (Utica, NY, USA), Elasto-Gel™ by SW Technologies (Kansas City, MO, USA), FlexiGel™ and Transigel™ produced by Smith & Nephew (London, UK), Kendall™ Curafil™ and Kendall™ Curagel™ both manufactured by Covidien (Dublin, Ireland), Normlgel® and Hypergel® from Molnlycke (Gothenburg, Sweden) [73] Health Care, Nu-gel® by Systagenix (Quincy, MA, USA), Tegagel™ offered by 3M (St. Paul, MN, USA), and Vigilon® by C.R. Bard (Murray Hill, NJ, USA), among others. In addition to providing a suitable environment for wound healing, traditional hydrogel wound dressings can be further enhanced by incorporating biomimetic components into bioprinted products. The studies on this method have demonstrated that biomimicry could positively influence the attachment, function, migration, and proliferation of both endogenous and exogenous cells [74].

By putting more effort into designing or upgrading 3D printers to protect cells from exposure to extreme conditions during the printing process, in combination with enhancing the performance of the materials by adding or changing the polymeric backbone, it is possible to produce biocompatible, mechanically stable, and non-immunogenic dressings with a proposed shape.

A wide variety of bioprinted materials is currently presented in the literature using bioinks. Inks are classified into two main groups based on the presence or absence of cells embedded in the materials' matrix. The most widely used type is a scaffold-based biomaterial, in which cells are loaded into hydrogels and bioprinted into 3D structures. Cell-loaded hydrogels allow cell proliferation and growth, facilitating tissue formation. In the second type, cells are bioprinted without an exogenous biomaterial referred to as the scaffold-free approach, which mimics embryonic development.

#### Scaffold-Based Bioink

With the help of 3D bioprinting technology, a scaffold-based bioink can be used to create biomimetic and functional tissue constructs. Considering their strong mechanical properties and ability to function with various biomaterials [75], which is a remarkable advantage of scaffold-based bioink, it is a promising technology with the potential to make significant contributions to tissue engineering and regenerative medicine. The notable disadvantage of scaffold-based bioink is the initial cell density and the possibility of tissue self-assembly. Currently, hydrogels are in the field of interest for wound dressings due to their superior water uptake and swelling properties, biocompatibility, and biodegradability.

Hydrogels are a class of cross-linked polymeric substances capable of absorbing and retaining large amounts of water. In the field of tissue engineering, hydrogels can be divided into two groups—naturally derived hydrogels and synthetically derived hydrogels. While synthetic polymers have been extensively used in the development of hydrogels, there is increasing interest in the use of natural polymers, also known as biopolymers, due to their advantages in terms of biocompatibility and biodegradability. Natural hy-

drogels (such as collagen and gelatin, composed of proteins) and polysaccharide-based hydrogels (including agarose and ALG) have been synthesized using natural polymers. On the other hand, synthetic hydrogels such as polyethylene glycol (PEG) are lacking biological features inherent in their structure, but possess suitable structures to obtain biological functions [76]. Hydrogels have numerous applications in biofabrication and tissue engineering, most of which relate to drug delivery [77], contact lenses [78] and wound dressings [79]. Some hydrogels can mimic the natural tissue environment, possessing several key properties of natural ECM components [80] that enable cell encapsulation in a highly aqueous, mechanically robust 3D environment, without sacrificing biocompatibility.

#### Scaffold-Free Bioink

The scaffold-free approach employs fundamental units such as cell sheets, spheroids, or tissue strands, composed of cells and an extracellular matrix, to construct 3D tissue structures. This methodology relies on the inherent capability of these building blocks to interlace, effectively minimizing the significance of cell proliferation and migration. Consequently, this leads to a substantial reduction in the requisite time for tissue formation. A notable advantage of the scaffold-free approach is its capacity to address the intricate architectural complexity of complex tissues and organs. This achievement is realized through the controlled assembly of heterogeneous building blocks encompassing diverse cell types. Nonetheless, this approach also encompasses certain limitations. Firstly, the individual structural units exhibit relatively modest mechanical properties, potentially rendering cells susceptible to damage during manipulation. Secondly, an immobilization period is imperative for the initial fusion of building blocks and the accumulation of ECM [75,81]. In conclusion, the scaffold-free approach holds promising prospects in the field of tissue engineering. Nevertheless, the constraints inherent to this approach, such as the modest mechanical attributes of individual structural units and the potential for cell damage during manipulation, underscore the need for further investigation and research.

- Tissue Spheroids

Tissue spheroids are a type of scaffold-free bioink material consisting of clusters of spherically arranged cells ranging from 200 to 400  $\mu\text{m}$  in diameter, which closely mimic the structure and function of the various types of tissue found in the human body. Tissue spheroids are widely used in tissue engineering research for modeling different diseases, and for drug testing purposes [82–85]. Additionally, they have been used to study the behavior and interactions of different cell types in the tissue microenvironment, which can both provide valuable insights into the mechanisms underlying various diseases and facilitate the development of new therapeutic strategies [86].

- Cell Pellet

A 3D cell layer is a cluster of cells formed through the centrifugation of suspended cells into a pellet form [87] that can easily be transferred to a micropipette or other mold, thereby enhancing intercellular interactions. The resulting scaffold-independent multicellular structures generate microtissues that closely mimic cell–cell/cell–ECM interactions and enable customization to achieve the desired cellular architecture. An agarose mold is used to support the extrusion of cell sheets-based bioinks into a restricted area. As a benefit of the model, heterocellular nerve grafts can be produced in tubular form [88].

- Tissue Strands

Tissue Strands are 3D structures composed of elongated cells that emulate the structure and function of specific types of tissue in the human body. Scaffold-free bioink materials have been utilized to encourage the growth and elongation of cells, leading to the formation of tissue strips [89,90]. For proper bioprinting, tissue strands must be matured optimally. Tissue engineering research has leveraged this technology for the development of various tissues, including blood vessels and cartilage, as well as drug screening experiments and the exploration of cell-to-cell interactions. For instance, Wu et al. deposited spheroids of

cells on agarose rod templates to create a structure that facilitated the construction of single and double-layered vascular channels and utilized microinjection techniques to produce tissue strips encapsulated in ALG capsules [89].

#### 4. 3D Bioprinting Techniques

3D bioprinting is an additive printing technology that allows production by layer-by-layer deposition. It depends on a digital design using imaging techniques such as CAD, MRI or CT. The 3D designed model can be easily converted into the stereolithography (.stl) format, and thus a physical, bioprinted construct is obtained (Figure 1D) [91–94].

The 3D bioprinting system was first introduced by Charles Hull with the invention and patenting of the stereolithography (SLA) printing technology. Hull then proceeded to found 3D Systems Corporation, a 3D printer manufacturing company. Card Deckard patented a selective laser sintering (SLS) technology in 1987 and Scott Crump patented a fused deposition modeling (FDM) [95] technology in 1989. Three-dimensional printers were first introduced in 1996: “Genisys” from Stratasys, “Actua 2100” from 3D Systems and “Z402” from Z Corporation. These technology systems had high costs and insufficient equipment. Following extensive research and development, this promising technology is now accessible, and enables the high-resolution printing of many inks.

As 3D printing allows for customized manufacturing, it has become increasingly popular in the healthcare industry, as it has replaced mass production with personalized manufacturing, and has allowed the development of layered bioinks based on complex 3D structures [96–98]. The ink employed in the bioprinting process must satisfy biocompatibility requirements and possess high strength and resolution properties to ensure that the ink will encourage cell growth [99]. Determining the bioprinting parameters of bioink depends on cell type and density, shear thinning, viscosity, degree of crosslinking, and gelation point [100]. Moreover, cell selection and immune behavior are critical for the performance of 3D-bioprinted dressings.

There are many different classifications according to the working principles of 3D bioprinting technologies. However, not every 3D bioprinting technology is preferred for the process of hydrogel materials, as processing hydrogel materials requires delicate rather than harsh conditions. This review focuses on examining materials and 3D bioprinting technologies that have been and/or can be developed for the 3D bioprinting of hydrogels for wound healing.

##### 4.1. Laser-Based Bioprinting

Developed in 1980, laser-based printing has led to the emergence of various techniques. It can be applied to achieve precisely printed hydrogel structures with inks composed of natural polymers, manipulated by light under the dispersion of laser energy and the ultraviolet (UV) distance (Figure 2A) [101]. With a UV laser, a thin single gel structure is formed, which can then be extruded out so subsequent layers can be built on top of the first layer. The 3D structures fabricated during this process flow directly from the fluid reservoir, meaning hydrogel composites can be formed in a light-curable organic–inorganic solution. Several subgroups of laser-based bioprinting technology exist, including SLA, two-photon polymerization (TPP), digital light processing (DLP), hybrid laser printing (HLP) and SLS (Figure 2). The details of the laser-based bioprinting method and the advantages and disadvantages are given in Tables 1 and 2, respectively.

##### 4.1.1. Stereolithography (SLA)

SLA is prototyped by combining 2D polymer layers cured with UV laser light [102,103]. Via sequential scanning by laser, the printed sheets are lowered, which allows the polymer to create one layer with a required thickness and to scan the following layer. Photopolymers converted into polymer chains bind to the next layer and form the structure. The resin that holds the printing scaffold during the process is removed when the printing is completed. SLA technology has an approximate resolution of 10  $\mu\text{m}$ , thus enabling the production

of sensitive biomedical products [104]. This technology has advantages of both high-resolution and multi-layer printing quality in producing large print volumes in the range of 200–2000 mm. In addition, the printing product, formed due to the easy control over printing parameters, has a consistent and stable structure [105]. The limited light-curing hydrogel structure is one of the advantages of SLA techniques in the production of hydrogel composites. However, the need for supporting structures during printing and the final curing process is the main downside of SLA printing technology.

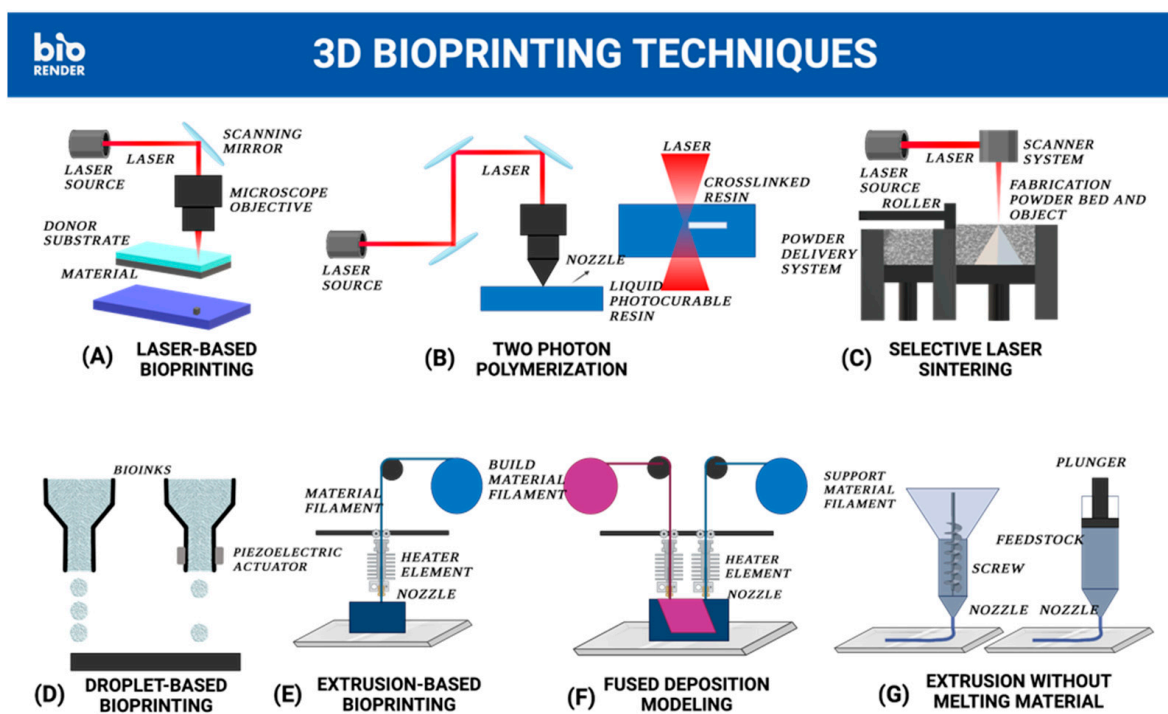


**Figure 2.** Schematic presentation of different types of 3D bioprinting techniques including laser-based bioprinting (A), two-photon polymerization (B), selective laser sintering (C), droplet-based bioprinting (D), extrusion-based bioprinting (E), fused deposition modeling (F), and extrusion without melting material (G). This figure was created using <https://app.biorender.com/> (accessed on 1 August 2023).

In the field of bioprinting, SLA is highly preferred because of its high resolution. Micro stereolithography technology, which controls tiny spaces with precise beam control, is divided into two subgroups. The first is the scanning  $\mu$ SLA, in which UV is focused on the bioink surface and avoids disadvantageous parameters such as poor focusing and low resolution during scanning [106,107]. Mask projection, another 3D printing method, is achieved under radiation with the help of a patterned mask, leaving each layer of liquid bioink under the influence of the beam. These bioprinting systems allow the 3D printing of structures in skin applications, wound dressings, and applications such as microelectromechanical systems (MEMS) due to their excellent printability properties on very small areas [108–110].

#### 4.1.2. Two-Photon Polymerization (TPP)

The TPP technique is a stereolithographic method used to create nano-sized structures without going through a layer-by-layer process (Figure 2B) [101,107]. The TPP strategy is formed by infrared (IR) laser pulses of femtosecond durations. Furthermore, with the IR light threshold intensity reaching up to 200 nm, TPP enables high-resolution 3D designs compared to other 3D techniques, with its low amount of focus, which makes it favored by

researchers [109,111]. During the polymerization process, free radicals are responsible for initiating the reaction.

The simultaneous absorption of two photons allows the molecule to switch to a high-energy electronic state at TPP, which causes photon voxels to increase up to 100 nm [112–114] and makes TPP a functional system for the 3D bioprinting of nano- and micro-sized materials. The speed of the TPP printing system is proven to be faster than traditional systems, with a speed of 20 mm s<sup>-1</sup> [115]. Beside all these advantages, the dependence of resolution on the laser beam diameter results in a longer bioprinting process, influencing the scaffold's size.

To date, various natural and synthetic resources have been used as bioinks during the TPP 3D bioprinting of hydrogel to solve the dimensional and bioprinting time-dependent problems of the technique [109,116]. Another disadvantage of TPP is the utilization of toxic two-photon initiators that results from organic solvent residues in the final product. A proof-of-concept study based on improvements in the bioink ingredient's biocompatibility and biodegradability was achieved using a new type of ionic carbazole water-soluble photoinitiator, 3,6-Bis[2-(1-methyl-pyridinium)vinyl]-9-methyl-carbazole diiodide (BMVMC), and cucurbit[7]uril (CB7) as the hydrogel monomer, to solve this problem [117]. A photoresist consisting of BMVMC and CB7 was prepared with a photoinitiator ratio of 0.12 wt. %. Then, an arbitrary 3D polymer structure was fabricated in the photoresist by scanning the laser beam over a predefined path over the substrate using a femtosecond laser direct writing setup. Here, the resulting material was produced with a low laser threshold at 3.7 mW and a high resolution at 180 nm. L929 mouse fibroblast cells were incubated in the Dulbecco's modified eagle medium (DMEM) solution containing BMVMC and CB7. Additionally, another batch of L929 cells were also cultured with printed scaffolds. Moreover, the cell viability tests show that the final samples have good biocompatibility and low cytotoxicity on L929 cells, making them a potential candidate for further applications in tissue engineering.

Recently, the production of photo-crosslinked silk fibroin (SF) via two-photon polymerization methods was introduced by Valente et al. [118]. Here, SF was prepared by degumming the fibers, then dissolving the fibers in lithium bromide and finally diluting the SF solution to 4% *w/v* concentration. Later, tris(2,2'-bipyridyl)dichlororuthenium(II) hexahydrate (ruthenium) and sodium persulfate were added to the SF solutions. The cross-linking of the SF-based hydrogel caused an increment in Young's modulus to range between 9.6 and 47.2 kPa. Scanning electron microscope (SEM) analysis revealed that the average pore sizes were in the range of 0.25–1.13 μm<sup>2</sup>. In addition, normal human dermal fibroblasts (NHDF) were added to the SF solution prior to 3D printing. Cytotoxicity assays showed an over 95% cell viability rate in 21 days, thus confirming the bioprinting suitability of this method. This is due to the fact that TPP does not apply shear force stress to cells caused by extrusion, and the literature demonstrates that IR radiation is safer than UV radiation [118–120]. The *in vitro* degradation analysis indicated that the size of the hydrogels fabricated with 800 mW lasers decreased by almost 90% after 60 min, whereas an increase in laser power resulted in a greater resistance to degradation; therefore, 1600 mW lasers were capable of fabricating hydrogels with 60% size reductions in 60 min [121].

#### 4.1.3. Digital Light Processing (DLP)

DLP was developed with the help of SLA biosignature technology. DLP light sources, combined with multiple lenses, allow 3D scaffolds with a resolution between 25 and 150 pixels [101,105,122]. Unlike traditional printing systems, DLP adopts the top-down method, which includes a beam source placed under the DLP system and cured bioink. Therefore, the structure system or carrier can be immersed in the bio-substrate and moved up after the layers are polymerized. During this process, bioink may also be delivered directly to the substrate via capillary action, and each repeated step can be completed within 15 s [101,123]. The DLP system can be run again spontaneously by the user without changing the parameters [109].

Due to its rapid and high-resolution printing capabilities, the DLP method is suitable for tissue engineering and fabricating wound dressings. For example, a CH/acrylamide (AM)-based hydrogel was successfully produced using the DLP system [123]. The bioink was prepared by dissolving CH in acetic acid solution, then adding methacrylic anhydride (MA) at 60 °C. Furthermore, the addition of AM to the bioink caused an increment in the maximum stress at fracture from 97 kPa to 345 kPa, resulting in an increase of 356% in compressive strength. Subsequently, the tensile stress increased from 47 kPa to 183 kPa. To assess the cytotoxicity of the hydrogel, CH/AM bioinks were placed on well plates and solidified with photocuring. Then, HUVECs were seeded on the surface of hydrogels and cultured for a few days. Although an increase in polymerized AM content resulted in less cellular attachment and activity, which limited the ability of cells to adhere to and proliferate on the surface, *in vitro* biocompatibility tests demonstrated adequate biocompatibility qualities.

For personalized disease management, micro-pyramid-decorated gelatin methacrylate (GelMA) hydrogels were introduced using the DLP technique [124]. GelMA was prepared by the methacrylation of gelatin type A, and the bioink was produced by dissolving GelMA in a solution involving phosphate buffered saline (PBS) and PEGDA. According to the mechanical tests, printed hydrogels exhibited a compressive modulus of 53 kPa, and the swelling ratio was approximately 400% in 5 h. The pyramids were designed to be 1.5 mm in length to ensure the dressing directly contacts the wound. The SEM results show that printed hydrogels kept their shape for 7 days in PBS immersion. To assess *in vitro* cytocompatibility tests, mouse fibroblasts were seeded on printed hydrogels. Furthermore, the cytotoxicity assays revealed 90% viability after 72 h of incubation. In order to evaluate the *in vivo* wound healing performance of the hydrogels, wound areas on rat skin were treated with GelMA hydrogels for 0, 7 and 14 days. Following this, an immunohistochemistry (IHC) assay for CD31 was carried out to further explain the healing mechanism. Consequently, the IHC assay confirmed more vascularization in hydrogels with heparin. *In vivo* tests demonstrated that hydrogels without heparin achieved 33% wound closure, while hydrogels conjugated with heparin achieved 67% wound closure after 14 days of treatment. Overall, the results indicate that the DLP method has significant potential in wound dressing production.

Besides the remarkable success achieved in the production of hydrogel-based biomaterials with DLP bioprinting, the most promising use of such biomaterials is the smart dressings combined with sensors. Recently, auxetic hydrogel wound dressings integrated with paper-based colorimetric sensors were developed to detect the pH and glucose concentrations of the wound. A 50 mL volume of hydrogel resin was prepared by mixing HEMA, PEGDA, and diphenyl-(2,4,6-trimethylbenzoyl)phosphine oxide (TPO) at a 1:1:0.05 ratio. In post processing, DLP-printed auxetic structures were washed with isopropyl alcohol, subjected to ultrasonication, and then UV-cured to remove residual monomers. According to mechanical tests, the average yield strength was 1.5 MPa and the Young's modulus was 0.6 MPa. Moreover, the hydrogels exhibited high water uptake and the integrated sensor exhibited an auspicious performance [125].

#### 4.1.4. Hybrid Laser Printing (HLP)

HLP is preferred for creating complex, large-sized and multi-ink printing bio-products. This bioprinting technique covers the connection between the “dead zone” in the continuous liquid interface production (CLIP) option and the “ablation z-range” interaction in the reduced multi-tone ablation (MPA) option. For this interaction, a crosslinking reaction is performed by selecting a light source with separate wavelengths from each other. It is passed through the harmonic generator to create the wavelength selected in the CLIP option. To create a cross-linked bio-product, a beam pattern is created according to the selected design. MPA is preferred in this technology to eliminate redundancies in the cross-linked layer. Although the resolution of the bio-print reaches down to micron levels [126,127], the

slow scanning property is the main drawback of this technology, which was first introduced by Kunwar and his colleagues [126].

#### 4.1.5. Selective Laser Sintering (SLS)

SLS is an additive manufacturing (AM) technique developed and patented by Carl Deckard and Joe Beaman in 1989 [128]. In this additive manufacturing technique, a laser beam is used to melt the powdered material (Figure 2C) obtained according to the design of the desired structure. Once the first layer is printed, the nozzle moves down, and a new layer of dust spreads on the platform for the next layer. This systematic process continues until the designed structure is fully completed [129] and excess dust is cleaned by brushing or using compressed air [96,130].

An important advantage of SLS is the capacity for producing large and complex structures. In addition, SLS does not need a supporting layer during the assembly process of dust particles, or solvent decay in the printing product [131]. On the other hand, the formation of a rough surface and its requirement of being polished are the main disadvantages of the SLS method [132]. At present, as far as we know, there is no ongoing research on wound dressings using SLS technology, but its potential is very promising due to its many advantages. For example, Chen et al. produced Poly- $\epsilon$ -caprolactone (PCL) scaffolds with differing pore structures and distributions using the SLS bioprinting method. The cartilage tissue engineering scaffolds were loaded with chondrocyte involving collagen gels. PCL/COL1 scaffolds showed better results than traditional scaffolds in terms of cell proliferation, cell survival and ECM production. Glycosaminoglycan and collagen II quantification also demonstrated the superior matrix secretion properties of PCL/COL1 scaffolds.

**Table 1.** Summary of laser-based bioprinting techniques.

3D Bioprinting Techniques	Power Source	Material	Printing Speed	Method	Accuracy ( $\mu\text{m}$ )	Resolution ( $\mu\text{m}$ )	Ref.
Stereolithography (SLA)	UV	PEGDA/PEDOT:PSS, p(HEMA-co-EGMA)/PEDOT:PSS, PEGDA/rGO, Ceramic	8 mm/s (PEGDA/PEDOT:PSS) 2.5 to 8.0 mm/s (p(HEMA-co-EGMA)/PEDOT:PSS) 1.5 to 2 s/layer (PEGDA/rGO) 20 mm/s (Ceramic)	Solidification of liquid resin by photopolymerization.	25–150	x: 10 y: 10 z: 15	[104,126,133–135]
Two Photon Polymerization (TPP)	UV	Polycaprolactone (PCL), trimethylene carbonate (TMC)	18–60 mm/s (PCL), 5 $\mu\text{m/s}$ (TMC)	The initiation of a photochemical reaction by focusing an ultrafast laser pulse on a photosensitive bioink.	100–400	100 $\mu\text{m}$	[136–141]
Digital Light Processing (DLP)	Projection	Ceramic, methacrylated gelatin/poly(vinyl alcohol) (GelMA/PVA), Polyethylene glycol diacrylate (PEGDA) Polyvinyl alcohol/acrylic acid/Polyethylene glycol diacrylate (PVA/AAc/PEGDA)	1–4 s (PEGDA) 500 mm/min (GelMA/PVA) 5 $\mu\text{m/s}$ (PEGDA) 50 mm/min (PVA/AAc/PEGDA) 10 mm/s (Ceramic)	The photosensitive bioink is cured with the aid of a projector.	10–25	x: 25 y: 25 z: 20	[16,104,136,142–144]
Hybrid Laser Printing (HLP)	UV	Polyethylene glycol diacrylate (PEGDA), gelatin methacrylate (GelMA)	100 $\mu\text{m/s}$ (PEGDA), 100 $\mu\text{m/s}$ (GelMA),	By combining Hybrid Laser Printing (HLP) and Continuous Liquid Interface Production (CLIP) with Multiphoton polymerization (MPP)/Multiphoton ablation (MPA) processes, it is possible to print bio-copies with micro-sizes and -properties in a short time.	-	25 $\mu\text{m}$	[126]
Selective Laser Sintering (SLS)	High Power Laser Beam	polyamide, polyethylene oxide (PEO), polycaprolactone (PCL)	2000 mm/s (polyamide) 300 mm/s polyethylene oxide (PEO) 1.257 m/s (PCL)	Laser-induced sintering of powder particles	300	x: 50 y: 50 z: 200	[16,104,145–148]

**Table 2.** Laser-based bioprinting advantages and disadvantages.

3D Bioprinting Techniques	Advantage	Disadvantage	Ref.
Stereolithography (SLA)	High drug loading capability, good bioprinting resolution, high tissue volume, fast printing and high cell viability, strong interlayer adhesion, and ability to model multiple resins in the same layer.	It is generally unsafe. Preference is given to liquid bio-products that can only be cured with light, and the material scale is low. Raw material toxicity, difficulty removing uncured resins, and the ability to print only flat layers.	[104,149,150]
Two Photon Polymerization (TPP)	The production of complex structures; precise control of parameters such as the number of pulses, pulse duration or pulse energy allows increasing the resolution. Also, 3D structures with micro/sub-micron properties can be produced precisely.	TPP technology is not fast in reaching mass production. Volumetric loss occurs during polymerization.	[151–154]
Digital Light Processing (DLP)	High resolution; simple, short biosignature time; better cell viability; uncured photopolymer is suitable for reuse.	Complex processing steps, high-precision instruments, material toxicity, low bioink scale, possible UV damage to DNA, difficulty printing large structures and difficulty in controlling the exact structural shape.	[104,155]
Hybrid Laser Printing (HLP)	Micro-size printing, complex product production, wide range of materials, high printing flexibility, low cost, control system is simple and automatic.	As you move from the corners of the printing product to the middle, the mechanical strength decreases.	[124,156]
Selective Laser Sintering (SLS)	High resolution, does not need a support structure, high strength, manufacturing in a short time, complex prints can be easily manufactured.	Finishing is necessary due to the roughness after printing. There are difficulties in material exchange.	[104]

#### 4.2. Droplet-Based Bioprinting

Droplet-based bioprinting is mainly based on inkjet printer technology. This technology allows the accumulation of materials by passing them through a special nozzle (Figure 2D). The precise deposition of droplets flowing from the nozzle enables the high resolution of the scaffold structures with a chemical or thermal curing process. However, due to factors such as viscosity [132], surface tension, and evaporation rate in the ink structure, this printing technology possesses great difficulties. Droplet-based bioprinting technology is divided into continuous inkjet and on-demand inkjet bioprinting. Continuous inkjet bioprinting is based on the strategy of dripping from a nozzle along with the pressure caused by bioprinting. Conductive bioink tends to be in the desired position under the influence of force (Figure 2). Optional inkjet bioprinting requires thermal, piezoelectric, and electrostatic effects for pressure pulses. Droplet-based bioink technology is ideal for complex structures due to the high accuracy (100  $\mu\text{m}$ ) of different bioinks and the ability to bioprint at a resolution of 50–500  $\mu\text{m}$  [157]. However, low-density bioink can be preferred for ink flow continuity and cell viability [158].

The rapid fabrication of complex structures with high accuracy is essential in many biomedical engineering applications. For this purpose, the preparation of human cell-derived artificial skin (hSKE) was introduced utilizing a unique technique based on droplet-based bioprinting technology [159]. The presented hSKE does not only imitate the dermis and epidermis of normal skin morphologically, but also mimics the keratinization process in the epidermis. Furthermore, the findings demonstrate that hSKE can enhance skin regeneration via wound grafting.

Another line of research has shown the effectiveness of droplet-based bioprinting techniques for manufacturing hydrogel–fiber composites [160]. The droplet deposition of structured hydrogels onto fibers and the homogenous distribution of high cell densities are used to achieve this approach. A solution consisting of collagen–ALG–fibrin was prepared, and to achieve a cross-linking bioink, a thrombin solution was produced with a DMEM solution involving calcium chloride. In order to obtain the desired cell printing density, pelletized cells were redissolved in a cross-linking bioink. Differences between composites generated with different fibroblast densities ( $5 \times 10^6$  and  $30 \times 10^6$  cells/mL) were also investigated. While 5 M cells/mL composite tissue precursors enhanced cell proliferation, 30 M cells/mL composites promoted quicker cellular migration, better fiber organization, and higher ECM synthesis. Despite the fiber-based substrate's porosity and surface roughness, the hydrogel component created an ECM-like environment that supported intimate cell–cell interactions. The needle-punched mesh served as an appropriate substrate for cells to move through the hydrogel and deposit ECM. Additionally, this method avoided filament dragging and weak adhesion problems on the initial layer of the printing surface. As a result, it is claimed that fibroblast infiltration and the creation of layered structures may imitate the skin layers of cell–hydrogel–microfiber composites.

In addition to the bioink composed of synthetic materials, living cells can also be printed with this technique. For example, the encapsulation of human stem cell spheroids into ALG hydrogels was achievable using droplet-based bioprinters [161]. In this study, cryopreserved human adipose-derived mesenchymal stem cells were thawed and cultured in a flask. Later, cells were plated into hydrogels and formed into spheroids. The average droplet diameter was in the range of 330–390  $\mu\text{m}$ , while increasing the flow rate resulted in decreased droplet size. The encapsulated stem cell spheroids had an average diameter of  $335 \pm 1$  to  $733 \pm 15$   $\mu\text{m}$ , with a lower concentration of surfactant resulting in larger diameters. The results indicate that droplet-based printing was effective in fabricating encapsulated hydrogel constructs.

Moreover, the effects of droplet impact velocity and droplet evaporation on the cell viability of thermal inkjet bioprinted primary human cells have been studied to understand the influence of the printing process on cell viability [162]. The cell concentration printability range was 1–4 million cells/mL, and a change in cell concentration (1–4 million cells/mL) showed no significant effect on the viability of the printed cells throughout the printing

process. A slower droplet impact rate reduced droplet spatter, enhanced printing accuracy, and increased printed cells' survival rate in sub-nanoliter droplets substantially. The PBS solution was used to evaluate the effect of droplet evaporation on cell viability, using PBS droplets with >90% cell load, a minimum droplet volume of 20 nL per dot, and a total printing time of 2 min per printed layer. The results of this study served as a foundation for other droplet-based bioprinting techniques that involve the non-contact spraying of nano-liter cell-loaded droplets across the nozzle-substrate distance.

#### 4.3. Extrusion-Based Bioprinting

The extrusion-based 3D bioprinting system is a technology that allows a system-guided nozzle to print a layer-by-layer structure. The nozzle moves the ink along the X and Y axes by creating a continuous flow and moves up or down in the Z-axis direction (Figure 2E). This technology can be divided into two subgroups: melt-based printing and non-material melt printing [163,164]. The accuracy and resolution of the extrusion-based bioprinting method with respect to the bioinks are summarized in Table 3, and the advantages and disadvantages of the method are summarized in Table 4.

Traditional extrusion technology consists of 3D printing by progressively extruding bioinks via the print head with pressure. A previous study was conducted to develop physically cross-linked chitosan–pectin (CS-PEC) hydrogels with good printability and dimensional integrity with this technology, making them suitable for wound dressings [165]. In addition, the integration of an upgraded static mixer to the 3D printer allows the use of bioinks with low viscosity [166]. Similarly, extrusion-based gradient 3D printing technology allows the 3D printing of bioink using two different syringes and two different softwares. It enables a composite bioink with a gradient structure using different syringe speed adjustments [167]. An alternative method is micro-extrusion 3D printing technology, which involves controlling the ink with computer software and extruding it onto the system layer. The bioprinting of the desired structure is created through four or five iterations [168].

In contrast to the methods described above, semi-solid extrusion (SSE) technology utilizes the layer-by-layer deposition of bioink to produce 3D constructions [169]. The primary distinction between SSE and other extrusion methods is in the raw materials used. The beginning material in SSE is a semi-solid or semi-molten substance, whereas the printing material in FDM is a solid filament or powder [170,171]. Because of the low temperatures necessary for bioprinting, live cell structures such as aortic valves and tissue healing may be created [172–175]. The distinct features of this biotechnology are currently being investigated in medication development to create novel dosage formulations [176]. SSE is a good contender for inclusion in healthcare settings or research laboratories due to its capacity to generate Printlets™ (3D-printed tablets) and other devices in minutes in a one-step procedure [177].

Extrusion-based bioprinting technologies with various bioink compositions have been frequently used in wound healing. For example, because of their low cytotoxicity and structural resemblance to ECM, cellulose nanofibrils (CNFs) in hydrogel form are proposed to be suitable for use in bioink formulation for extrusion-based bioprinting. A research group successfully printed low-concentration nanocellulose with 1% *w/v* TEMPO-oxidized CNF and less than 1% *w/v* GelMA [178]. The bioink was prepared by both mixing GelMA powder and loading GelMA solution into CNF hydrogels. It was noted that CNF and GelMA had a strong physical interaction, and the mechanical strength of the scaffolds was regulated between 2.5 and 5 kPa. Experiments with 3T3 fibroblast cell culture revealed that it evokes non-cytotoxic and biocompatible qualities in formulated inks and printed scaffolds. The incorporation of GelMA into the CNF hydrogel increased fibroblast growth. This study concludes that 3D printing shows considerable promise for wound healing applications.

Another research effort focused on the vascularization of 3D-printed full-layer skin grafts to improve current techniques. Dermal–epithelial grafts were implanted into a naked mouse model to evaluate integration with host tissue and wound healing. To produce micro-vessels in skin grafts, human dermal fibroblasts, keratinocytes, and microvascular

endothelial cells were developed and constructed using an extruded 3D printer. Human dermal fibroblasts and human microvascular endothelial cells were combined, with a gelatin–sodium ALG composite hydrogel as the dermis and human keratinocytes were mixed with gel as the epithelium. A full-thickness wound formed on the backs of naked mice and was then closed with a double-layer skin graft. The cell survival rate was kept at >90% per day, which indicates that the composite hydrogel meets the requirements for material for printing cells, while the wound contraction was improved by about 10% compared to the control. In the first week after surgery, no significant observations of differences in wound healing performance between the 3D-printed skin graft and control groups with no endothelial cells and no cells were seen. In the fourth week, however, the wound healing rate of the 3D-printed skin graft was relatively lower than both control groups. Histological examination revealed that the new skin looks like normal skin, and has a significant degree of angiogenesis [179].

A 3D-printed self-assembling peptide nanofiber hydrogel scaffold (SLg) combined with UV-cured GelMA possessing interpenetrating polymer networks was examined using the SSE printing method in terms of the elasticity and absorbency [180]. Photosensitive GelMA was prepared by dissolving gelatin in PBS and then MA was poured into the solution. Peptide hydrogels were obtained in the water mixture. The swelling rates of GelMA variations after 4 h ranged 462–729%, while the swelling rate after 24 h was between 472 and 649%. In order to study wound healing and angiogenesis performance, full-thickness wounds were incised on rats. Following this, the IHC test was performed to assess the biocompatibility and vascularization capabilities of the hydrogels. In vivo studies have demonstrated that the modified GelMA/SLg scaffolds promoted the adhesion and proliferation of HUVECs. The growth rate was parallel to that of L929 fibroblasts, and the proliferation of endothelial cells on GelMA/SLg20 exhibited the highest cell activity. Dermal tissue regeneration analysis utilizing a rat model revealed that on the 28th day, the GelMA/SLg20 group had the greatest regular and collagen fibrous structure, increased collagen type III capacity, and symmetrically distributed fibers. In conclusion, the addition of SLg into the scaffolds improved angiogenesis, vascular regeneration, and dermal tissue growth according to in vivo results.

Recently, two promising studies have been conducted on the development of 3D-printed cellulose/ $\epsilon$ -polylysine (CP) hydrogel and a 3D-printed GelMA hydrogel patch encapsulating VEGF, both decorated with photoactive and antibacterial tetrapodal zinc oxide (t-ZnO) microparticles for wound therapy. To prepare the CP hydrogels, CMC and  $\epsilon$ -polylysine were placed under weak acidic conditions with glycidyl methacrylate. Afterwards, both materials were dissolved in the I2959 solution. The first dressing showed swelling rates of CP hydrogels of 253.41% compared to hydrogels that had a lower CP concentration (333.07%), due to the crosslinking of hydrogels resulting in smaller pore size (25–100  $\mu$ m) and more balanced internal structures. Degradation time varied between 180 and 250 h, depending on the CP content. CP hydrogels resisted 62%~87% strain and endured 280 kPa compression stress. Antioxidant activity was assessed using 2,2-diphenyl-1-picrylhydrazyl (DPPH) free radical scavenging methods, and different concentrations of CP hydrogels revealed  $59 \pm 5\%$ ,  $82 \pm 5\%$ , and  $88.5 \pm 4\%$  antioxidant properties. Cytotoxic evaluation demonstrated no toxicity in CP hydrogels, and cell viability was over 98%. The antibacterial activity of the CP hydrogels also revealed that hydrogels with varying CP contents killed  $\approx 93 \pm 2\%$ – $96 \pm 2\%$  of *E. coli* and  $88 \pm 3\%$ – $95 \pm 1\%$  of *S. aureus*. To evaluate in vivo wound healing performance, full-thickness skin incision was performed on rats, and the wounds were treated with each hydrogel dressings. On the seventh day, the wound treated with CP hydrogel was sealed. After 14 days, the CP group was almost fully healed. Ultimately, the wound healing assay showed CP hydrogels' ability to heal 5 times faster than the control group, which promotes tissue growth, revascularization, and collagen accumulation [181].

The other study conducted with a 1% t-ZnO-VEGF GelMA hydrogel-based dressing caused a significant decrease in the wound by about  $24.90\% \pm 4.21\%$  after one week, and this

reached  $3.48\% \pm 6.03\%$  at the end of two weeks. Additionally, the wound treated with this dressing provided much higher epidermal thickness, with  $101.2 \mu\text{m} \pm 12.3 \mu\text{m}$ , compared to the untreated wound's thickness of  $19.7 \mu\text{m} \pm 4.1 \mu\text{m}$ . GelMA hydrogels involving t-ZnO microparticles adequately decreased bacterial concentrations, and promoted the re-growth of human umbilical vein endothelial cells (HUVEC) and C2C12 myoblasts. The VEGF produced optimal microenvironments on t-ZnO for enhancing endothelial cell growth while retaining antibacterial activity. In vivo tests were performed on mice using non-infected wound models and IHC staining methods. Finally, the printed scaffold containing t-ZnO-VEGF exhibited adequate biological stability and improved angiogenesis, cell proliferation, and anti-inflammatory responses at the wound site, leading to rapid wound healing [182].

The optimization of structures constructed in a 3D bioprinting system complicates the production of traditional approaches due to the variety in bioink type and the geometric complexity of the scaffolds. To address these shortcomings, an artificial intelligence-assisted high-throughput print condition scanning system (AI-HTPCSS) was introduced. It included a programmable pneumatic extrusion bioprinter and an artificial intelligence-assisted image analysis algorithm. The printing conditions were screened efficiently using AI-HTPCSS to produce uniformly organized hydrogel structures. The results reveal that the scaffolds printed under optimal conditions have adequate mechanical properties in vitro and are effective in accelerating diabetic wound healing in vivo. The authors envisage that the unique AI-HTPCSS will provide a platform technology for the future modernization of tissue engineering scaffold manufacturing using 3D bioprinting techniques [183].

#### 4.3.1. Direct Ink Writing (DIW)

DIW is a unique process that benefits extrusion to produce three-dimensional structures at micrometer and nanometer scales, offering a greater degree of customization and control than conventional stereolithography [184]. As part of the DIW process, polymers, ceramics, metals, or even biologically active cells with a certain viscosity are extruded layer by layer through a fine needle onto a substrate and allowed to flow along a predetermined path, in accordance with CAD data, to produce the desired 3D object [185,186]. By solidifying or drying the deposited layers, three-dimensional structures become complex and robust. Moreover, there are various printing modes available, and there is no need to constantly change the printhead [187].

For instance, the cell delivery and degradation of 3D-printed cellulose nanofiber (CNF) hydrogels produced with DIW were studied. Two different sources, tempo-oxidized bacterial cellulose (TOBC) and tempo-oxidized plant cellulose (TOPC), were used to produce hydrogels, and in comparison, TOBC showed a higher water uptake ( $72 \pm 24.4$  g of water per g of CNF) than TOPC ( $57 \pm 15$  g of water per g of CNF). The degradation time varied between 5 and 26 h, depending on their infill density. Prior to the cell viability assay, mouse fibroblasts (NIH-3T3) were encapsulated in TOPC and TOBC. Then, cell-containing hydrogels were transferred into syringes, which the 3D printer uses to produce hydrogel scaffolds. The viability of delivered cells demonstrated that pluripotency was maintained throughout the utilization of hydrogels. Overall, the results show that CNF hydrogels are suitable for the distribution, storage, and encapsulation of mammalian cells [188].

#### 4.3.2. Fused Deposition Modeling (FDM)

FDM is one of the more rapid production methods first introduced to the literature in 1980 by Scott Crump [189]. FDM is a printing method based on the deposition of various polymers in filament or powder form layer by layer from the printhead to the device by melting them with heat (Figure 2F). During printing, the position of the printhead is monitored by the device program. The designed printing shape is deposited in the XY plane. After the layer is printed, it completes the layer-by-layer process by moving the specified distance along the z-axis to print the upper layer. This process is repeated until the design is printed [190,191].

Among the advantages of FDM technology, it allows the possibility of multiple extrusions using various polymers [192,193]. This process uses nozzles containing different thermoplastic materials, controls them via the system, and decouples them sequentially, and a complete model is obtained by combining various characteristics. This bio-printing system does not contain solvents, so it does not need organic solvents that can often damage cells in other systems. However, the number of usable thermoplastic materials is disadvantageously limited [130,194].

Recently, researchers have developed novel bioinks suitable for FDM printing, while simultaneously contributing to biomedical engineering. For example, a research group demonstrated that grafting a polyvinylpyrrolidone (PVP) hydrogel on the surface of polylactic acid (PLA) flat discs and 3D-printed scaffolds increases hydrophilicity. In this study, PVPs of two molecular masses were used in separate variations: 10 kDa and 360 kDa. The mean mass of printed scaffolds was  $330.8 \text{ mg} \pm 22.3 \text{ mg}$ . The SEM photography of scaffolds revealed a hexagon-shaped pore with  $560\text{--}590 \text{ }\mu\text{m}$  sides. The printed hydrogels were placed on wells containing mouse fibroblast cells with DMEM and incubated for 24 h. Cell viability analysis using mouse fibroblasts revealed that grafted scaffolds except the 360 kDa variant could retain viability above 70%, in compliance with ISO10993 [195]. This study proves that PVP grafting is suitable for more complex, porous 3D prints, albeit polymers with high molecular weight may generate cytotoxicity [196]. In another study, wound dressings consisting of CH-pectin (PEC) hydrogels were prepared for the delivery of lidocaine hydrochloride (LDC), using an extrusion-based 3D printer. LDC loaded hydrogels showed swelling rates and water contents of 2265% and 96%, correspondingly, whereas the hydrogel-only group displayed a swelling rate of 2832% and water content of 97%. In vitro drug assays revealed a fast, but controlled, LDC release over 5 h in all variations. The printed hydrogels had bioadhesion strength values of 86.5–126.9 g, like the commercially available wound dressings. Overall, the study confirmed that 3D-printed CH-PEC hydrogels can be used in fabricating wound dressings [165].

#### 4.3.3. Extrusion without Melting Material

Extrusion technology without melting material can be divided into two groups: pneumatic and mechanical (screw and reciprocating), according to deposition mechanisms. In pneumatic 3D printing technology, the bioink is removed from the printhead at a controlled flow rate using air or gas pressure (Figure 2G). Due to adjustable air pressure, various bioinks can be used in this 3D printing technology [197]. However, when compared with the mechanical method, it is difficult to achieve precise control of the mass accumulated in the printhead due to delays associated with the volume of compressed gas. Piston and screw-based mechanical 3D bioprinting technology, on the other hand, uses a linearly positioned piston and screw to push the ink out of the print head. Mechanical technology advances the control of the flow of biofilms and increases the printability of high-viscosity biofilms. However, this mechanical interaction can damage the structure of the biomass [197,198].

A study was conducted on the bioprinting of bioinks consisting of quince seed mucilage and cellulose nanofibrils (QSM-CNF), prepared and 3D-printed into cage structures [199]. The compressive and Young's modulus of printed structures doubled as the CNF concentration increased ( $10.7 \pm 0.5$  and  $64 \pm 2 \text{ kPa}$ , respectively). The swelling ratio and degradation rate were in the range of 1120–1690% and 6.4–10.6%, respectively. To assess cytocompatibility, HepG2 cells were seeded on samples and cultured for 1, 3 and 7 days. Later, an optical density assay was undertaken by adding WST-1 reagent to each well. As the cell viability in all samples was over 90%, no cytotoxic effects were observed, and the printed hydrogels promoted cell adhesion and proliferation.

**Table 3.** Summary of extrusion bioprinting techniques.

3D Bioprinting Techniques	Power Source	Material	Printing Speed	Method	Accuracy ( $\mu\text{m}$ )	Resolution ( $\mu\text{m}$ )	Ref.
Direct Ink Writing (DIW)	UV	GelMA/PEDOT:PSS, MC/kCA/PEDOT:PSS, PAA/PPy-Ki, PLLA/PPy	5 to 10 mm/s (GelMA/PEDOT:PSS) 1, 2, 4, 6 and 8 mm/s (MC/kCA/PEDOT:PSS) 2 mm/s (PAA/PPy-Ki) 140 mm/min (PLLA/PPy)	Extrusion of ink and powder liquid binder	100	x: 10 y: 10 z: 50	[16,134]
Fused Deposition Modeling (FDM)	Thermal Energy	Acrylonitrile butadiene styrene (ABS), Polylactic Acid (PLA), Polycaprolactone/graphene oxide (PCL/rGO), PCL/PANI, GelMA/PEGDA	20 mm/s (PCL/PANI) 0.3 mm/s (PCL/rGO), 1 mm/s (ABS) 150 mm/s (PLA) 20 mm/s (GelMA/PEGDA)	The molten biomaterial is deposited in layers on top of each other. Each layer allows the formation of a 3D structure by merging with the previous layer.	350	x: 100 y: 100 z: 250	[16,104,133,149–207]
Extrusion Without Melting Material	Thermal Energy	PCL/rGO, Nano-fibrillated cellulose (NFC) + ALG, Calcium silicate + Magnesium + PVA, GelMA/PEGDA, gelatin,	5 mm/s (Nano-fibrillated cellulose (NFC) + ALG) 6 mm/s (Calcium silicate + Magnesium + PVA) 1.4 mm/s (PCL/rGO) 12.5 mm/s (GelMA/PEGDA) 5 mm/s (gelatin)	Extrusion of inks containing paste or gel layer by layer to create a 3D object	350	x: 100 y: 100 z: 250	[16,104,145,201,203,206]

**Table 4.** Extrusion bioprinting advantages and disadvantages.

3D Bioprinting Techniques	Advantage	Disadvantage	Ref.
Direct Ink Writing (DIW)	Prints complex 3D objects without frequent nozzle changes, allowing nonlinear patterns via parameter adjustments. Compatible with diverse materials and multiple solidification methods.	The process of bioprinting is long. The spectrum of materials available for bioprinting is restricted and small-scaled prints require unique ink formulations or process adjustments.	[12,187]
Fused Deposition Modeling (FDM)	Enables hollow object production using diverse polymers. User-friendly, cost-effective, compact, and supports various shapes and colors. Compatible with FDA-approved thermoplastics (PLA, polycaprolactone, polyglycolic acid), facilitating healthcare integration. Offers versatility with faster speed than SLA.	Less soluble than SLS and SLA. Long processing time and strong shear forces from nozzles result in rough surfaces. Requires support, parts may exhibit reduced strength compared to solid polymers.	[104,145,149,152,156]
Extrusion Without Melting Material	Adjustable pressure allows for a wide range of bioinks. Mechanical 3D printing allows for fine flow control through the nozzle, allowing for greater viscosity bioink to be used due to enhanced deposition forces.	Following the mass control of the bio-product flowing through the nozzle is challenging with pneumatic extrusion. During pressure, the nozzle's thrust force might damage cell membranes.	[197,207]

#### 4.4. Other Techniques

##### 4.4.1. Magnetic Bioprinting Techniques

An alternative method for 3D bioprinting is the magnetic bioprinting technique, which is used to combine cells in different ways without contact [208]. In this method, two different approaches have been tested. In the first method, label-free diamagnetophoretic printing, the cell medium is mixed with a paramagnetic buffer and exposed to an external magnetic field. Cells floating in the air are directed towards a region with a lower magnetic field strength. The shape of 3D cell assemblies is controlled by changing the magnet configuration. In the second approach, the cells are magnetized by incubating with magnetic nanoparticles (NPs) overnight. The magnetized cells are planted on a low-adhesive plate and cell aggregates are formed through air elevation. Then, the magnetized cell clusters are put back into suspension. Spatial modeling of the magnetic template used to create the desired morphology of cell aggregates is performed using the method of variable variations in shape. However, the cytotoxicity of the magnetic NPs taken into the cells and possible internal stresses can lead to negative effects that can damage the cells [208].

Ito et al. pioneered magnetic bioprinting technology. Using magnetite NPs and magnetic force, structures were created from biological materials (diameter 3 mm; length 10 mm; magnetic induction 1300 G). Magnetite NPs were produced within cationic liposomes, delivered to target cells and consequently magnetically labeled. Labeled cells were then placed on ultra-low-binding plates with a magnet underneath, and post-culture cells formed a surface layer. The magnet was placed in a silicone tube with an outer diameter of 5 mm, an inner diameter of 3 mm and a length of 25 mm. When the cell layer was wrapped around a cylindrical magnet, the magnetic force attracted the cells, forming a tubular structure. Finally, the magnet was removed, and a tubular structure remained as a result [209]. In another study, Leonard et al. used magnetic levitation and bioprinting methods to create 3D cancer cell spheroids. After incubating cells with magnetic NPs overnight, cells were placed on top of the spheroid drive, thus allowing them to form a spheroid shape [210]. Conclusively, this approach is effective for sculpting and organizing biological materials [209].

##### 4.4.2. Freeform Reversible Embedding of Suspended Hydrogels (FRESH) Bioprinting Techniques

One of the most difficult obstacles facing effective bioprinting is the breakdown of soft and liquid-like bioinks due to gravity, and the resultant decrease in print quality. It might be difficult to create a robust structure without physical support when printing multiple bioinks layer by layer. Another issue is not curing the structure quickly enough and with the right hardness throughout the printing process. To solve this issue, the Freeform Reversible Embedding of Suspended Hydrogels (FRESH) approach was created. The bioinks are extruded in efficient stress-support water, allowing them to remain in the appropriate position until cured. This successfully solves the issue of structural stability while printing [211–215].

Lee et al. have successfully recreated the tissue and organ functions of the human heart, from capillary to full organ scale, using the FRESH 3D bioprinting technique. As a result of the measurements performed, they evaluated the conformity of the print with the original model. For the mechanical functionality analysis, they integrated the valve into an arterial pumped flow system to mimic physiological pressures and observed the valve leaflets cyclically opening and closing. During this observation, the flow rate through the leaflets was measured and showed <15% backflow (regurgitation) with a maximum open area of 19.5% [211].

#### 4.4.3. Sacrificial Writing into Functional Tissue Bioprinting (SWIFT) Bioprinting Techniques

The Sacrificial Writing into Functional Tissue Bioprinting (SWIFT) biomanufacturing approach includes embedding the 3D printing of a sacrificial ink into a live organoid-based matrix to construct perfusable channels in the form of single or branched conduits. After the sacrificial ink is removed, the resultant channels are perfused with hyperoxygenated media to assist the tissue construct's development and maturation. This approach allows for the formation of organ-specific tissues with high cell density, maturation, and desired functioning, and it holds enormous therapeutic promise in regenerative medicine [216].

#### 4.4.4. In Situ Techniques

In situ 3D bioprinting technology relies on emulating human physiology to bioprint tissue with minimal damage to body tissues. In situ 3D bioprinting technology has been described as a new system for highly personalized medicine [217].

There are two main options for in situ 3D bioprinting technology. The first is the portable device-based approach that allows direct printing. In this method, thanks to the small size of the system, it moves easily in and around the wound area and directly presses the defect area. This system is preferred due to its sterile operation and low cost compared to other technologies [218,219]. The second system is a specialist-controlled approximation of the X, Y, and Z axes [220]. The texture to be printed is designed in a digital file format. The device, ready for printing in a controlled manner by the specialist, can print many bioinks with different formulations in the same system. The location of the defect within the complex structure can be easily printed with this system simulating complex tissues and implants [221,222].

With on-site 3D bioprinting, it is challenging to print personalized dressings in the defect area. The creation of the printing product in compliance with the morphology structure, and the selection of optimum conditions, are the main drawbacks that limit the wide use of the in situ 3D technology [223].

CH hydrogels are becoming increasingly popular for their biocompatibility, antibacterial activity, biodegradability, and their cost; however, they occasionally involve toxic and organic solvents in their composition. To address this problem, a study was conducted for manufacturing high-strength (2.31 MPa) CH hydrogels via DIW [224]. The researchers produced an ink wherein CH was dissolved in an alkaline aqueous solution that presents considerable potential in tissue engineering. Another research inquiry showed the efficacy of VEGF-containing bioprinted GelMA hydrogels in treating full-thickness wounds in a pig model. When compared to empty GelMA and topical VEGF therapy, wounds treated with VEGF-releasing GelMA showed less shrinkage ( $18 \pm 4\%$ ) and a lower SEI (scar elevation index) ( $1.09 \pm 0.01$ ). The number of rete ridges and the neopidermis thickness were greater in wounds treated with VEGF-releasing GelMA, compared to empty GelMA and topical VEGF therapy. This work established in vitro and in vivo bioprinting of VEGF-loaded GelMA hydrogel [225].

#### 4.4.5. Microfluidic-Based Techniques

Microfluidic devices are functional in vitro structures that strive to miniaturize a structure's in vivo physiology. They do so by employing various cell types and ECM while retaining the chemical and mechanical characteristics of micro-level surroundings [226]. During the production, cleanroom technology is essential to prevent dust or particle accumulation in microchannels [132,227]. Given the valve integrations and time-consuming procedures, these technologies result in intensive resource consumption and time-consuming activities. Microfluidic devices cannot be used due to production constraints and complexity. These constraints, along with the benefits of 3D printers, have piqued researchers' interest in the fabrication of microfluidic devices. A 3D printer comprises bioink and a printed design in a digital file for the creation of microfluidic devices using 3D bioprinting technology. The 3D printer travels in the X, Y, and Z directions, allowing 3D printing to be

created. The X and Y axes reflect the nozzle's lateral motions, while the Z axis represents its vertical movement [228–230].

Among the 3D bioprinting technologies of microfluidic devices, laser-based bioprinting, droplet-based bioprinting, and molten deposition modeling are commonly employed. The layers created by fused deposition modeling (FDM) biotechnology have heights ranging from 50 to 400 microns. Low layer length improves accuracy; nevertheless, this approach requires more time and money to develop the bioprinter. In comparison to FDM biotechnology, they are extensively employed in the 3D manufacture of SLA and SLS microfluidic devices because of their benefits such as high sensitivity, rapid production time, and low cost [231–234]. Owing to the indicated advantages, one study produced a graphene oxide (GO)-mediated photothermal responsive dextran hydrogel scaffold using microfluidic 3D printing technique. According to mechanical and in vitro tests, the storage modulus ( $G'$ ) increased gradually with differing GO concentrations from 2 to 8 mg/mL and the degradation rate was delayed as the concentration was increased. A Live/Dead assay has shown no cytotoxicity towards cells, and normal cell proliferation occurred. After near-infrared (NIR) laser exposure for 5 min, the DEX/GO5 hydrogel exhibited an approximately 100% antibacterial effect against *E. coli*, *S. aureus* and *C. albicans*, proving the photothermal antibacterial properties of DEX/GO hydrogels. In vivo wound-healing tests were conducted on rats with *S. aureus*-infected wounds and after 11 days, the DEX/GO5/VEGF+NIR group had the smallest wound area at  $5.3\% \pm 0.8\%$ . When loaded with VEGF and used as a wound dressing, the scaffold achieved adjustable mechanical, photothermal antibacterial properties, followed by angiogenesis during the wound healing process. According to the study, the GO hybrid hydrogel revealed an evident stiffness decrease, a good photothermal antibacterial performance, as well as effectively stimulating cargo release with NIR light [235].

#### 4.4.6. Cell Laden Spheroids

Two bioprinting approaches have been devised to manufacture cell-loaded spheroids using 3D bioprinting: direct cell extrusion and sacrificial bioink printing. Direct cell extrusion 3D bioprinter allows the production of complex 3D structures resembling living tissues and organs in vitro. These structures are obtained by the precise and flexible printing of complex products such as cell-containing biosimilars, ECM and cytokines [236].

Bioprinters create repeatable and systematic biological structures using additive manufacturing and layer-by-layer deposition processes. Large numbers of spheroids may be created in vitro in this manner. Spheroids are created by extruding droplets containing cell-loaded bioinks. Bioinks with cell adhesion capabilities are essential in the spheroid generation process. Bioinks with cell-adhesive characteristics promote stable cell attachment and proliferation in an environment comparable to ECM. As a result, inside the droplet, a spheroid is entirely filled with cell forms [237–241].

Cell aggregation and intercellular adhesion are stimulated by a drop of cell-repellent bioink, resulting in the creation of a small spheroid. However, in bioprinting, numerous bioink parameters such as viscosity, shear thinning, viscoelasticity, biodegradation, crosslinking, and cellular adhesion must be chosen. These characteristics are crucial for achieving the required structures [242–244].

It is proposed to use a sacrificial bioink rather than a hydrogel to fabricate precise 3D patterned spheroids. After printing the polymer barrier and matrix biomaterial as a supporting medium, the cell-loaded sacrificial bioink was pierced into the matrix biomaterial. The matrix biomaterials were selectively cross-linked, and the sacrificial bioink that surrounded the cells was dissolved, resulting in holes sealed within the matrix biomaterial. Imprinted cells inside the holes were able to form spheres in situ because of ongoing culture, and the accurate 3D placement of the spheres was achieved in a single simultaneous procedure. Spheroid size control and correct spheroid localization were also established. Although sacrificial bioink 3D bioprinting allows for exact spheroid production at a specific

location, its practical use is restricted since it is more expensive, difficult to handle, and time-consuming than other procedures [240,245].

## 5. Recent Advances in Hydrogel-Based 3D Printing for Wound Healing

### 5.1. Drug Delivery

In recent years, 3D printing has attracted significant attention to drug delivery research because of its capability to produce highly customized products in an efficient manner. Thanks to the customization options of bioinks, it is possible to load drugs into hydrogels during the printing process. For instance, HA and carboxymethylcellulose (CMC) were used to produce a highly elastic, biocompatible, and microporous hydrogel network that was capable of being printed in multiple layers without the need to add additional materials or post-printing processes [246]. This method rapidly self-crosslinks hydrogels in the 3D printing process and is capable of rapid self-healing without damaging the integrated cells. *In vitro* drug release and cell culture studies revealed that 3D-printed structures (pore size  $\cong 50 \mu\text{m}$ ) formed thicker networks caused by higher stress during the needle extrusion, displaying slower drug release from the printed gel until 96 h and Live/Dead ratios of  $78 \pm 8$ , and  $68 \pm 2$  for 1 h to 24 h, respectively. *In vivo* studies were undertaken by placing hydrogels subcutaneously on mice. At 1 week after injection, the angiogenesis in the HA-CMC groups was  $14.8 \pm 2.8$ , which was significantly higher than the control group ( $4.8 \pm 1.3$ ). At 4 weeks after injection, the angiogenesis in the HA-CMC groups was  $17.6 \pm 2.4$ , which was approximately 20% higher than the control group. The conducted *in vivo* studies revealed 80% infiltration of the surrounding tissues after one week, and all the hydrogel groups did not degrade after four weeks. For the treatment of impetigo, a common and highly contagious bacterial skin infection that mostly affects young children and infants, a new PF-127-CH hydrogel containing cephalexin NPs was developed as a topical antibacterial delivery system. By embedding polymeric NPs into the heat-sensitive hydrogel, the authors achieved improved tissue targeting, reduced burst release, and a controlled drug release rate. In this study, Salatin et al. used CH, known for its antibacterial and bioadhesive properties. The resulting heat-sensitive and bioadhesive cephalexin nanohydrogel shows great potential as a topical antibacterial delivery system that can not only reduce therapy costs, but also minimize antibiotic-associated adverse effects [247].

The controlled release of drugs is achievable using photo-responsive materials in drug delivery. 3D-printed hydrogel/PCL core/shell fiber scaffolds were produced to show NIR-triggered drug release for cancer therapy and wound healing. Gel/PCL/PDA scaffolds were prepared by firstly 3D-printing core scaffolds, then dipping them in PCL solution, and finally coating them with PDA. The 30% PCL-coated ALG–gelatin hydrogels had a tensile strength and Young's modulus of  $253 \pm 51.1 \text{ KPa}$  and  $2.98 \pm 0.2 \text{ MPa}$ , respectively. Compared to uncoated gel scaffolds, the PCL coating increased tensile strength and modulus by 4–6 times, although PDA (Polydopamine) coating did not alter mechanical properties since the scaffold thickness was only 50 nm. The 3D-printed Gel/PCL/PDA scaffolds showed a fast degradation rate, and only 15% of weight remained after 28 days of incubation. To assess drug release *in vivo*, doxorubicin-loaded scaffolds were placed hypodermically into the wound areas of mice. *In vivo* photothermal effect evaluation revealed that Gel/PCL/PDA scaffolds reached  $55 \text{ }^\circ\text{C}$  after NIR laser irradiation ( $0.5 \text{ W/cm}^2$ ) for 3 min, while the Gel/PCL scaffold reached  $42 \text{ }^\circ\text{C}$ , confirming the good photothermal conversion capability of PDA coated scaffolds. *In vivo* drug release tests showed that Gel/PCL/PDA scaffolds' doxorubicin loading efficiency was  $80.0 \pm 2.9\%$ ; most of the drugs were still preserved. According to wound healing assays, Gel/PCL/PDA scaffold-treated wounds contained more blood vessels and hair follicles than control and PCL samples, and cytotoxicity analysis showed no adverse effects on mice [15].

Another study introduced 3D-printable ink for treating diabetic wounds, including citric acid and sodium CMC solution (Figure 3A) [248]. The ink was printed in a cylindrical shape and then freeze-dried for 24 h at  $-80\text{ }^{\circ}\text{C}$  (Figure 3A) [248]. The dried structure was then crosslinked by thermal treatment at  $120\text{ }^{\circ}\text{C}$  for 7 min. The printed CMC scaffold was incubated with platelet-rich plasma (PRP) for 2 h at  $22\text{ }^{\circ}\text{C}$ . SEM analysis demonstrated that a sponge-like structure was obtained due to the homogeneously dispersed microporous structure of the scaffold. After 2 h of soaking in water, the swelling rates of platelet-rich plasma and 0.9% NaCl were 40% and 15%, respectively. The swelling test achieved 17.5% and 55.2% weight loss in the NaCl solution after 2 and 24 h, respectively (Figure 3(A3–A5)) [248]. The growth factor releases of the structure prepared in NaCl solution was investigated. In the first 6 h, burst release was observed. After 72 h of incubation, the total protein release was  $232\text{ }\mu\text{g}$  per mg scaffold. On the seventh day, the dressing had completely disintegrated, so all content was assumed to have been released. It was reported that the wound closures in cell experiments were almost at their maximum values at 24 h. To evaluate *in vivo* wound healing, healthy rats were injected with streptozotocin to promote diabetes. Later, full-thickness wounds were incised on rats and scaffolds were applied accordingly. The *in vivo* wound healing experiments revealed that control, CMC and CMC-PRP scaffolds had a wound closure rate of 35.8%, 44.1% and 50.2% after 3 days, respectively. After 7 days, the healing rates of the treated wounds were less than 50%, while the CMC and CMC-PRP scaffolds were 58.0% and 62.8%, respectively (Figure 3(A1,A2)) [248]. As a result of the experiments, the CMC-PRP material exhibited the best performance, with a wound healing rate of 88.6%.

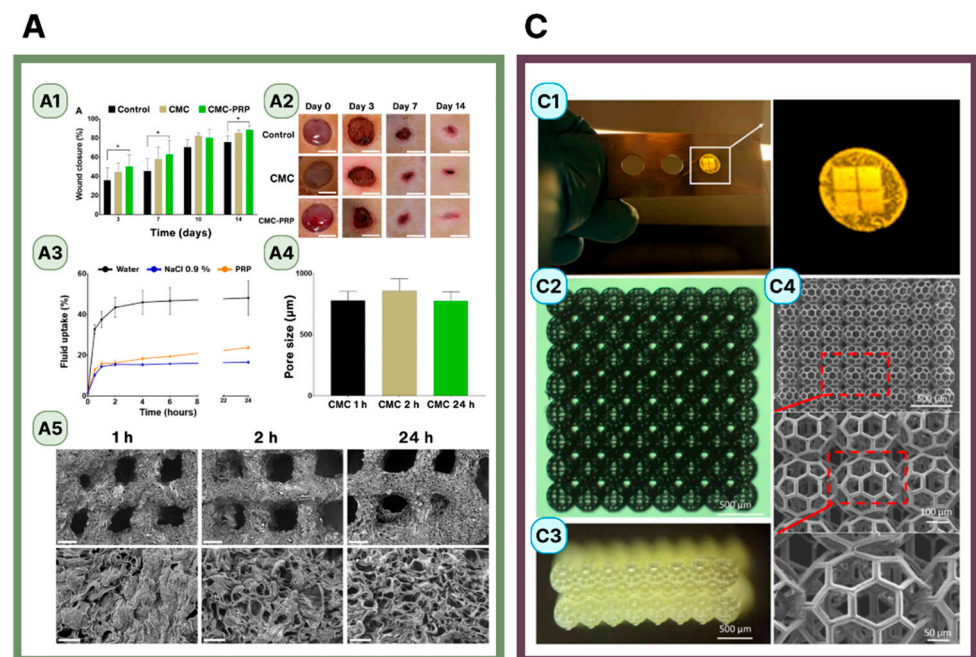
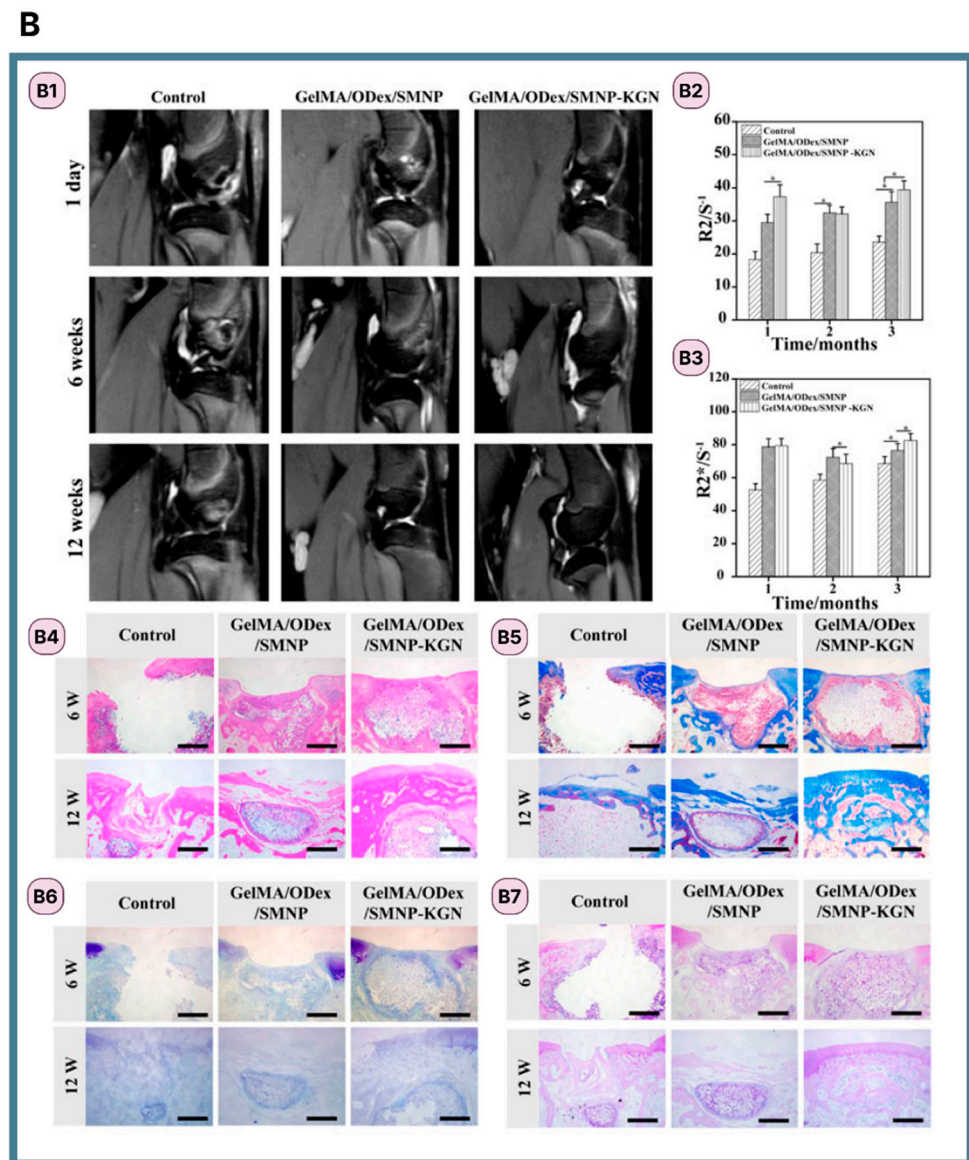


Figure 3. Cont.



**Figure 3.** (A) The effect of 3D-printed carboxymethyl cellulose scaffolds for autologous growth factors' delivery in a wound healing application. Reproduced/adapted with permission from Ref. [248] (B) In situ cartilage regeneration monitoring by MRI with the help of GelMA-based hydrogel-loaded kartogenin. Reproduced/adapted with permission from Ref. [249]. (C) 3D-printed large-scale and highly porous biodegradable tissue engineering scaffolds from poly(trimethylene-carbonate). Reproduced/adapted with permission from Ref. [250]. 3D-printed large-scale and highly porous biodegradable tissue engineering scaffolds from poly(trimethylene-carbonate). (A1) Graph representing the wound healing efficiency after 3, 7, 10 and 14 days of wound formation, Tukey's honestly significant difference test (HSD) and one-way analysis of variance (ANOVA) were conducted for evaluation and comparison of the data ((\*) for  $p < 0.05$ , ( $n = 7$ )); and (A2) a representative image of wound healing in treated and untreated groups. Images taken on day 0 indicate fresh wounds that have not been treated with scaffolds. The scaffolds remained transparent on day three. (A3) Swelling kinetic plot for CMC scaffolds when incubated in water, NaCl 0.9% or PRP for 24 h. (A4) The graph illustrates the pore size changes after incubation in NaCl 0.9%  $w/v$  for 1, 2 or 24 h. (A5) SEM images of freeze-dried CMC scaffolds after incubation with the same incubation times.

(B1) T2-weighted MR image of articular cartilage, (B2) R2/S-1 (One-way ANOVA test was performed to obtain significance analysis (\*) for  $p < 0.05$ ) and (B3) R2\*/S-1 value derived from MR imaging (\*) for  $p < 0.05$ ). (B4) H&E, (B5) Masson, (B6) toluidine (B7) PAS staining images of in vivo cartilage regeneration at 6 and 12 weeks. (C1) Illustration for in vivo printing and photo-crosslinking of GelMA precursor enriched with VEGF. (C2) Photograph of portable printers and their components. (C3) Photograph of hydrogel scaffold printed during the process, flow rate versus percentage of maximum speed range and diameter versus printing speed of bioink graph of resultant material. (C4) SEM images of hydrogel scaffold.

Then, highly complex structures consisting of two-layer 3D-bioprinted hydrogel-based dressing were proposed for the treatment of diabetic wounds [251]. The first layer formed from the 3D bioprinting strip of 2-(acryloyloxy) ethyl Trimethylammonium chloride (Bio-IL) and GelMA. The second layer was 3D-printed on a doxycycline hydrochloride-loaded (DOXH) and ROS-degradable polyurethane nanofibrous membrane. UV irradiation was applied to final dressings to activate immunomodulation and electroconductivity features. The dressing promoted the migration of endothelial cells and the polarization of macrophages to the anti-inflammatory phenotype (M2) in vitro. Rats were injected with streptozotocin to induce diabetes, and then full-thickness wounds were created on their bodies. Then, the scaffolds were applied to the wounds to assess their efficacy in promoting in vivo wound healing. As a result of this test, the combination of conductivity and DOXH was most effective in accelerating wound healing, collagen deposition, revascularization, and re-epithelialization. This combination reduced ROS and inflammatory factor levels and increased the ratio of M2 macrophages.

To prevent melanoma recurrence after surgical operation, a hybrid hydrogel scaffold with a mixture of sodium ALG, gellan gum and polydopamine NPs was manufactured. The printed hybrid hydrogel scaffold displayed good mechanical strength and biocompatibility. Polydopamine NPs provided a decent photothermal effect to the scaffold. They can also provide photothermal chemotherapy by coating it with a heat-sensitive gelatin hydrogel loaded with doxorubicin. Consequently, this method can accelerate drug release, suppress tumor cell proliferation, and recurrence after surgical resection. Due to the porous structure of the hydrogel scaffolds, HUVEC can increase proliferation and migration as well as tissue growth. Thus, it supports post-operative wound healing [252].

To inhibit the irregular remodeling of ECM that causes scar tissue to form in the wound healing process, another team prepared a polyvinylidene fluoride/sodium ALG piezoelectric hydrogel scaffold involving modified zinc oxide NPs with 3D printing technology [253]. The scaffold has dual piezoelectric response patterns, mainly comprising vertical swelling and horizontal friction. It can be used to simulate and amplify endogenous bioelectricity to promote wound healing and prevent wound formation. Ultimately, the proposed dual piezoelectric response models provided a novel solution to accelerate the wound healing process, prevent scarring, and expand the application of piezoelectric materials in wound dressings.

Recently, Bergonzi et al. examined active dressing: a hydrogel-based 3D printing dressing consisting of CH/ALG for wound healing [77]. A freeze deposition 3D printing method was used to fabricate CH/ALG hydrogels with modifiable thickness and interconnected pore structures. The printed hydrogels were further crosslinked to enhance their mechanical properties and stability. The ALG hydrogels were loaded with 0.75% *w/v* silver sulfadiazine (SSD), a drug model typically used for the treatment of infected burn wounds. Four alternative 3D CH/ALG structures were constructed to regulate the release of the indicated active molecule. The water content, flexibility, and porosity of the CH/ALG structures were remarkable. The Young's modulus of ALG and CH hydrogels was  $0.582 \pm 0.019$  MPa and  $0.365 \pm 0.015$  MPa, respectively. The water content in ALG was 93.18% and 0.88%, while the water content in CH was 92.76% and 1.17%. ALG and CH/ALG constructs were positioned with the surface of the CH facing the membrane in the donor chamber of the Franz cell. The receptor chamber was filled with simulated wound fluid and samples were taken at 5, 10, 30, 60, 180, and 300 min. When in vitro SSD

release studies were performed using vertical diffusion Franz cells, statistically significant differences were detected in the amount and in the kinetics of released drugs as a function of structure. Furthermore, depending on the structure, this experiment demonstrated a strong antimicrobial effect against *Staphylococcus aureus* and *Pseudomonas aeruginosa*, providing proof of concept that 3D printing techniques can be efficiently applied to the production of hydrogels for controlled drug delivery.

### 5.2. Imaging (MRI, PET, etc.)

In tissue engineering, the 3D manufacturing processes of modeled body tissues and organs start primarily with acquiring sliced anatomical images via modalities in the radiology department, such as MRI, CT, etc. Like artificial organs and tissues, 3D hydrogel scaffolds designed for wound healing can also easily be produced using imaging modalities and computer-aided design software programs [254]. SEM images allow the analysis of the cross-sectional morphologies of 3D-printed hydrogels [130,255–259].

Since manufactured hydrogel models contain an abundance of water molecules, they present an excellent high signal-to-noise ratio (SNR) for MRI based on the magnetic precession of hydrogen atoms in tissues. MRI also provides for the easy characterization of hydrogel-based wound dressings through its non-invasive, high spatial resolution, multi-planar, and ionizing radiation-free imaging characteristics. The chemical structure and physical properties of hydrogels (including distribution of materials, pore size, stiffness, water diffusion, and gelation process of different compositions) can be analyzed in detail during the manufacturing process under MRI [249,260–264]. Moreover, the level of skin reconstruction and wound healing can also be tracked and assessed in terms of the spatial distribution of the surviving transplanted cells on a hydrogel matrix, acute and chronic inflammation, or epidermal and dermal formation using MRI and fluorescence microscopy images [262,263]. For instance, Zhang et al. prepared a kartogenin (KGN) and gelatin-/dextran-based hydrogel for regenerating cartilage defects, and combined this with Fe-chelated synthetic melanin nanoparticles for monitoring the hydrogel state and regenerated cartilage in real time under MRI (Figure 3(B1–B7)) [249].

On the other hand, chemical exchange saturation transfer (CEST) can eliminate the disadvantages of MRI for visualizing solute protons and molecules into water. CEST is a type of molecular magnetic resonance imaging (MRI) method originating from the fast exchange rate of saturated solute protons or molecules through water using selective radio frequency (RF) pulses. Therefore, many recent studies benefit from the enhanced sensitivity property of CEST imaging when monitoring liposomal hydrogels with different concentrations, as well as to evaluate hydrogel degradation and drug release with varied materials [265–274].

### 5.3. Tissue Engineering

In tissue engineering, the 3D-printing of scaffolds has enabled researchers to combine different materials with desired shapes and characteristics for the treatment of various complications. For example, Palcone et al. created a keratin-based hydrogel scaffold by formulating a photo-crosslinkable resin involving riboflavin-sodium persulfate-hydroquinone (initiator-catalyst-inhibitor) solution [275]. They applied it in a DLP 3D printer to study for tissue engineering and regenerative medicine applications. The scaffold's compressive modulus was in the range of 5.49–15.45 kPa, between the 4 and 6% keratin hydrogels. An in vitro cytotoxicity assay was conducted by placing the scaffolds directly on top of the wells seeded with L929 mouse fibroblast cells. Under direct exposure to keratin, the metabolic activity of the cell was maintained at  $96.3 \pm 28.8\%$ . Consequently, the study showed that a keratin-based printing resin and printing methodology have minimal cytotoxicity. Further, the fabricated hydrogels behave no differently from other keratin-based constructions and commercially available non-cytotoxic substances, with decent printing resolution, adequate mechanical properties, uptake, and swelling capacities.

A subsequent investigation was conducted to determine the biological properties and the use of photosensitive GelMA hydrogel solutions for tissue engineering applications. GelMA hydrogel was fabricated using a 780 nm femtosecond laser by mixing GelMA hydrogel with a VA-086 photoinitiator and Rose Bengal photosensitizer in a solution. For both HPF-1 human lung fibroblasts for the cytotoxicity assay and CCC-ESF-1 human skin fibroblasts for the cell attachment assay, cells were seeded in well plates and afterwards scaffolds were placed in the wells. The photosensitive gel-hydrogel solution produced by TPP technology was utilized to obtain solutions with 66.3% cell viability suitable for cell binding. Further, a micro/nano 3D-printed scaffold with superior biocompatibility was produced using a photosensitive GelMA hydrogel solution. The production of scaffolds by TPP technology was performed at 150 m per second, at a power of 7.8 mW, with a layer distance of 150 nanometers, and at a concentration of 12% [276].

Another line of research successfully 3D-printed an artificial skin structure containing hair follicles, epidermis and dermis using gelatin GelMA/hyaluronic acid methacryloyl (HAMA) hydrogels as the bioink. A DLP printer was used to 3D-print papillary molds, and an extrusion-based bioprinter was used to 3D-print skin equivalents. A micropored culture dish was then used to mature the skin equivalents. The average pore sizes of GelMA/HAMA hydrogels were  $118.40 \pm 12.32 \mu\text{m}$ . Mechanical tests revealed  $59.02 \pm 22.96 \text{ kPa}$  compressive stress and a Young's modulus of  $15.72 \pm 3.9 \text{ kPa}$  on average. Further, cytotoxicity assays displayed that 99.6% of the cells were alive. The papillary layer was able to support epidermis-dermis interaction, and to promote the growth of laden cells. Ultimately, these findings suggest that GelMA/HAMA hydrogels can be utilized in tissue engineering as therapeutic scaffolds [277].

Moreover, the formulation of a specialized photosensitive, biodegradable, and biocompatible resin, based on a three-armed methacrylated poly(trimethylene-carbonate) (PTMC-MA) and its printability in 3D bioprinting, have been examined and tested for their biocompatibility (Figure 3(C1)). PTMC-MA macromer was synthesized by polymerizing TMC and then reacting the resulting PTMC oligomer with MA. Afterwards, a PTMC resin was prepared by dissolving PTMC-MA in tetrahydrofuran (THF), adding a photoinitiator, and evaporating the THF. To remove the air bubbles, the solution was placed in a vacuum before dividing into sample holders and the bioink was heated to  $50 \text{ }^\circ\text{C}$  before printing. The volume of PTMC-MA-based wound dressing was significantly increased with a large size of  $18 \times 18 \times 0.9 \text{ mm}$ , a volume of  $292 \text{ mm}^3$  and 96% porosity when a low magnification objective was used ( $\times 10$ , numerical aperture was 0.4) and rapidly written ( $1000 \text{ mm s}^{-1}$ ) during the TPP bioprinting process (Figure 3(C2–C4)). Before the cell viability assay, 3D-printed scaffolds were sterilized in 70% ethanol and incubated in DMEM-fetal bovine serum (FBS) solution for 24 h. Subsequently, human adipose-derived mesenchymal stem cells were seeded on the top of scaffolds in agarose-coated well plates separately. As a result, the PTMC-MA-based dressing showed excellent cell compatibility, which supports the attachment, proliferation, and differentiation of human adipose-derived mesenchymal stem cells into osteogenic and chondrogenic lineages [250].

#### 5.4. Others

In addition to the above-mentioned application areas, a synergistic approach involving combining different techniques could accelerate wound healing. For instance, AI can monitor a wound under a multifunctional hydrogel. Not only do the hydrogel-based dressings have antibacterial, hemostatic, and adhesive properties that effectively promote wound healing, but also, AI can monitor the wound condition in real-time.

The entire intelligent wound monitoring process basically consists of three parts: wound recognition, real-time condition monitoring, and personalized wound management. The customized hydrogel wound dressing can precisely match the contours of the wound for precision treatment. In addition, the personalized wound management model can use convolutional neural network (CNN) machine learning algorithms to analyze and evaluate wound healing and infection status through the colorimetric signal of the hydrogel wrap.

Machine learning has a high accuracy rate of 94.47%. Integrating precision treatment, real-time monitoring and personalized management for intelligent wound monitoring, this multifunctional hydrogel wound cover provides an advanced solution to accelerate wound healing and reduce bacterial infections. It shall play a vital step in intelligent wound management in the future [278].

## 6. Adaptability of 3D Bioprinting to Industry

### 6.1. Sustainability

Three-dimensional bioprinting enables the recycling and repurposing of materials. Renewable resources play a pivotal role in advancing environmental sustainability. Derived from these resources, sustainable materials demonstrate commendably low carbon footprints and energy consumption. Biopolymers assume a critical function in establishing a nexus between renewable reservoirs and biomaterials; thereby these materials contribute significantly to the sustainability of 3D bioprinting by offering environmentally responsible production opportunities [279].

The materials of 3D-bioprinted hydrogel dressings are effective and smart biomaterials that can be made from natural (such as collagen, ALG, and gelatin) or synthetic (like synthetic fibers, peptides, and elastomers) materials. Although hydrogels of natural origin offer advantages such as easy recognition of cellular growth factors and biomolecules, as well as their natural degradation by the body, synthetic hydrogels are more popularly used in 3D bioprinting due to their improved mechanical properties, biocompatibility, and having less batch-to-batch variation [280].

Hydrogels have gained significant prominence within the realm of tissue engineering due to their inherent biocompatibility, a property that fosters and enhances cellular differentiation and proliferation. In contrast, traditional 3D printing frameworks exploit the utilization of established hydrogel-based scaffold materials such as ALG, GelMA, and ultra-short peptides. This strategic utilization enables the fabrication of softer and more delicate tissue, or even harder tissue structures [281–284]. These key features define hydrogels as intelligent biomaterials that provide suitable microenvironments for a plethora of cells that require specialized culture media such as neurons, chondrocytes, osteoblasts, and stem cells.

### 6.2. Scaling Up

Therapeutic products require approval from regulatory authorities such as Australia's Therapeutic Goods Administrative (TGA) agency, the FDA of the United States and the European Medicines Agency (EMA) to ensure superior quality, safety and efficacy. Using products without these authorities' approval or a license can cause serious life-threatening hazards. Even though 3D bioprinting technology has been extensively researched in recent years, this technology is still not fully developed as a result of several challenges and limitations, including finding a suitable material and appropriate crosslinking mode suitable for wounds in terms of physical, mechanical, and biological requirements, as well as difficulties creating a microvascular network in wound dressings during 3D bioprinting to supply nutrition to the wound area [285].

The production of manipulated bioprinting products must comply with Good Manufacturing Practice (cGMP) standards and include sterility assurance levels for microbiological evaluation. Achieving a market-ready, clinically tested and ethically approved product is a long and labor-intensive process that involves high initial capital costs. These high initial capital costs can make the commercialization of expensive bioprinting products difficult due to process complexity and stringent regulations. However, it is necessary to assess the cost of such bioprinting products not only in terms of cost per unit of production, but also indirectly, by considering factors such as the overall reduction in hospital costs, length of stay and number of reconstructive surgeries after major burns. In the early stages of treatment, until basic standards of care are reached, experienced and highly trained healthcare teams are needed in clinics. Therefore, the scaling-up of wound dressing is not

solely determined by the technology itself, but also by the awareness and flexibility of the sectors [286–288].

### 6.3. Lifespan and Durability

Three-dimensional-bioprinted dressings are highly versatile and can be customized to suit wound needs. Nevertheless, traditional dressings are often composed and structured in a manner that may not always correspond exactly to the wound's requirements. Using bioprinting, the dressing's composition, structure and mechanical properties can be precisely controlled. Due to the technologies' flexibility in using different types of materials individually and together as bioink, dressings can be designed that are tailored to specific wound types and stages of healing. An additional important function of dressings is to adapt to the dynamic environment of a healing wound through their mechanical and physical durability. Creating an effective wound dressing requires the synchronization of the degradation of the dressing with the growth of new tissue. For instance, the hydrogels specifically chosen for application in wound healing models must maintain their structure for a minimum of 14 days before being applied in vivo [289]. Along with the degradation, the mechanical forces generated by daily body movements can disrupt the integrity of the hydrogel mesh structure, which can reduce the therapeutic effect of the hydrogel. Despite this, hydrogel materials with self-healing abilities can maintain structural and functional integrity in a different manner than traditional dressings. When the network structure is disrupted, self-healing hydrogels can extend the lifespan of bioprinting products and improve safety compared to conventional wound dressings [289–291].

### 6.4. Mass-Production

The most important factors limiting the use of 3D printing are high material costs and technological limitations. In addition, factors such as the lack of precision, color and surface quality of the print make this technology limited to special cases. However, despite these limitations, the existing literature has enumerated several economic benefits of 3D printing. While 3D printing technology reduces device requirements by making the manufacturing stage more accessible, it is also mentioned in the literature that energy use can be lower for complex parts [292–295].

This technology also offers the possibility to create new supply chains for the development of innovative products. Configurations that are difficult or impossible with traditional manufacturing methods become realizable with 3D printing. Moreover, 3D printing transforms the competition for quality, making the quality of the final product dependent not on the manufacturing process, but on the perspective of the computer-based CAD file [292,293].

Compared to traditional manufacturing methods, 3D printing reorganizes economies of scale and scope, while shortening lead times through instantaneous production. This approach further decentralizes production activities and reduces supply chain times. In this framework, the constraints and economic advantages of 3D printing technology come together to transform production processes, while the commoditization of production infrastructure contributes to the emergence of a broader ecosystem and increased flexibility in production [296,297].

During the COVID-19 pandemic, the market size of additive manufacturing (AM) within the healthcare sector reached an estimated USD 1.45 billion in 2021 [298]. It is projected that the economic growth of 3D-printed medical models and devices in the healthcare market will reach USD 6.25 billion by 2032 [299]. Given the significant interest in biopolymers for AM, it becomes essential to emphasize recent advancements and the role of environmentally sustainable biomaterials in advanced healthcare systems [300].

## 7. Conclusions and Future Directions

Wound healing is a complex process that depends on the synergistic interplay of many factors and intricate signaling pathways. Recently, hydrogel-based wound dressings have

emerged as promising candidates, providing the following benefits: establishing a proper environment for wound healing and expediting the healing process. The ability to fabricate intricate constructs incorporating living cells, therapeutic agents, and customized hydrogels enables bioprinting to fit perfectly into patient-specific needs. As a result of recent improvements in hydrogel-based dressings and the maturation of 3D bioprinting procedures, several studies have demonstrated that these innovations can be utilized to enhance wound closure, re-epithelialization, and angiogenesis, while avoiding cytotoxicity concerns.

Recent advances in 3D printing technology have concentrated on developing customized 3D printer configurations that are meticulously calibrated to meet the unique needs of individual patients. As a result of these technological advances, a variety of innovative approaches have been developed, including sophisticated scanning systems, robotic mechanisms integrated into 3D bioprinting applications, the seamless integration of artificial intelligence paradigms, and the pioneering application of bioinks for in situ bioprinting, leading to accelerated wound healing processes. Bioprinting technologies possessing four, five, and six axes of motion point towards the possibility of the facile fabrication of intricate 3D structures, necessitating nuanced treatment options for wounds with a wide range of depths. The following factors must be addressed in order for 3D-bioprinted dressings to become practical in clinical settings in the near future:

- (i) During the 3D bioprinter design process, the priority should be to reduce the size of the device without compromising advanced features such as creating complex tissue architectures with cellular precision, so that an acceptable wound dressing can be developed and translated into a patient-friendly form;
- (ii) The role of specialists should be limited to controlling 3D printing parameters. Using artificial intelligence to regulate 3D bioprinting parameters would be a significant step towards precision and high-quality dressing production;
- (iii) It is difficult to develop personalized therapies in this field of research due to a lack of tissue availability, a high morbidity rate at harvest sites, as well as the extremely time-consuming extraction and culturing processes. Researchers have recently conducted studies on the design of bioreactors for the mass production of skin tissue components and their integration with 3D bioprinters, which may enable the production of 3D-bioprinted dressings with patient-specific bioinks in the future;
- (iv) In situ bioprinting plays an essential role in shaping 3D bioprinting's future within this broader context. A new technology, in situ bioprinting, involves the direct placement of viable cells and biomaterials onto wound sites, which facilitates the recovery of wounds even after severe injuries.

The future holds great promise, with wound healing, hydrogel dressings, and 3D bioprinting converging to redefine wound care paradigms, resulting in personalized, effective, and efficient wound care.

**Author Contributions:** Conceptualization, E.B. (Engin Baysoy) G.K.-C. and B.A.; writing—original draft preparation, E.B. (Emirhan Bayrak), S.B.B., F.A. and E.U.; writing—review and editing, E.B. (Engin Baysoy), G.K.-C. and B.A.; visualization, E.B. (Emirhan Bayrak) and G.K.-C.; supervision, E.B. (Engin Baysoy), G.K.-C. and B.A. All authors have read and agreed to the published version of the manuscript.

**Funding:** Engin Baysoy acknowledges the funding from the Scientific and Technological Research Council of Turkey (2219-1059B192100591).

**Institutional Review Board Statement:** Not applicable.

**Informed Consent Statement:** Not applicable.

**Data Availability Statement:** Not applicable.

**Conflicts of Interest:** The authors declare no conflict of interest.

## References

1. Pasparakis, M.; Haase, I.; Nestle, F.O. Mechanisms regulating skin immunity and inflammation. *Nat. Rev. Immunol.* **2014**, *14*, 289–301. [[CrossRef](#)]
2. Pereira, R.F.; Sousa, A.; Barrias, C.C.; Bayat, A.; Granja, P.L.; Bártolo, P.J. Advances in bioprinted cell-laden hydrogels for skin tissue engineering. *Biomanufacturing Rev.* **2017**, *2*, 1. [[CrossRef](#)]
3. Proksch, E.; Brandner, J.M.; Jensen, J.-M. The skin: An indispensable barrier. *Exp. Dermatol.* **2008**, *17*, 1063–1072. [[CrossRef](#)]
4. Ud-Din, S.; Volk, S.W.; Bayat, A. Regenerative healing, scar-free healing and scar formation across the species: Current concepts and future perspectives. *Exp. Dermatol.* **2014**, *23*, 615–619. [[CrossRef](#)] [[PubMed](#)]
5. Delavary, B.M.; van der Veer, W.M.; van Egmond, M.; Niessen, F.B.; Beelen, R.H.J. Macrophages in skin injury and repair. *Immunobiology* **2011**, *216*, 753–762. [[CrossRef](#)] [[PubMed](#)]
6. Sidgwick, G.P.; Bayat, A. Extracellular matrix molecules implicated in hypertrophic and keloid scarring. *J. Eur. Acad. Dermatol. Venereol.* **2012**, *26*, 141–152. [[CrossRef](#)]
7. Guo, S.; DiPietro, L.A. Factors Affecting Wound Healing. *J. Dent. Res.* **2010**, *89*, 219–229. [[CrossRef](#)]
8. Dhivya, S.; Padma, V.V.; Santhini, E. Wound dressings—A review. *Biomedicine* **2015**, *5*, 22. [[CrossRef](#)]
9. Asadi, N.; Pazoki-Toroudi, H.; Del Bakhshayesh, A.R.; Akbarzadeh, A.; Davaran, S.; Annabi, N. Multifunctional hydrogels for wound healing: Special focus on biomacromolecular based hydrogels. *Int. J. Biol. Macromol.* **2021**, *170*, 728–750. [[CrossRef](#)]
10. Chen, G.; Yu, Y.; Wu, X.; Wang, G.; Ren, J.; Zhao, Y. Bioinspired Multifunctional Hybrid Hydrogel Promotes Wound Healing. *Adv. Funct. Mater.* **2018**, *28*, 1801386. [[CrossRef](#)]
11. Liang, Y.; He, J.; Guo, B. Functional Hydrogels as Wound Dressing to Enhance Wound Healing. *ACS Nano* **2021**, *15*, 12687–12722. [[CrossRef](#)] [[PubMed](#)]
12. Xiang, J.; Shen, L.; Hong, Y. Status and future scope of hydrogels in wound healing: Synthesis, materials and evaluation. *Eur. Polym. J.* **2020**, *130*, 109609. [[CrossRef](#)]
13. Dalisson, B.; Barralet, J. Bioinorganics and Wound Healing. *Adv. Healthc. Mater.* **2019**, *8*, 1900764. [[CrossRef](#)] [[PubMed](#)]
14. Brumberg, V.; Astrelina, T.; Malivanova, T.; Samoilov, A. Modern Wound Dressings: Hydrogel Dressings. *Biomedicines* **2021**, *9*, 1235. [[CrossRef](#)]
15. Liu, C.; Wang, Z.; Wei, X.; Chen, B.; Luo, Y. 3D printed hydrogel/PCL core/shell fiber scaffolds with NIR-triggered drug release for cancer therapy and wound healing. *Acta Biomater.* **2021**, *131*, 314–325. [[CrossRef](#)]
16. Tsegay, F.; Elsherif, M.; Butt, H. Smart 3D Printed Hydrogel Skin Wound Bandages: A Review. *Polymers* **2022**, *14*, 1012. [[CrossRef](#)]
17. MacDonald, E.; Wicker, R. Multiprocess 3D printing for increasing component functionality. *Science* **2016**, *353*, aaf2093. [[CrossRef](#)]
18. Ho, C.M.B.; Ng, S.H.; Yoon, Y.-J. A review on 3D printed bioimplants. *Int. J. Precis. Eng. Manuf.* **2015**, *16*, 1035–1046. [[CrossRef](#)]
19. Webb, P.A. A review of rapid prototyping (RP) techniques in the medical and biomedical sector. *J. Med. Eng. Technol.* **2000**, *24*, 149–153. [[CrossRef](#)]
20. Gilaberte, Y.; Prieto-Torres, L.; Pastushenko, I.; Juarranz, A. Anatomy and Function of the Skin. In *Nanoscience in Dermatology*; Academic Press: Cambridge, MA, USA, 2016; pp. 1–14. [[CrossRef](#)]
21. Groves, R.B. Quantifying the Mechanical Properties of Skin In Vivo and Ex Vivo to Optimize Microneedle Device Design. Ph.D. Thesis, Institute of Medical Engineering & Medical Physics School of Engineering, Cardiff, UK, 2012.
22. Fuchs, E.; Raghavan, S. Getting under the skin of epidermal morphogenesis. *Nat. Rev. Genet.* **2002**, *3*, 199–209. [[CrossRef](#)]
23. Gallagher, A.J.; Ni Annadh, A.; Bruyere, K.; Otténio, M.; Xie, H.; Gilchrist, M.D. Dynamic tensile properties of human skin. In Proceedings of the IRCOBI Conference (International Research Council on the Biomechanics of Injury), Dublin, Ireland, 12–14 September 2012; Volume 59.
24. Grice, E.A.; Segre, J.A. The skin microbiome. *Nat. Rev. Microbiol.* **2011**, *9*, 244–253. [[CrossRef](#)] [[PubMed](#)]
25. Wong, R.; Geyer, S.; Weninger, W.; Guimberteau, J.-C.; Wong, J.K. The dynamic anatomy and patterning of skin. *Exp. Dermatol.* **2016**, *25*, 92–98. [[CrossRef](#)] [[PubMed](#)]
26. Betts, J.G.; Young, K.A.; Wise, J.A.; Johnson, E.; Poe, B.; Kruse, D.H.; Korol, O.; Johnson, J.E.; Womble, M.; DeSaix, P. *Anatomy & Physiology*; OpenStax College, Rice University: Houston, TX, USA, 2013.
27. Joodaki, H.; Panzer, M.B. Skin mechanical properties and modeling: A review. *Proc. Inst. Mech. Eng. Part H J. Eng. Med.* **2018**, *232*, 323–343. [[CrossRef](#)] [[PubMed](#)]
28. Kalra, A.; Lowe, A.; Al-Jumaily, A.M. Mechanical behaviour of skin: A review. *J. Mater. Sci. Eng.* **2016**, *5*, 1000254. [[CrossRef](#)]
29. Fjeldborg, K.; Pedersen, S.B.; Møller, H.J.; Christiansen, T.; Bennetzen, M.; Richelsen, B. Human Adipose Tissue Macrophages Are Enhanced but Changed to an Anti-Inflammatory Profile in Obesity. *J. Immunol. Res.* **2014**, *2014*, 309548. [[CrossRef](#)]
30. Guimberteau, J.C.; Delage, J.P.; McGrouther, D.A.; Wong, J.K.F. The microvacuolar system: How connective tissue sliding works. *J. Hand Surg.* **2010**, *35*, 614–622. [[CrossRef](#)]
31. Lee, S.D.; Tontonoz, P. Eosinophils in Fat: Pink Is the New Brown. *Cell* **2014**, *157*, 1249–1250. [[CrossRef](#)]
32. Nguyen, K.D.; Qiu, Y.; Cui, X.; Sharon Goh, Y.P.; Mwangi, J.; David, T.; Mukundan, L.; Brombacher, F.; Locksley, R.M.; Chawla, A. Alternatively activated macrophages produce catecholamines to sustain adaptive thermogenesis. *Nature* **2011**, *480*, 104–108. [[CrossRef](#)]
33. Stienstra, R.; Dijk, W.; van Beek, L.; Jansen, H.; Heemskerk, M.; Houtkooper, R.H.; Denis, S.; van Harmelen, V.; Willems van Dijk, K.; Tack, C.J.; et al. Mannose-Binding Lectin Is Required for the Effective Clearance of Apoptotic Cells by Adipose Tissue Macrophages During Obesity. *Diabetes* **2014**, *63*, 4143–4153. [[CrossRef](#)]

34. Raziyeva, K.; Kim, Y.; Zharkinbekov, Z.; Kassymbek, K.; Jimi, S.; Saparov, A. Immunology of Acute and Chronic Wound Healing. *Biomolecules* **2021**, *11*, 700. [[CrossRef](#)]
35. Nguyen, A.V.; Soulika, A.M. The Dynamics of the Skin's Immune System. *Int. J. Mol. Sci.* **2019**, *20*, 1811. [[CrossRef](#)] [[PubMed](#)]
36. Cañedo-Dorantes, L.; Cañedo-Ayala, M. Skin Acute Wound Healing: A Comprehensive Review. *Int. J. Inflamm.* **2019**, *2019*, 3706315. [[CrossRef](#)] [[PubMed](#)]
37. Garraud, O.; Hozzein, W.N.; Badr, G. Wound healing: Time to look for intelligent, 'natural' immunological approaches? *BMC Immunol.* **2017**, *18*, 23. [[CrossRef](#)]
38. Su, L.; Zheng, J.; Wang, Y.; Zhang, W.; Hu, D. Emerging progress on the mechanism and technology in wound repair. *Biomed. Pharmacother.* **2019**, *117*, 109191. [[CrossRef](#)] [[PubMed](#)]
39. Lucas, T.; Waisman, A.; Ranjan, R.; Roes, J.; Krieg, T.; Müller, W.; Roers, A.; Eming, S.A. Differential Roles of Macrophages in Diverse Phases of Skin Repair. *J. Immunol.* **2010**, *184*, 3964–3977. [[CrossRef](#)] [[PubMed](#)]
40. Zaidi, A.; Green, L. Physiology of haemostasis. *Anaesth. Intensive Care Med.* **2019**, *20*, 152–158. [[CrossRef](#)]
41. Wilkinson, H.N.; Hardman, M.J. Wound healing: Cellular mechanisms and pathological outcomes. *Open Biol.* **2020**, *10*, 200223. [[CrossRef](#)]
42. Anderson, K.; Hamm, R.L. Factors that impair wound healing. *J. Am. Coll. Clin. Wound Spec.* **2012**, *4*, 84–91. [[CrossRef](#)]
43. Schneider, L.A.; Korber, A.; Grabbe, S.; Dissemond, J. Influence of pH on wound-healing: A new perspective for wound-therapy? *Arch. Dermatol. Res.* **2007**, *298*, 413–420. [[CrossRef](#)]
44. Dong, R.; Guo, B. Smart wound dressings for wound healing. *Nano Today* **2021**, *41*, 101290. [[CrossRef](#)]
45. Li, R.; Liu, K.; Huang, X.; Li, D.; Ding, J.; Liu, B.; Chen, X. Bioactive materials promote wound healing through modulation of cell behaviors. *Adv. Sci.* **2022**, *9*, 2105152. [[CrossRef](#)] [[PubMed](#)]
46. Yamakawa, S.; Hayashida, K. Advances in surgical applications of growth factors for wound healing. *Burn. Trauma* **2019**, *7*, s41038-019. [[CrossRef](#)] [[PubMed](#)]
47. Edwards, J.V.; Yager, D.R.; Cohen, I.K.; Diegelman, R.F.; Montante, S.; Bertoniere, N.; Bopp, A.F. Modified cotton gauze dressings that selectively absorb neutrophil elastase activity in solution. *Wound Repair Regen.* **2001**, *9*, 50–58. [[CrossRef](#)]
48. Han, G.; Ceilley, R. Chronic Wound Healing: A Review of Current Management and Treatments. *Adv. Ther.* **2017**, *34*, 599–610. [[CrossRef](#)] [[PubMed](#)]
49. Pinho, E.; Soares, G. Functionalization of cotton cellulose for improved wound healing. *J. Mater. Chem. B* **2018**, *6*, 1887–1898. [[CrossRef](#)]
50. Shi, C.; Wang, C.; Liu, H.; Li, Q.; Li, R.; Zhang, Y.; Liu, Y.; Shao, Y.; Wang, J. Selection of Appropriate Wound Dressing for Various Wounds. *Front. Bioeng. Biotechnol.* **2020**, *8*, 182. [[CrossRef](#)]
51. Ahmed, E.M. Hydrogel: Preparation, characterization, and applications: A review. *J. Adv. Res.* **2015**, *6*, 105–121. [[CrossRef](#)]
52. Wichterle, O.; Lim, D. Hydrophilic Gels for Biological Use. *Nature* **1960**, *185*, 117–118. [[CrossRef](#)]
53. Li, J.; Mooney, D.J. Designing hydrogels for controlled drug delivery. *Nat. Rev. Mater.* **2016**, *1*, 16071. [[CrossRef](#)]
54. Drury, J.L.; Mooney, D.J. Hydrogels for tissue engineering: Scaffold design variables and applications. *Biomaterials* **2003**, *24*, 4337–4351. [[CrossRef](#)]
55. Peppas, N.A.; Langer, R. New Challenges in Biomaterials. *Science* **1994**, *263*, 1715–1720. [[CrossRef](#)]
56. Kawecki, M.; Labuś, W.; Klama-Baryla, A.; Kitala, D.; Kraut, M.; Glik, J.; Misiuga, M.; Nowak, M.; Bielecki, T.; Kasperczyk, A. A review of decellurization methods caused by an urgent need for quality control of cell-free extracellular matrix' scaffolds and their role in regenerative medicine. *J. Biomed. Mater. Res. B Appl. Biomater.* **2018**, *106*, 909–923. [[CrossRef](#)]
57. Madhumathi, K.; Shalumon, K.T.; Divya Rani, V.V.; Tamura, H.; Furuie, T.; Selvamurugan, N.; Nair, S.V.; Jayakumar, R. Wet chemical synthesis of chitosan hydrogel-hydroxyapatite composite membranes for tissue engineering applications. *Int. J. Biol. Macromol.* **2009**, *45*, 12–15. [[CrossRef](#)]
58. Ouyang, L.; Highley, C.B.; Sun, W.; Burdick, J.A. A Generalizable Strategy for the 3D Bioprinting of Hydrogels from Nonviscous Photo-crosslinkable Inks. *Adv. Mater.* **2017**, *29*, 1604983. [[CrossRef](#)]
59. Pilehvar-Soltanahmadi, Y.; Dadashpour, M.; Mohajeri, A.; Fattahi, A.; Sheervalilou, R.; Zarghami, N. An Overview on Application of Natural Substances Incorporated with Electrospun Nanofibrous Scaffolds to Development of Innovative Wound Dressings. *Mini-Rev. Med. Chem.* **2018**, *18*, 414–427. [[CrossRef](#)] [[PubMed](#)]
60. Lu, J.; Chen, Y.; Ding, M.; Fan, X.; Hu, J.; Chen, Y.; Li, J.; Li, Z.; Liu, W. A 4arm-PEG macromolecule crosslinked chitosan hydrogels as antibacterial wound dressing. *Carbohydr. Polym.* **2022**, *277*, 118871. [[CrossRef](#)] [[PubMed](#)]
61. Zhang, S.; Zhou, H.; Huang, C.; Sun, J.; Qu, X.; Lu, Y. A novel corneal adhesive based on functionally coupled PEG-lysozyme hydrogel for wound closure after surgical eye surgery. *Chin. Chem. Lett.* **2022**, *33*, 4321–4325. [[CrossRef](#)]
62. Cai, C.; Wang, T.; Han, X.; Yang, S.; Lai, C.; Yuan, T.; Feng, Z.; He, N. In situ wound sprayable double-network hydrogel: Preparation and characterization. *Chin. Chem. Lett.* **2022**, *33*, 1963–1969. [[CrossRef](#)]
63. Lu, J.; Fan, X.; Hu, J.; Li, J.; Rong, J.; Wang, W.; Chen, Y.; Liu, W.; Chen, J.; Chen, Y. Construction and function of robust and moist bilayer chitosan-based hydrogel wound dressing. *Mater. Des.* **2023**, *226*, 111604. [[CrossRef](#)]
64. Irmukhametova, G.S.; Mun, G.A.; Khutoryanskiy, V.V. Hydrogel dressings. In *Therapeutic Dressings and Wound Healing Applications*; John Wiley & Sons: Hoboken, NJ, USA, 2020; pp. 185–207. [[CrossRef](#)]
65. Tottoli, E.M.; Dorati, R.; Genta, I.; Chiesa, E.; Pisani, S.; Conti, B. Skin Wound Healing Process and New Emerging Technologies for Skin Wound Care and Regeneration. *Pharmaceutics* **2020**, *12*, 735. [[CrossRef](#)]

66. Singh, D.; Singh, D.; Han, S.S. 3D Printing of Scaffold for Cells Delivery: Advances in Skin Tissue Engineering. *Polymers* **2016**, *8*, 19. [[CrossRef](#)] [[PubMed](#)]
67. Sultan, S.; Siqueira, G.; Zimmermann, T.; Mathew, A.P. 3D printing of nano-cellulosic biomaterials for medical applications. *Curr. Opin. Biomed. Eng.* **2017**, *2*, 29–34. [[CrossRef](#)]
68. Habib, M.A.; Khoda, B. A Rheological Study of Bio-Ink: Shear Stress and Cell Viability. In *Volume 1: Additive Manufacturing; Advanced Materials Manufacturing; Biomanufacturing; Life Cycle Engineering; Manufacturing Equipment and Automation*; American Society of Mechanical Engineers: New York, NY, USA, 2021. [[CrossRef](#)]
69. West, J.L.; Hubbell, J.A. Polymeric biomaterials with degradation sites for proteases involved in cell migration. *Macromolecules* **1999**, *32*, 241–244. [[CrossRef](#)]
70. Murphy, S.V.; Atala, A. 3D bioprinting of tissues and organs. *Nat. Biotechnol.* **2014**, *32*, 773–785. [[CrossRef](#)]
71. O'Brien, F.J. Biomaterials & scaffolds for tissue engineering. *Mater. Today* **2011**, *14*, 88–95. [[CrossRef](#)]
72. Cui, R.; Zhang, L.; Ou, R.; Xu, Y.; Xu, L.; Zhan, X.Y.; Li, D. Polysaccharide-based hydrogels for wound dressing: Design considerations and clinical applications. *Front. Bioeng. Biotechnol.* **2022**, *10*, 845735. [[CrossRef](#)]
73. Broussard, K.C.; Powers, J.G. Wound dressings: Selecting the most appropriate type. *Am. J. Clin. Dermatol.* **2013**, *14*, 449–459. [[CrossRef](#)]
74. Hersel, U.; Dahmen, C.; Kessler, H. RGD modified polymers: Biomaterials for stimulated cell adhesion and beyond. *Biomater.* **2003**, *24*, 4385–4415. [[CrossRef](#)]
75. Ovsianikov, A.; Khademhosseini, A.; Mironov, V. The synergy of scaffold-based and scaffold-free tissue engineering strategies. *Trends Biotechnol.* **2018**, *36*, 348–357. [[CrossRef](#)]
76. Gao, G.; Hubbell, K.; Schilling, A.F.; Dai, G.; Cui, X. Bioprinting Cartilage Tissue from Mesenchymal Stem Cells and PEG Hydrogel. In *3D Cell Culture*; Humana Press: New York, NY, USA, 2017; pp. 391–398. [[CrossRef](#)]
77. Bergonzi, C.; Bianchera, A.; Remaggi, G.; Ossiprandi, M.C.; Bettini, R.; Elviri, L. 3D Printed Chitosan/Alginate Hydrogels for the Controlled Release of Silver Sulfadiazine in Wound Healing Applications: Design, Characterization and Antimicrobial Activity. *Micromachines.* **2023**, *14*, 137. [[CrossRef](#)]
78. Tran, N.-P.-D.; Yang, M.-C. Synthesis and Characterization of Silicone Contact Lenses Based on TRIS-DMA-NVP-HEMA Hydrogels. *Polymers* **2019**, *11*, 944. [[CrossRef](#)]
79. Ge, Q.; Chen, Z.; Cheng, J.; Zhang, B.; Zhang, Y.; Li, H.; He, X.; Yuan, C.; Liu, J.; Magdassi, S.; et al. 3D printing of highly stretchable hydrogel with diverse UV curable polymers. *Sci. Adv.* **2021**, *7*, eaba4261. [[CrossRef](#)] [[PubMed](#)]
80. Simsa, R.; Rothenbücher, T.; Gürbüz, H.; Ghosheh, N.; Emneus, J.; Jenndahl, L.; Kaplan, D.L.; Bergh, N.; Serrano, A.M.; Fogelstrand, P. Brain organoid formation on decellularized porcine brain ECM hydrogels. *PLoS ONE* **2021**, *16*, e0245685. [[CrossRef](#)] [[PubMed](#)]
81. Khoshnood, N.; Zamanian, A. A comprehensive review on scaffold-free bioinks for bioprinting. *Bioprinting.* **2020**, *19*, e00088. [[CrossRef](#)]
82. Ayan, B.; Celik, N.; Zhang, Z.; Zhou, K.; Kim, M.H.; Banerjee, D.; Wu, Y.; Costanzo, F.; Ozbolat, I.T. Aspiration-assisted freeform bioprinting of pre-fabricated tissue spheroids in a yield-stress gel. *Commun. Phys.* **2020**, *3*, 183. [[CrossRef](#)] [[PubMed](#)]
83. Ayan, B.; Wu, Y.; Karuppagounder, V.; Kamal, F.; Ozbolat, I.T. Aspiration-assisted bioprinting of the osteochondral interface. *Sci. Rep.* **2020**, *10*, 13148. [[CrossRef](#)]
84. Ayan, B. Aspiration-Assisted Bioprinting. Ph.D. Dissertation, Penn State University, University Park, PA, USA, 2020.
85. Ayan, B.; Heo, D.N.; Zhang, Z.; Dey, M.; Povilianskas, A.; Drapaca, C.; Ozbolat, I. Aspiration-assisted bioprinting for precise positioning of biologics. *Sci. Adv.* **2020**, *6*, eaaw5111. [[CrossRef](#)]
86. Jang, J.; Yi, H.-G.; Cho, D.-W. 3D Printed Tissue Models: Present and Future. *ACS Biomater. Sci. Eng.* **2016**, *2*, 1722–1731. [[CrossRef](#)]
87. Khalil, M.; Shariat-Panahi, A.; Tootle, R.; Ryder, T.; McCloskey, P.; Roberts, E.; Hodgson, H.; Selden, C. Human hepatocyte cell lines proliferating as cohesive spheroid colonies in alginate markedly upregulate both synthetic and detoxificatory liver function. *J. Hepatol.* **2001**, *34*, 68–77. [[CrossRef](#)]
88. Owens, C.M.; Marga, F.; Forgacs, G.; Heesch, C.M. Biofabrication and testing of a fully cellular nerve graft. *Biofabrication* **2013**, *5*, 045007. [[CrossRef](#)]
89. Wu, Y.; Ayan, B.; Moncal, K.K.; Kang, Y.; Dhawan, A.; Koduru, S.V.; Ravnic, D.J.; Kamal, F.; Ozbolat, I.T. Hybrid Bioprinting of Zonally Stratified Human Articular Cartilage Using Scaffold-Free Tissue Strands as Building Blocks. *Adv. Health Mater.* **2020**, *9*, 2001657. [[CrossRef](#)] [[PubMed](#)]
90. Schon, B.S.; Schrobback, K.; van der Ven, M.; Stroebel, S.; Hooper, G.J.; Woodfield, T.B.F. Validation of a high-throughput microtissue fabrication process for 3D assembly of tissue engineered cartilage constructs. *Cell Tissue Res.* **2012**, *347*, 629–642. [[CrossRef](#)] [[PubMed](#)]
91. de Oliveira, R.S.; Fantaus, S.S.; Guillot, A.J.; Melero, A.; Beck, R.C.R. 3D-Printed Products for Topical Skin Applications: From Personalized Dressings to Drug Delivery. *Pharmaceutics* **2021**, *13*, 1946. [[CrossRef](#)] [[PubMed](#)]
92. Shahrubudin, N.; Lee, T.C.; Ramlan, R. An Overview on 3D Printing Technology: Technological, Materials, and Applications. *Procedia Manuf.* **2019**, *35*, 1286–1296. [[CrossRef](#)]
93. Trenfield, S.J.; Awad, A.; Goyanes, A.; Gaisford, S.; Basit, A.W. 3D Printing Pharmaceuticals: Drug Development to Frontline Care. *Trends Pharmacol. Sci.* **2018**, *39*, 440–451. [[CrossRef](#)]

94. Trenfield, S.J.; Madla, C.M.; Basit, A.W.; Gaisford, S. The Shape of Things to Come: Emerging Applications of 3D Printing in Healthcare. In *3D Printing of Pharmaceuticals*; Springer: Cham, Switzerland, 2018; pp. 1–19. [CrossRef]
95. Soni, G.; Yadav, K.S. Nanogels as potential nanomedicine carrier for treatment of cancer: A mini review of the state of the art. *Saudi Pharm. J.* **2016**, *24*, 133–139. [CrossRef]
96. Cho, H.; Jammalamadaka, U.; Tappa, K. Nanogels for Pharmaceutical and Biomedical Applications and Their Fabrication Using 3D Printing Technologies. *Materials* **2018**, *11*, 302. [CrossRef]
97. He, P.; Zhao, J.; Zhang, J.; Li, B.; Gou, Z.; Gou, M.; Li, X. Bioprinting of skin constructs for wound healing. *Burn. Trauma* **2018**, *6*. [CrossRef]
98. Groll, J.; Burdick, J.A.; Cho, D.-W.; Derby, B.; Gelinsky, M.; Heilshorn, S.C.; Jüngst, T.; Malda, J.; Mironov, V.A.; Nakayam, K. A definition of bioinks and their distinction from biomaterial inks. *Biofabrication* **2018**, *11*, 013001. [CrossRef]
99. Gopinathan, J.; Noh, I. Recent trends in bioinks for 3D printing. *Biomater. Res.* **2018**, *22*, 11. [CrossRef]
100. Panwar, A.; Tan, L.P. Current Status of Bioinks for Micro-Extrusion-Based 3D Bioprinting. *Molecules* **2016**, *21*, 685. [CrossRef]
101. Billiet, T.; Vandenhaute, M.; Schelphout, J.; Van Vlierberghe, S.; Dubruel, P. A review of trends and limitations in hydrogel-rapid prototyping for tissue engineering. *Biomaterials* **2012**, *33*, 6020–6041. [CrossRef] [PubMed]
102. Bhargav, A.; Sanjairaj, V.; Rosa, V.; Feng, L.W.; Fuh, Y.H. Applications of additive manufacturing in dentistry: A review. *J. Biomed. Mater. Res. B Appl. Biomater.* **2018**, *106*, 2058–2064. [CrossRef] [PubMed]
103. Vashishtha, V.K.; Mehla, N. Advancement of Rapid Prototyping in Aerospace Industryda Review Water Generation from Atmospheric Air View Project Solar Tilt Angle Orientation View Project. 2011. Available online: <https://www.researchgate.net/publication/50984934> (accessed on 20 June 2023).
104. Han, T.; Kundu, S.; Nag, A.; Xu, Y. 3D Printed Sensors for Biomedical Applications: A Review. *Sensors* **2019**, *19*, 1706. [CrossRef] [PubMed]
105. Melchels, F.P.W.; Feijen, J.; Grijpma, D.W. A review on stereolithography and its applications in biomedical engineering. *Biomaterials* **2010**, *31*, 6121–6130. [CrossRef] [PubMed]
106. Beluze, L.; Bertsch, A.; Renaud, P. Microstereolithography: A new process to build complex 3D objects. In *Design, Test, and Microfabrication of MEMS and MOEMS*; Courtois, B., Crary, S.B., Ehrfeld, W., Fujita, H., Karam, J.M., Markus, K.W., Eds.; SPIE: Bellingham, WA, USA, 1999; p. 808. [CrossRef]
107. Choi, J.S.; Kang, H.-W.; Lee, I.H.; Ko, T.J.; Cho, D.-W. Development of micro-stereolithography technology using a UV lamp and optical fiber. *Int. J. Adv. Manuf. Technol.* **2009**, *41*, 281–286. [CrossRef]
108. Bertsch, A.; Bernhard, P.; Vogt, C.; Renaud, P. Rapid prototyping of small size objects. *Rapid Prototyp. J.* **2000**, *6*, 259–266. [CrossRef]
109. Jang, T.-S.; Jung, H.-D.; Pan, H.M.; Han, W.T.; Chen, S.; Song, J. 3D printing of hydrogel composite systems: Recent advances in technology for tissue engineering. *Int. J. Bioprint* **2018**, *4*, 126. [CrossRef]
110. Sun, C.; Fang, N.; Wu, D.M.; Zhang, X. Projection micro-stereolithography using digital micro-mirror dynamic mask. *Sens. Actuators A Phys.* **2005**, *121*, 113–120. [CrossRef]
111. Weiß, T.; Hildebrand, G.; Schade, R.; Liefelth, K. Two-Photon polymerization for microfabrication of three-dimensional scaffolds for tissue engineering application. *Eng. Life Sci.* **2009**, *9*, 384–390. [CrossRef]
112. Farsari, M.; Chichkov, B.N. Two-photon fabrication. *Nat. Photonics* **2009**, *3*, 450–452. [CrossRef]
113. Park, S.-H.; Yang, D.-Y.; Lee, K.-S. Two-photon stereolithography for realizing ultraprecise three-dimensional nano/microdevices. *Laser Photonics Rev.* **2009**, *3*, 1–11. [CrossRef]
114. Zipfel, W.R.; Williams, R.M.; Webb, W.W. Nonlinear magic: Multiphoton microscopy in the biosciences. *Nat. Biotechnol.* **2003**, *21*, 1369–1377. [CrossRef] [PubMed]
115. Perevoznic, D.; Nazir, R.; Kiyani, R.; Kurselis, K.; Koszarna, B.; Gryko, D.T.; Chichkov, B.N. High-speed two-photon polymerization 3D printing with a microchip laser at its fundamental wavelength. *Opt. Express* **2019**, *27*, 25119. [CrossRef]
116. Bell, A.; Kofron, M.; Nistor, V. Multiphoton crosslinking for biocompatible 3D printing of type I collagen. *Biofabrication* **2015**, *7*, 035007. [CrossRef]
117. Gao, W.; Chao, H.; Zheng, Y.C.; Zhang, W.C.; Liu, J.; Jin, F.; Dong, X.Z.; Liu, Y.H.; Li, S.J.; Zheng, M.L. Ionic Carbazole-Based Water-Soluble Two-Photon Photoinitiator and the Fabrication of Biocompatible 3D Hydrogel Scaffold. *ACS Appl. Mater. Interfaces* **2021**, *13*, 27796–27805. [CrossRef] [PubMed]
118. Kim, H.S.; Yeon, Y.K.; Lee, J.M.; Chao, J.R.; Lee, Y.J.; Seo, Y.B.; Sultan, M.T.; Lee, O.J.; Lee, J.S.; Yoon, S.; et al. Precisely printable and biocompatible silk fibroin bioink for digital light processing 3D printing. *Nat. Commun.* **2018**, *9*, 1620. [CrossRef]
119. Ma, X.; Qu, X.; Zhu, W.; Li, Y.S.; Yuan, S.; Zhang, H.; Liu, J.; Wang, P.; Lai, C.S.E.; Zanella, F.; et al. Deterministically patterned biomimetic human iPSC-derived hepatic model via rapid 3D bioprinting. *Proc. Natl. Acad. Sci. USA* **2016**, *113*, 2206–2211. [CrossRef]
120. Keriquel, V.; Oliveira, H.; Rémy, M.; Ziane, S.; Delmond, S.; Rousseau, B.; Rey, S.; Catros, S.; Amédée, J.; Guillemot, F.; et al. In situ printing of mesenchymal stromal cells, by laser-assisted bioprinting, for in vivo bone regeneration applications. *Sci. Rep.* **2017**, *7*, 1778. [CrossRef]
121. Valente, F.; Hepburn, M.S.; Chen, J.; Aldana, A.A.; Allardyce, B.J.; Shafei, S.; Doyle, B.J.; Kennedy, B.F.; Dilley, R.J. Bioprinting silk fibroin using two-photon lithography enables control over the physico-chemical material properties and cellular response. *Bioprinting* **2022**, *25*, e00183. [CrossRef]

122. Ni, J.; Huang, X.; Bai, Y.; Zhao, B.; Han, Y.; Han, S.; Xu, T.; Si, C.; Zhang, C. Resistance to aggregation-caused quenching: Chitosan-based solid carbon dots for white light-emitting diode and 3D printing. *Adv. Compos. Hybrid Mater.* **2022**, *5*, 1865–1875. [[CrossRef](#)]
123. He, Y.; Wang, F.; Wang, X.; Zhang, J.; Wang, D.; Huang, X. A photocurable hybrid chitosan/acrylamide bioink for DLP based 3D bioprinting. *Mater. Des.* **2021**, *202*, 109588. [[CrossRef](#)]
124. Joshi, A.; Kaur, T.; Joshi, A.; Gugulothu, S.B.; Choudhury, S.; Singh, N. Light-Mediated 3D Printing of Micro-Pyramid-Decorated Tailorable Wound Dressings with Endogenous Growth Factor Sequestration for Improved Wound Healing. *ACS Appl Mater Interfaces* **2023**, *15*, 327–337. [[CrossRef](#)] [[PubMed](#)]
125. Tsegay, F.; Elsherif, M.; Alam, F.; Butt, H. Smart 3D Printed Auxetic Hydrogel Skin Wound Dressings. *ACS Appl. Bio. Mater.* **2022**, *5*, 5545–5553. [[CrossRef](#)]
126. Kunwar, P.; Xiong, Z.; Zhu, Y.; Li, H.; Filip, A.; Soman, P. Hybrid Laser Printing of 3D, Multiscale, Multimaterial Hydrogel Structures. *Adv. Opt. Mater.* **2019**, *7*, 1900656. [[CrossRef](#)]
127. Liu, C.; Xu, N.; Zong, Q.; Yu, J.; Zhang, P. Hydrogel prepared by 3D printing technology and its applications in the medical field. *Colloid Interface Sci. Commun.* **2021**, *44*, 100498. [[CrossRef](#)]
128. Beaman, J.J.; Deckard, C.R. Selective laser sintering with assisted powder handling. U.S. Patent No. 4,938,816., 1990.
129. Mazzoli, A.; Ferretti, C.; Gigante, A.; Salvolini, E.; Mattioli-Belmonte, M. Selective laser sintering manufacturing of polycaprolactone bone scaffolds for applications in bone tissue engineering. *Rapid Prototyp. J.* **2015**, *21*, 386–392. [[CrossRef](#)]
130. Tamay, D.G.; Usal, T.D.; Alagoz, A.S.; Yucel, D.; Hasirci, N.; Hasirci, V. 3D and 4D Printing of Polymers for Tissue Engineering Applications. *Front. Bioeng. Biotechnol.* **2019**, *7*, 164. [[CrossRef](#)]
131. Muzaffar, A.; Ahamed, M.B.; Deshmukh, K.; Kovářik, T.; Křenek, T.; Pasha, S.K.K. 3D and 4D Printing of pH-Responsive and Functional Polymers and Their Composites. In *3D and 4D Printing of Polymer Nanocomposite Materials*; Elsevier: Amsterdam, The Netherlands, 2020; pp. 85–117. [[CrossRef](#)]
132. Prabhakar, P.; Sen, R.K.; Dwivedi, N.; Khan, R.; Solanki, P.R.; Srivastav, A.K.; Dhand, C. 3D-Printed Microfluidics and Potential Biomedical Applications. *Front. Nanotechnol.* **2021**, *3*, 609355. [[CrossRef](#)]
133. Athukorala, S.S.; Tran, T.S.; Balu, R.; Truong, V.K.; Chapman, J.; Dutta, N.K.; Roy Choudhury, N. 3D Printable Electrically Conductive Hydrogel Scaffolds for Biomedical Applications: A Review. *Polymers* **2021**, *13*, 474. [[CrossRef](#)]
134. Placone, J.K.; Engler, A.J. Recent Advances in Extrusion-Based 3D Printing for Biomedical Applications. *Adv. Healthc. Mater.* **2018**, *7*, 1701161. [[CrossRef](#)] [[PubMed](#)]
135. Zhang, G.; Jiang, J.; Wang, H.; Qian, L.; Lan, H. Continuous DLP-based ceramic 3D printing using a composite oxygen-rich film. *J. Manuf. Process.* **2021**, *64*, 341–348. [[CrossRef](#)]
136. Claeysens, F.; Hasan, E.A.; Gaidukeviciute, A.; Achilleos, D.S.; Ranella, A.; Reinhardt, C.; Ovsianikov, A.; Shizhou, X.; Fotakis, C.; Vamvakaki, M.; et al. Three-Dimensional Biodegradable Structures Fabricated by Two-Photon Polymerization. *Langmuir* **2009**, *25*, 3219–3223. [[CrossRef](#)] [[PubMed](#)]
137. Kwon, I.K.; Matsuda, T. Photo-polymerized microarchitectural constructs prepared by microstereolithography ( $\mu$ SL) using liquid acrylate-end-capped trimethylene carbonate-based prepolymers. *Biomaterials* **2005**, *26*, 1675–1684. [[CrossRef](#)] [[PubMed](#)]
138. LaFratta, C.N.; Baldacchini, T. Two-Photon Polymerization Metrology: Characterization Methods of Mechanisms and Microstructures. *Micromachines* **2017**, *8*, 101. [[CrossRef](#)]
139. Liao, C.; Wuethrich, A.; Trau, M. A material odyssey for 3D nano/microstructures: Two photon polymerization based nanolithography in bioapplications. *Appl. Mater. Today* **2020**, *19*, 100635. [[CrossRef](#)]
140. Thompson, J.R.; Worthington, K.S.; Green, B.J.; Mullin, N.K.; Jiao, C.; Kaalberg, E.E.; Wiley, L.A.; Han, I.C.; Russell, S.R.; Sohn, E.H.; et al. Two-photon polymerized poly(caprolactone) retinal cell delivery scaffolds and their systemic and retinal biocompatibility. *Acta Biomater.* **2019**, *94*, 204–218. [[CrossRef](#)]
141. Zhou, X.; Hou, Y.; Lin, J. A review on the processing accuracy of two-photon polymerization. *AIP Adv.* **2015**, *5*, 030701. [[CrossRef](#)]
142. Hu, Q.; Lu, R.; Liu, S.; Liu, Y.; Gu, Y.; Zhang, H. 3D printing GelMA/PVA interpenetrating polymer networks scaffolds mediated with CuO nanoparticles for angiogenesis. *Macromol. Biosci.* **2022**, *22*, 2200208. [[CrossRef](#)]
143. Mau, R.; Nazir, J.; John, S.; Seitz, H. Preliminary Study on 3D printing of PEGDA Hydrogels for Frontal Sinus Implants using Digital Light Processing (DLP). *Curr. Dir. Biomed. Eng.* **2019**, *5*, 249–252. [[CrossRef](#)]
144. Caprioli, M.; Roppolo, I.; Chiappone, A.; Larush, L.; Pirri, C.F.; Magdassi, S. 3D-printed self-healing hydrogels via Digital Light Processing. *Nat. Commun.* **2021**, *12*, 2462. [[CrossRef](#)] [[PubMed](#)]
145. Al-Dulimi, Z.; Wallis, M.; Tan, D.K.; Maniruzzaman, M.; Nokhodchi, A. 3D printing technology as innovative solutions for biomedical applications. *Drug Discov. Today* **2021**, *26*, 360–383. [[CrossRef](#)] [[PubMed](#)]
146. Fina, F.; Goyanes, A.; Madla, C.M.; Awad, A.; Trenfield, S.J.; Kuek, J.M.; Patel, P.; Gaisford, S.; Basit, A.W. 3D printing of drug-loaded gyroid lattices using selective laser sintering. *Int. J. Pharm.* **2018**, *547*, 44–52. [[CrossRef](#)] [[PubMed](#)]
147. Ude, C.; Hentrop, T.; Lindner, P.; Lücking, T.H.; Scheper, T.; Beut, S. New perspectives in shake flask pH control using a 3D-printed control unit based on pH online measurement. *Sens. Actuators B Chem.* **2015**, *221*, 1035–1043. [[CrossRef](#)]
148. Williams, J.M.; Adewunmi, A.; Schek, R.M.; Flanagan, C.L.; Krebsbach, P.H.; Feinberg, S.E.; Hollister, S.J.; Das, S. Bone tissue engineering using polycaprolactone scaffolds fabricated via selective laser sintering. *Biomaterials* **2005**, *26*, 4817–4827. [[CrossRef](#)]
149. Ahangar, P.; Cooke, M.E.; Weber, M.H.; Rosenzweig, D.H. Current Biomedical Applications of 3D Printing and Additive Manufacturing. *Appl. Sci.* **2019**, *9*, 1713. [[CrossRef](#)]

150. Beg, S.; Almalki, W.H.; Malik, A.; Farhan, M.; Aatif, M.; Rahman, Z.; Alruwaili, N.K.; Alrobaian, M.; Tarique, M.; Rahman, M. 3D printing for drug delivery and biomedical applications. *Drug Discov. Today* **2020**, *25*, 1668–1681. [[CrossRef](#)]
151. Lin, J.; Kan, Y.; Jing, X.; Lu, M. Design and Fabrication of a Three-Dimensional Artificial Compound Eye Using Two-Photon Polymerization. *Micromachines* **2018**, *9*, 336. [[CrossRef](#)]
152. Lin, Y.; Zhou, R.; Xu, J. Superhydrophobic Surfaces Based on Fractal and Hierarchical Microstructures Using Two-Photon Polymerization: Toward Flexible Superhydrophobic Films. *Adv. Mater. Interfaces* **2018**, *5*, 1801126. [[CrossRef](#)]
153. Mahmood, M.A.; Popescu, A.C. 3D Printing at Micro-Level: Laser-Induced Forward Transfer and Two-Photon Polymerization. *Polymers* **2021**, *13*, 2034. [[CrossRef](#)]
154. Paz, V.F.; Emons, M.; Obata, K.; Ovsianikov, A.; Peterhänsel, S.; Frenner, K.; Reinhardt, C.; Chichkov, B.; Morgner, U.; Osten, W. Development of functional sub-100 nm structures with 3D two-photon polymerization technique and optical methods for characterization. *J. Laser Appl.* **2012**, *24*, 042004. [[CrossRef](#)]
155. Zhang, M.; Zhang, C.; Li, Z.; Fu, X.; Huang, S. Advances in 3D skin bioprinting for wound healing and disease modeling. *Regen. Biomater.* **2023**, *10*, rbac105. [[CrossRef](#)]
156. Liu, Y.; Ouyang, W.; Wu, H.; Xu, Z.; Sheng, I.; Zou, Q.; Zhang, M.; Zhang, W.; Jiao, J. Improving surface quality and superficial microstructure of LDED Inconel 718 superalloy processed by hybrid laser polishing. *J. Mater. Process. Technol.* **2022**, *300*, 117428. [[CrossRef](#)]
157. Li, J.; Wu, C.; Chu, P.K.; Gelinsky, M. 3D printing of hydrogels: Rational design strategies and emerging biomedical applications. *Mater. Sci. Eng. R Rep.* **2020**, *140*, 100543. [[CrossRef](#)]
158. Tabriz, A.G.; Douroumis, D. Recent advances in 3D printing for wound healing: A systematic review. *J. Drug Deliv. Sci. Technol.* **2022**, *74*, 103564. [[CrossRef](#)]
159. Lee, S.-G.; Lee, S.; Bae, H.-K.; Lee, K.Y.; Park, C.; Kim, M.S.; Lee, D.H.; Chung, H.M.; Kim, C.-Y. Evaluation of the therapeutic efficacy of human skin equivalents manufactured through droplet-based bioprinting/nebulization technology. *Mol. Cell Toxicol.* **2023**, *19*, 1–10. [[CrossRef](#)]
160. Kotlarz, M.; Ferreira, A.M.; Gentile, P.; Russell, S.J.; Dalgarno, K. Droplet-based bioprinting enables the fabrication of cell–hydrogel–microfibre composite tissue precursors. *Bioresour. Manuf.* **2022**, *5*, 512–528. [[CrossRef](#)]
161. Mesquita, C.R.S.; Charelli, L.E.; Baptista, L.S.; Naveira-Cotta, C.P.; Balbino, T.A. Continuous-mode encapsulation of human stem cell spheroids using droplet-based glass-capillary microfluidic device for 3D bioprinting technology. *Biochem. Eng. J.* **2021**, *174*, 108122. [[CrossRef](#)]
162. Ng, W.L.; Huang, X.; Shkolnikov, V.; Goh, G.L.; Suntornnond, R.; Yeong, W.Y. Controlling Droplet Impact Velocity and Droplet Volume: Key Factors to Achieving High Cell Viability in Sub-Nanoliter Droplet-based Bioprinting. *Int. J. Bioprint.* **2021**, *8*, 424. [[CrossRef](#)]
163. Dumpa, N.; Butreddy, A.; Wang, H.; Komanduri, N.; Bandari, S.; Repka, M.A. 3D printing in personalized drug delivery: An overview of hot-melt extrusion-based fused deposition modeling. *Int. J. Pharm.* **2021**, *600*, 120501. [[CrossRef](#)]
164. Pranzo, D.; Larizza, P.; Filippini, D.; Percoco, G. Extrusion-Based 3D Printing of Microfluidic Devices for Chemical and Biomedical Applications: A Topical Review. *Micromachines* **2018**, *9*, 374. [[CrossRef](#)] [[PubMed](#)]
165. Long, J.; Etxeberria, A.E.; Nand, A.V.; Bunt, C.R.; Ray, S.; Seyfoddin, A. A 3D printed chitosan-pectin hydrogel wound dressing for lidocaine hydrochloride delivery. *Mater. Sci. Eng. C* **2019**, *104*, 109873. [[CrossRef](#)]
166. Puertas-Bartolomé, M.; Włodarczyk-Biegun, M.K.; del Campo, A.; Vázquez-Lasa, B.; San Román, J. 3D Printing of a Reactive Hydrogel Bio-Ink Using a Static Mixing Tool. *Polymers* **2020**, *12*, 1986. [[CrossRef](#)] [[PubMed](#)]
167. Bakarich, S.E.; Gorkin, R.; Gately, R.; Naficy, S.; Panhuis, M.I.H.; Spinks, G.M. 3D printing of tough hydrogel composites with spatially varying materials properties. *Addit. Manuf.* **2017**, *14*, 24–30. [[CrossRef](#)]
168. Meng, Y.; Cao, J.; Chen, Y.; Yu, Y.; Ye, L. 3D printing of a poly(vinyl alcohol)-based nano-composite hydrogel as an artificial cartilage replacement and the improvement mechanism of printing accuracy. *J. Mater. Chem. B* **2020**, *8*, 677–690. [[CrossRef](#)]
169. Firth, J.; Basit, A.W.; Gaisford, S. The Role of Semi-Solid Extrusion Printing in Clinical Practice. In *3D Printing of Pharmaceuticals*; Springer: Cham, Switzerland, 2018; pp. 133–151. [[CrossRef](#)]
170. Goyanes, A.; Allahham, N.; Trenfield, S.J.; Stoyanov, E.; Gaisford, S.; Basit, A.W. Direct powder extrusion 3D printing: Fabrication of drug products using a novel single-step process. *Int. J. Pharm.* **2019**, *567*, 118471. [[CrossRef](#)] [[PubMed](#)]
171. Henry, S.; Samaro, A.; Marchesini, F.H.; Shaqour, B.; Macedo, J.; Vanhoorne, V.; Vervaeke, C. Extrusion-based 3D printing of oral solid dosage forms: Material requirements and equipment dependencies. *Int. J. Pharm.* **2021**, *598*, 120361. [[CrossRef](#)]
172. Liaskoni, A.; Wildman, R.D.; Roberts, C.J. 3D printed polymeric drug-eluting implants. *Int. J. Pharm.* **2021**, *597*, 120330. [[CrossRef](#)]
173. Samaro, A.; Janssens, P.; Vanhoorne, V.; Van Renterghem, J.; Eeckhout, M.; Cardon, L.; De Beer, T.; Vervaeke, C. Screening of pharmaceutical polymers for extrusion-based Additive Manufacturing of patient-tailored tablets. *Int. J. Pharm.* **2020**, *586*, 119591. [[CrossRef](#)]
174. Cui, X.; Breitenkamp, K.; Finn, M.G.; Lotz, M.; D’Lima, D.D. Direct Human Cartilage Repair Using Three-Dimensional Bioprinting Technology. *Tissue Eng. Part A* **2012**, *18*, 1304–1312. [[CrossRef](#)]
175. Duan, B.; Kapetanovic, E.; Hockaday, L.A.; Butcher, J.T. Three-dimensional printed trileaflet valve conduits using biological hydrogels and human valve interstitial cells. *Acta Biomater.* **2014**, *10*, 1836–1846. [[CrossRef](#)] [[PubMed](#)]
176. Park, B.J.; Choi, H.J.; Moon, S.J.; Kim, S.J.; Bajracharya, R.; Min, H.Y.; Han, H.K. Pharmaceutical applications of 3D printing technology: Current understanding and future perspectives. *J. Pharm. Investig.* **2018**, *49*, 575–585. [[CrossRef](#)]

177. Seoane-Viaño, I.; Januskaite, P.; Alvarez-Lorenzo, C.; Basit, A.W.; Goyanes, A. Semi-solid extrusion 3D printing in drug delivery and biomedicine: Personalised solutions for healthcare challenges. *J. Control Release* **2021**, *332*, 367–389. [CrossRef] [PubMed]
178. Xu, W.; Molino, Z.; Cheng, F.; Molino, P.J.; Yue, Z.; Su, D.; Wang, X.; Willför, S.; Xu, C.; Wallace, G.G. On Low-Concentration Inks Formulated by Nanocellulose Assisted with Gelatin Methacrylate (GelMA) for 3D Printing toward Wound Healing Application. *ACS Appl. Mater. Interfaces* **2019**, *11*, 8838–8848. [CrossRef]
179. Huyan, Y.; Lian, Q.; Zhao, T.; Li, D.; He, J. Pilot Study of the Biological Properties and Vascularization of 3D Printed Bilayer Skin Grafts. *Int. J. Bioprint.* **2020**, *6*, 246. [CrossRef]
180. Chu, B.; He, J.-M.; Wang, Z.; Liu, L.-L.; Li, X.-L.; Wu, C.-X.; Chen, C.S.; Tu, M. Proangiogenic peptide nanofiber hydrogel/3D printed scaffold for dermal regeneration. *Chem. Eng. J.* **2021**, *424*, 128146. [CrossRef]
181. Wang, X.; Qi, J.; Zhang, W.; Pu, Y.; Yang, R.; Wang, P.; Liu, S.; Tan, S.; Chi, B. 3D-printed antioxidant antibacterial carboxymethyl cellulose/ $\epsilon$ -polylysine hydrogel promoted skin wound repair. *Int. J. Biol. Macromol.* **2021**, *187*, 91–104. [CrossRef]
182. Siebert, L.; Luna-Cerón, E.; García-Rivera, L.E.; Oh, J.; Jang, J.; Rosas-Gómez, D.A.; Pérez-Gómez, M.D.; Maschkowitz, G.; Fickenscher, H.; Ocegüera-Cuevas, D.; et al. Light-Controlled Growth Factors Release on Tetrapodal ZnO-Incorporated 3D-Printed Hydrogels for Developing Smart Wound Scaffold. *Adv. Funct. Mater.* **2021**, *31*, 2007555. [CrossRef]
183. Chen, B.; Dong, J.; Ruelas, M.; Ye, X.; He, J.; Yao, R.; Fu, Y.; Liu, Y.; Hu, J.; Wu, T.; et al. Artificial Intelligence-Assisted High-Throughput Screening of Printing Conditions of Hydrogel Architectures for Accelerated Diabetic Wound Healing. *Adv. Funct. Mater.* **2022**, *32*, 2201843. [CrossRef]
184. Smay, J.E.; Gratson, G.M.; Shepherd, R.F.; Cesarano, J.; Lewis, J.A. Directed Colloidal Assembly of 3D Periodic Structures. *Adv. Mater.* **2002**, *14*, 1279–1283. [CrossRef]
185. Yuk, H.; Zhao, X. A New 3D Printing Strategy by Harnessing Deformation, Instability, and Fracture of Viscoelastic Inks. *Adv. Mater.* **2018**, *30*, 1704028. [CrossRef] [PubMed]
186. Zhang, Y.; Shi, G.; Qin, J.; Lowe, S.E.; Zhang, S.; Zhao, H.; Zhong, Y.L. Recent Progress of Direct Ink Writing of Electronic Components for Advanced Wearable Devices. *ACS Appl. Electron. Mater.* **2019**, *1*, 1718–1734. [CrossRef]
187. Jiang, P.; Lin, P.; Yang, C.; Qin, H.; Wang, X.; Zhou, F. 3D Printing of Dual-Physical Cross-linking Hydrogel with Ultrahigh Strength and Toughness. *Chem. Mater.* **2020**, *32*, 9983–9995. [CrossRef]
188. Das, R.; Lee, C.P.; Prakash, A.; Hashimoto, M.; Fernandez, J.G. Geometrical control of degradation and cell delivery in 3D printed nanocellulose hydrogels. *Mater. Today Commun.* **2022**, *30*, 103023. [CrossRef]
189. Casavola, C.; Cazzato, A.; Moramarco, V.; Pappalettere, C. Orthotropic mechanical properties of fused deposition modelling parts described by classical laminate theory. *Mater. Des.* **2016**, *90*, 453–458. [CrossRef]
190. Xu, N.; Ye, X.; Wei, D.; Zhong, J.; Chen, Y.; Xu, G.; He, D. 3D Artificial Bones for Bone Repair Prepared by Computed Tomography-Guided Fused Deposition Modeling for Bone Repair. *ACS Appl. Mater. Interfaces* **2014**, *6*, 14952–14963. [CrossRef]
191. Yuan, B.; Zhou, S.; Chen, X. Rapid prototyping technology and its application in bone tissue engineering. *J. Zhejiang Univ.-Sci. B* **2017**, *18*, 303–315. [CrossRef]
192. Thavornnyutikarn, B.; Chantarapanich, N.; Sithiseripratip, K.; Thouas, G.A.; Chen, Q. Bone tissue engineering scaffolding: Computer-aided scaffolding techniques. *Prog. Biomater.* **2014**, *3*, 61–102. [CrossRef]
193. Wang, X.; Jiang, M.; Zhou, Z.; Gou, J.; Hui, D. 3D printing of polymer matrix composites: A review and prospective. *Compos. B Eng.* **2017**, *110*, 442–458. [CrossRef]
194. Chia, H.N.; Wu, B.M. Recent advances in 3D printing of biomaterials. *J. Biol. Eng.* **2015**, *9*, 4. [CrossRef]
195. ISO 10993-1:2018; Biological Evaluation of Medical Devices—Part 1: Evaluation and Testing within a Risk Management Process. ISO: Geneva, Switzerland, 2018. Available online: <https://www.iso.org/standard/68936.html> (accessed on 1 October 2018).
196. Kowalczyk, P.; Trzaskowska, P.; Łojszczyk, I.; Podgórski, R.; Ciach, T. Production of 3D printed polylactide scaffolds with surface grafted hydrogel coatings. *Colloids Surf B Biointerfaces* **2019**, *179*, 136–142. [CrossRef]
197. Ning, L.; Chen, X. A brief review of extrusion-based tissue scaffold bio-printing. *Biotechnol. J.* **2017**, *12*, 1600671. [CrossRef]
198. Rajabi, M.; McConnell, M.; Cabral, J.; Ali, M.A. Chitosan hydrogels in 3D printing for biomedical applications. *Carbohydr. Polym.* **2021**, *260*, 117768. [CrossRef]
199. Baniasadi, H.; Polez, R.T.; Kimiaei, E.; Madani, Z.; Rojas, O.J.; Österberg, M.; Seppälä, J. 3D printing and properties of cellulose nanofibrils-reinforced quince seed mucilage bio-inks. *Int. J. Biol. Macromol.* **2021**, *192*, 1098–1107. [CrossRef] [PubMed]
200. Sood, A.K.; Ohdar, R.K.; Mahapatra, S.S. Parametric appraisal of mechanical property of fused deposition modelling processed parts. *Mater. Des.* **2010**, *31*, 287–295. [CrossRef]
201. Tappa, K.; Jammalamadaka, U. Novel biomaterials used in medical 3D printing techniques. *J. Funct. Biomater.* **2018**, *9*, 17. [CrossRef] [PubMed]
202. Herreros-Pomares, A.; Zhou, X.; Calabuig-Fariñas, S.; Lee, S.-J.; Torres, S.; Esworthy, T.; Hann, S.Y.; Jantus-Lewintre, E.; Camps, C.; Zhang, L.G. 3D printing novel in vitro cancer cell culture model systems for lung cancer stem cell study. *Mater. Sci. Eng. C* **2021**, *122*, 111914. [CrossRef]
203. Seyedsalehi, A.; Daneshmandi, L.; Barajaa, M.; Riordan, J.; Laurencin, C.T. Fabrication and characterization of mechanically competent 3D printed polycaprolactone-reduced graphene oxide scaffolds. *Sci. Rep.* **2020**, *10*, 22210. [CrossRef]
204. Duan, J.; Cao, Y.; Shen, Z.; Cheng, Y.; Ma, Z.; Wang, L.; Zhang, Y.; An, Y.; Sang, S. 3D bioprinted GelMA/PEGDA hybrid scaffold for establishing an in vitro model of melanoma. *J. Microbiol. Biotechnol.* **2022**, *32*, 531–540. [CrossRef]

205. Ashammakhi, N.; Ahadian, S.; Xu, C.; Montazerian, H.; Ko, H.; Nasiri, R.; Barros, N.; Khademhosseini, A. Bioinks and bioprinting technologies to make heterogeneous and biomimetic tissue constructs. *Mater. Today Bio.* **2019**, *1*, 100008. [[CrossRef](#)]
206. Ali, M.A.; Rajabi, M.; Sali, S.S. Additive manufacturing potential for medical devices and technology. *Curr. Opin. Chem. Eng.* **2020**, *28*, 127–133. [[CrossRef](#)]
207. Van de Walle, A.; Perez, J.E.; Wilhelm, C. Magnetic bioprinting of stem cell-based tissues. *Bioprinting* **2023**, *30*, e00265. [[CrossRef](#)]
208. Lee, M.J.; Sing, S.L.; Zhou, M.; Yeong, W.Y. 3D bioprinting processes: A perspective on classification and terminology. *Int. J. Bioprinting* **2018**, *4*, 151. [[CrossRef](#)] [[PubMed](#)]
209. Ito, A.; Ino, K.; Hayashida, M.; Kobayashi, T.; Matsunuma, H.; Kagami, H.; Ueda, M.; Hond, H. Novel methodology for fabrication of tissue-engineered tubular constructs using magnetite nanoparticles and magnetic force. *Tissue Eng.* **2005**, *11*, 1553–1561. [[CrossRef](#)]
210. Leonard, F.; Godin, B. 3D in vitro model for breast cancer research using magnetic levitation and bioprinting method. In *Breast Cancer Methods in Molecular Biology*; Humana Press: New York, NY, USA, 2016; pp. 239–251. [[CrossRef](#)]
211. Lee, A.R.H.A.; Hudson, A.R.; Shiward, D.J.; Tashman, J.W.; Hinton, T.J.; Yerneni, S.; Bliley, J.M.; Campbell, P.G.; Feinberg, A.W. 3D bioprinting of collagen to rebuild components of the human heart. *Science* **2019**, *365*, 482–487. [[CrossRef](#)]
212. Hinton, T.J.; Jallerat, Q.; Palchesko, R.; Park, J.H.; Grodzicki, M.S.; Shue, H.-J.; Ramadan, M.H.; Hudson, A.R.; Feinberg, A.W. Three-dimensional printing of complex biological structures by freeform reversible embedding of suspended hydrogels. *Sci. Adv.* **2015**, *1*, e1500758. [[CrossRef](#)]
213. Shiward, D.J.; Hudson, A.R.; Tashman, J.W.; Feinberg, A.W. Emergence of FRESH 3D printing as a platform for advanced tissue biofabrication. *APL Bioeng.* **2021**, *5*, 010904. [[CrossRef](#)]
214. Kreimendahl, F.; Kniebs, C.; Sobreiro, A.M.T.; Schmitz-Rode, T.; Jockenhoevel, S.; Thiebes, A.L. FRESH bioprinting technology for tissue engineering—the influence of printing process and bioink composition on cell behavior and vascularization. *J. Appl. Biomater. Funct. Mater.* **2021**, *19*. [[CrossRef](#)]
215. Mirdamadi, E.; Tashman, J.W.; Shiward, D.J.; Palchesko, R.N.; Feinberg, A.W. FRESH 3D bioprinting a full-size model of the human heart. *ACS Biomater. Sci. Eng.* **2020**, *6*, 6453–6459. [[CrossRef](#)]
216. Skylar-Scott, M.A.; Uzel, S.G.M.; Nam, L.L.; Ahrens, J.H.; Truby, R.L.; Damaraju, S.; Lewis, J.A. Biomufacturing of organ-specific tissues with high cellular density and embedded vascular channels. *Sci. Adv.* **2019**, *5*, eaaw2459. [[CrossRef](#)]
217. Russell, C.S.; Mostafavi, A.; Quint, J.P.; Panayi, A.C.; Baldino, K.; Williams, T.J.; Daubendiek, J.G.; Sánchez, V.H.; Bonick, Z.; Trujillo-Miranda, M.; et al. In Situ Printing of Adhesive Hydrogel Scaffolds for the Treatment of Skeletal Muscle Injuries. *ACS Appl. Bio. Mater.* **2020**, *3*, 1568–1579. [[CrossRef](#)] [[PubMed](#)]
218. Li, X.; Lian, Q.; Li, D.; Xin, H.; Jia, S. Development of a Robotic Arm Based Hydrogel Additive Manufacturing System for In-Situ Printing. *Appl. Sci.* **2017**, *7*, 73. [[CrossRef](#)]
219. Ma, K.; Zhao, T.; Yang, L.; Wang, P.; Jin, J.; Teng, H.; Xia, D.; Zhu, L.; Li, L.; Jiang, Q.; et al. Application of robotic-assisted in situ 3D printing in cartilage regeneration with HAMA hydrogel: An in vivo study. *J. Adv. Res.* **2020**, *23*, 123–132. [[CrossRef](#)] [[PubMed](#)]
220. O’Connell, C.D.; Konate, S.; Onofrillo, C.; Kapsa, R.; Baker, C.; Duchi, S.; Eekel, T.; Yue, Z.; Beirne, S.; Barnsley, G. Free-form co-axial bioprinting of a gelatin methacryloyl bio-ink by direct in situ photo-crosslinking during extrusion. *Bioprinting* **2020**, *19*, e00087. [[CrossRef](#)]
221. Agostinacchio, F.; Mu, X.; Dirè, S.; Motta, A.; Kaplan, D.L. In Situ 3D Printing: Opportunities with Silk Inks. *Trends Biotechnol.* **2021**, *39*, 719–730. [[CrossRef](#)]
222. Wu, Y.; Ravnic, D.J.; Ozbolat, I.T. Intraoperative Bioprinting: Repairing Tissues and Organs in a Surgical Setting. *Trends Biotechnol.* **2020**, *38*, 594–605. [[CrossRef](#)]
223. Li, L.; Shi, J.; Shen, S.; Teng, H.; Yang, J.; Wang, X.; Jiang, Q. In situ repair of bone and cartilage defects using 3D scanning and 3D printing. *Sci. Rep.* **2017**, *7*, 9416. [[CrossRef](#)]
224. Zhou, L.; Ramezani, H.; Sun, M.; Xie, M.; Nie, J.; Lv, S.; Cai, J.; Fu, J.; He, Y. 3D printing of high-strength chitosan hydrogel scaffolds without any organic solvents. *Biomater. Sci.* **2020**, *8*, 5020–5028. [[CrossRef](#)]
225. Nuutila, K.; Samandari, M.; Endo, Y.; Zhang, Y.; Quint, J.; Schmidt, T.A.; Tamayol, A.; Sinha, I. In vivo printing of growth factor-eluting adhesive scaffolds improves wound healing. *Bioact. Mater.* **2022**, *8*, 296–308. [[CrossRef](#)]
226. Webster, A.; Greenman, J.; Haswell, S.J. Development of microfluidic devices for biomedical and clinical application. *J. Chem. Technol. Biotechnol.* **2011**, *86*, 10–17. [[CrossRef](#)]
227. Sommonte, F.; Denora, N.; Lamprou, D.A. Combining 3D Printing and Microfluidic Techniques: A Powerful Synergy for Nanomedicine. *Pharmaceuticals* **2023**, *16*, 69. [[CrossRef](#)] [[PubMed](#)]
228. Chiesa-Estomba, C.M.; González-García, J.; Sistiaga-Suarez, J.A.; Fernández, I.G. A Novel Computer-Aided Design/Computer-Aided Manufacturing (CAD/CAM) 3D Printing Method for Nasal Framework Reconstruction Using Microvascular Free Flaps. *Cureus* **2022**, *14*, e28971. [[CrossRef](#)]
229. Ellakany, P.; Fouda, S.M.; Mahrous, A.A.; AlGhamdi, M.A.; Aly, N.M. Influence of CAD/CAM Milling and 3D-Printing Fabrication Methods on the Mechanical Properties of 3-Unit Interim Fixed Dental Prosthesis after Thermo-Mechanical Aging Process. *Polymers* **2022**, *14*, 4103. [[CrossRef](#)] [[PubMed](#)]
230. Wang, H.; Chi, Y.; Huang, H.; Su, S.; Xue, H.; Hou, J. Combined use of 3D printing and computer-assisted navigation in the clinical treatment of multiple maxillofacial fractures. *Asian J. Surg.* **2022**, *46*, 2284–2292. [[CrossRef](#)] [[PubMed](#)]

231. Kafle, A.; Luis, E.; Silwal, R.; Pan, H.M.; Shrestha, P.L.; Bastola, A.K. 3D/4D Printing of Polymers: Fused Deposition Modelling (FDM), Selective Laser Sintering (SLS), and Stereolithography (SLA). *Polymers* **2021**, *13*, 3101. [[CrossRef](#)]
232. Karakurt, I.; Aydoğdu, A.; Çıkrıkçı, S.; Orozco, J.; Lin, L. Stereolithography (SLA) 3D printing of ascorbic acid loaded hydrogels: A controlled release study. *Int. J. Pharm.* **2020**, *584*, 119428. [[CrossRef](#)]
233. Xiao, R.; Ding, M.; Wang, Y.; Gao, L.; Fan, R.; Lu, Y. Stereolithography (SLA) 3D printing of carbon fiber-graphene oxide (CF-GO) reinforced polymer lattices. *Nanotechnology* **2021**, *32*, 235702. [[CrossRef](#)]
234. Xu, X.; Goyanes, A.; Trenfield, S.J.; Diaz-Gomez, L.; Alvarez-Lorenzo, C.; Gaisford, S.; Basit, A.W. Stereolithography (SLA) 3D printing of a bladder device for intravesical drug delivery. *Mater. Sci. Eng. C* **2021**, *120*, 111773. [[CrossRef](#)]
235. Ding, X.; Yu, Y.; Yang, C.; Wu, D.; Zhao, Y. Multifunctional GO Hybrid Hydrogel Scaffolds for Wound Healing. *Research* **2022**, *2022*, 9850743. [[CrossRef](#)]
236. Ahn, S.; Kim, D.; Cho, K.; Koh, W.-G. Microfabrication methods for 3D spheroids formation and their application in biomedical engineering. *Korean J. Chem. Eng.* **2023**, *40*, 311–324. [[CrossRef](#)]
237. Daly, A.C.; Davidson, M.D.; Burdick, J.A. 3D bioprinting of high cell-density heterogeneous tissue models through spheroid fusion within self-healing hydrogels. *Nat. Commun.* **2021**, *12*, 753. [[CrossRef](#)] [[PubMed](#)]
238. Daly, A.C.; Kelly, D.J. Biofabrication of spatially organised tissues by directing the growth of cellular spheroids within 3D printed polymeric microchambers. *Biomaterials* **2019**, *197*, 194–206. [[CrossRef](#)] [[PubMed](#)]
239. El Khoury, R.; Nagiah, N.; Mudloff, J.A.; Thakur, V.; Chattopadhyay, M.; Joddar, B. 3D Bioprinted Spheroidal Droplets for Engineering the Heterocellular Coupling between Cardiomyocytes and Cardiac Fibroblasts. *Cyborg Bionic Syst.* **2021**, *2021*, 9864212. [[CrossRef](#)] [[PubMed](#)]
240. Mandrycky, C.; Wang, Z.; Kim, K.; Kim, D.-H. 3D bioprinting for engineering complex tissues. *Biotechnol. Adv.* **2016**, *34*, 422–434. [[CrossRef](#)]
241. Velasco, V.; Shariati, S.A.; Esfandyarpour, R. Microtechnology-based methods for organoid models. *Microsyst. Nanoeng.* **2020**, *6*, 76. [[CrossRef](#)]
242. Clua-Ferré, L.; Chiara, F.D.; Rodríguez-Comas, J.; Comelles, J.; Martinez, E.; Godeau, A.L.; García-Alamán, A.; Gasa, R.; Ramón-Azcón, J. Collagen-Tannic Acid Spheroids for  $\beta$ -Cell Encapsulation Fabricated Using a 3D Bioprinter. *Adv. Mater. Technol.* **2022**, *7*, 2101696. [[CrossRef](#)]
243. Tarassoli, S.P.; Jessop, Z.M.; Jovic, T.; Hawkins, K.; Whitaker, I.S. Candidate Bioinks for Extrusion 3D Bioprinting—A Systematic Review of the Literature. *Front. Bioeng. Biotechnol.* **2021**, *9*, 616753. [[CrossRef](#)]
244. Williams, S.K.; Touroo, J.S.; Church, K.H.; Hoying, J.B. Encapsulation of Adipose Stromal Vascular Fraction Cells in Alginate Hydrogel Spheroids Using a Direct-Write Three-Dimensional Printing System. *BioRes. Open Access* **2013**, *2*, 448–454. [[CrossRef](#)]
245. Jeon, S.; Heo, J.; Kim, M.K.; Jeong, W.; Kang, H. High-Precision 3D Bio-Dot Printing to Improve Paracrine Interaction between Multiple Types of Cell Spheroids. *Adv. Funct. Mater.* **2020**, *30*, 2005324. [[CrossRef](#)]
246. Janarthanan, G.; Shin, H.S.; Kim, I.-G.; Ji, P.; Chung, E.-J.; Lee, C.; Noh, I. Self-crosslinking hyaluronic acid–carboxymethylcellulose hydrogel enhances multilayered 3D-printed construct shape integrity and mechanical stability for soft tissue engineering. *Biofabrication* **2020**, *12*, 045026. [[CrossRef](#)]
247. Salatin, S.; Lotfipour, F.; Jelvehgari, M. Preparation and characterization of a novel thermosensitive and bioadhesive cephalixin nanohydrogel: A promising platform for topical antibacterial delivery. *Expert Opin. Drug Deliv.* **2020**, *17*, 881–893. [[CrossRef](#)] [[PubMed](#)]
248. Diaz-Gomez, L.; Gonzalez-Prada, I.; Millan, R.; Silva-Candal, A.D.; Bugallo-Casal, A.; Campos, F.; Concheiro, A.; Alvarez-Lorenzo, C. 3D printed carboxymethyl cellulose scaffolds for autologous growth factors delivery in wound healing. *Carbohydr. Polym.* **2022**, *278*, 118924. [[CrossRef](#)] [[PubMed](#)]
249. Zhang, H.; Fang, W.; Zhao, T.; Zhang, H.; Gao, L.; Li, J.; Wang, R.; Xu, W. Real-Time MRI Monitoring of GelMA-Based Hydrogel-Loaded Kartogenin for In Situ Cartilage Regeneration. *Front. Bioeng. Biotechnol.* **2022**, *10*, 940735. [[CrossRef](#)]
250. Weisgrab, G.; Guillaume, O.; Guo, Z.; Heimel, P.; Slezak, P.; Poot, A.; Grijpma, D.; Ovsianikov, A. 3D Printing of large-scale and highly porous biodegradable tissue engineering scaffolds from poly(trimethylene-carbonate) using two-photon-polymerization. *Biofabrication* **2020**, *12*, 045036. [[CrossRef](#)]
251. Cao, W.; Peng, S.; Yao, Y.; Xie, J.; Li, S.; Tu, C.; Gao, C. A nanofibrous membrane loaded with doxycycline and printed with conductive hydrogel strips promotes diabetic wound healing in vivo. *Acta Biomater.* **2022**, *152*, 60–73. [[CrossRef](#)]
252. Xu, L.; Chen, Y.; Zhang, P.; Tang, J.; Xue, Y.; Luo, H.; Dai, R.; Jina, J.; Liu, J. 3D printed heterogeneous hybrid hydrogel scaffolds for sequential tumor photothermal-chemotherapy and wound healing. *Biomater. Sci.* **2022**, *10*, 5648–5661. [[CrossRef](#)]
253. Liang, J.; Zeng, H.; Qiao, L.; Jiang, H.; Ye, Q.; Wang, Z.; Liu, B.; Fan, Z. 3D Printed Piezoelectric Wound Dressing with Dual Piezoelectric Response Models for Scar-Prevention Wound Healing. *ACS Appl. Mater. Interfaces* **2022**, *14*, 30507–30522. [[CrossRef](#)]
254. Advincula, R.C.; Dizon, J.R.C.; Caldon, E.B.; Viers, R.A.; Siacor, F.D.C.; Maalihan, R.D.; Espera, A.H., Jr. On the progress of 3D-printed hydrogels for tissue engineering. *MRS Commun.* **2021**, *11*, 539–553. [[CrossRef](#)]
255. Ganguly, K.; Espinal, M.M.; Dutta, S.D.; Patel, D.K.; Patil, T.V.; Luthfikasari, R.; Lim, K.-T. Multifunctional 3D platforms for rapid hemostasis and wound healing: Structural and functional prospects at biointerfaces. *Int. J. Bioprint.* **2022**, *9*, 648. [[CrossRef](#)]
256. Nizioł, M.; Paleczny, J.; Junka, A.; Shavandi, A.; Dawiec-Liśniewska, A.; Podstawczyk, D. 3D Printing of Thermoresponsive Hydrogel Laden with an Antimicrobial Agent towards Wound Healing Applications. *Bioengineering* **2021**, *8*, 79. [[CrossRef](#)]

257. Zhang, Y.; Wang, C. Recent advances in 3D printing hydrogel for topical drug delivery. *MedComm–Biomater. Appl.* **2022**, *1*. [[CrossRef](#)]
258. Kirillova, A.; Maxson, R.; Stoychev, G.; Gomillion, C.T.; Ionov, L. 4D Biofabrication Using Shape-Morphing Hydrogels. *Adv. Mater.* **2017**, *29*, 1703443. [[CrossRef](#)] [[PubMed](#)]
259. Albanna, M.; Binder, K.W.; Murphy, S.V.; Kim, J.; Qasem, S.A.; Zhao, W.; Tan, J.; El-Amin, I.B.; Dice, D.D.; Marco, J.; et al. In Situ Bioprinting of Autologous Skin Cells Accelerates Wound Healing of Extensive Excisional Full-Thickness Wounds. *Sci. Rep.* **2019**, *9*, 1856. [[CrossRef](#)]
260. Kimberlee, P.; Adrian, C.T.; Laurence, H. Mapping of the spatial variation in alginate concentration in calcium alginate gels by magnetic resonance imaging(MRI). *Carbohydr. Res.* **1993**, *246*, 43–49. [[CrossRef](#)]
261. Simpson, N.E.; Grant, S.C.; Blackband, S.J.; Constantinidis, I. NMR properties of alginate microbeads. *Biomaterials* **2003**, *24*, 4941–4948. [[CrossRef](#)] [[PubMed](#)]
262. Corradini, V.; Pajewski, L.A.; Di Censo, D.; Alecci, M.; Galante, A. Characterization of a Novel Packaged Hydrogel Wound Dressing by 2.35 T Magnetic Resonance Imaging. 35 T Magnetic Resonance Imaging. *Electronics* **2023**, *12*, 188. [[CrossRef](#)]
263. Austin, D.T.R.; Hills, B.P. Two-dimensional NMR relaxation study of the pore structure in silicone hydrogel contact lenses. *Appl. Magn. Reson.* **2009**, *35*, 581–591. [[CrossRef](#)]
264. Grant, S.C.; Celper, S.; Gauffin-Holmberg, I.; Simpson, N.E.; Blackband, S.J.; Constantinidis, I. Alginate assessment by NMR microscopy. *J. Mater. Sci. Mater. Med.* **2005**, *16*, 511–514. [[CrossRef](#)]
265. Degrassi, A.; Toffanin, R.; Paoletti, S.; Hall, L.D. A better understanding of the properties of alginate solutions and gels by quantitative magnetic resonance imaging (MRI). *Carbohydr. Res.* **1998**, *306*, 19–26. [[CrossRef](#)]
266. van Zijl, P.C.M.; Yadav, N.N. Chemical exchange saturation transfer (CEST): What is in a name and what isn't? *Magn. Reson. Med.* **2011**, *65*, 927–948. [[CrossRef](#)]
267. Han, X.; Lai, J.H.C.; Huang, J.; Park, S.W.; Liu, Y.; Chan, K.W.Y. Imaging Self-Healing Hydrogels and Chemotherapeutics Using CEST MRI at 3 T. *ACS Appl. Bio. Mater.* **2021**, *4*, 5605–5616. [[CrossRef](#)] [[PubMed](#)]
268. Ward, K.M.; Aletras, A.H.; Balaban, R.S. A New Class of Contrast Agents for MRI Based on Proton Chemical Exchange Dependent Saturation Transfer (CEST). *J. Magn. Reson.* **2000**, *143*, 79–87. [[CrossRef](#)] [[PubMed](#)]
269. Han, X.; Huang, J.; To, A.K.W.; Lai, J.H.C.; Xiao, P.; Wu, E.X.; Xu, J.; Chan, K.W.Y. CEST MRI detectable liposomal hydrogels for multiparametric monitoring in the brain at 3T. *Theranostics* **2020**, *10*, 2215–2228. [[CrossRef](#)] [[PubMed](#)]
270. Zhu, W.; Chu, C.; Kuddannaya, S.; Yuan, Y.; Walczak, P.; Singh, A.; Song, X.; Bult, J.W.M. In Vivo Imaging of Composite Hydrogel Scaffold Degradation Using CEST MRI and Two-Color NIR Imaging. *Adv. Funct. Mater.* **2019**, *29*, 1903753. [[CrossRef](#)] [[PubMed](#)]
271. Shazeeb, M.S.; Corazzini, R.; Konowicz, P.A.; Fogle, R.; Bangari, D.S.; Johnson, J.; Ying, X.; Dhal, P.K. Assessment of in vivo degradation profiles of hyaluronic acid hydrogels using temporal evolution of chemical exchange saturation transfer (CEST) MRI. *Biomaterials* **2018**, *178*, 326–338. [[CrossRef](#)] [[PubMed](#)]
272. Liang, Y.; Bar-Shir, A.; Song, X.; Gilad, A.A.; Walczak, P.; Bulte, J.W.M. Label-free imaging of gelatin-containing hydrogel scaffolds. *Biomaterials* **2015**, *42*, 144–150. [[CrossRef](#)] [[PubMed](#)]
273. Jin, T.; Nicholls, F.J.; Crum, W.R.; Ghuman, H.; Badylak, S.F.; Modo, M. Diamagnetic chemical exchange saturation transfer (diaCEST) affords magnetic resonance imaging of extracellular matrix hydrogel implantation in a rat model of stroke. *Biomaterials* **2017**, *113*, 176–190. [[CrossRef](#)]
274. Lock, L.L.; Li, Y.; Mao, X.; Chen, H.; Staedtke, V.; Bai, R.; Ma, W.; Lin, R.; Li, Y.; Liu, G.; et al. One-Component Supramolecular Filament Hydrogels as Theranostic Label-Free Magnetic Resonance Imaging Agents. *ACS Nano* **2017**, *11*, 797–805. [[CrossRef](#)]
275. Placone, J.K.; Navarro, J.; Laslo, G.W.; Lerman, M.J.; Gabard, A.R.; Herendeen, G.J.; Falco, E.E.; Tomblynn, S.; Burnett, L.; Fisher, J.P. Development and Characterization of a 3D Printed, Keratin-Based Hydrogel. *Ann. Biomed. Eng.* **2017**, *45*, 237–248. [[CrossRef](#)]
276. Yuan, Y.; Chen, L.; Shi, Z.; Chen, J. Micro/Nanoarchitectonics of 3D Printed Scaffolds with Excellent Biocompatibility Prepared Using Femtosecond Laser Two-Photon Polymerization for Tissue Engineering Applications. *Nanomaterials* **2022**, *12*, 391. [[CrossRef](#)]
277. Kang, M.S.; Kwon, M.; Lee, S.H.; Kim, W.H.; Lee, G.W.; Jo, H.J.; Kim, B.; Yang, S.Y.; Kim, K.S.; Han, D.W. 3D Printing of Skin Equivalents with Hair Follicle Structures and Epidermal-Papillary-Dermal Layers Using Gelatin/Hyaluronic Acid Hydrogels. *Chem. Asian J.* **2022**, *17*, e202200620. [[CrossRef](#)] [[PubMed](#)]
278. Wang, L.; Zhou, M.; Xu, T.; Zhang, X. Multifunctional hydrogel as wound dressing for intelligent wound monitoring. *Chem. Eng. J.* **2022**, *433*, 134625. [[CrossRef](#)]
279. de León, E.H.P.; Valle-Pérez, A.U.; Khan, Z.N.; Hauser, C.A.E. Intelligent and smart biomaterials for sustainable 3D printing applications. *Curr. Opin. Biomed. Eng.* **2023**, *26*, 100450. [[CrossRef](#)]
280. Sánchez, M.E.; Gómez-Blanco, J.C.; Nieto, E.L.; Casado, J.G.; Macías-García, A.; Díaz Díez, M.A.; Carrasco-Amador, J.P.; Martín, D.T.; Sánchez-Margallo, F.M.; Pagador, J.B. Hydrogels for bioprinting: A systematic review of hydrogels synthesis, bioprinting parameters, and bioprinted structures behavior. *Front. Bioeng. Biotechnol.* **2020**, *8*, 776. [[CrossRef](#)]
281. Saadi, M.A.S.R.; Maguire, A.; Pottackal, N.T.; Thakur, M.S.H.; Ikram, M.M.; Hart, A.J.; Ajayan, P.M.; Rahman, M.M. Direct ink writing: A 3D printing technology for diverse materials. *Adv. Mater.* **2022**, *34*, 2108855. [[CrossRef](#)]
282. Khan, Z.N.; Albalawi, H.I.; Valle-Pérez, A.U.; Aldoukhi, A.; Hammad, N.; León, E.H.-P.; Abdelrahman, S.; Hauser, C.A.E. From 3D printed molds to bioprinted scaffolds: A hybrid material extrusion and vat polymerization bioprinting approach for soft matter constructs. *Mater. Sci. Addit. Manuf.* **2022**, *1*, 7.

283. Wang, M.; Li, W.; Hao, J.; Gonzales, A.; Zhao, Z.; Flores, R.S.; Kuang, X.; Mu, X.; Ching, T.; Tang, G. Molecularly cleavable bioinks facilitate high-performance digital light processing-based bioprinting of functional volumetric soft tissues. *Nat. Commun.* **2022**, *13*, 3317. [CrossRef]
284. Falcone, G.; Mazzei, P.; Piccolo, A.; Esposito, T.; Mencherini, T.; Aquino, R.P.; Gaudio, P.D.; Russo, P. Advanced printable hydrogels from pre-crosslinked alginate as a new tool in semi solid extrusion 3D printing process. *Carbohydr. Polym.* **2022**, *276*, 118746. [CrossRef]
285. Zhang, B.; Luo, Y.; Ma, L.; Gao, L.; Li, Y.; Xue, Q.; Yang, H.; Cui, Z. 3D bioprinting: An emerging technology full of opportunities and challenges. *Bio-Des. Manuf.* **2018**, *1*, 2–13. [CrossRef]
286. Dearman, B.L.; Boyce, S.T.; Greenwood, J.E. Advances in skin tissue bioengineering and the challenges of clinical translation. *Front. Surg.* **2021**, *8*, 640879. [CrossRef]
287. Ozbolat, I.T. Bioprinting scale-up tissue and organ constructs for transplantation. *Trends Biotechnol.* **2015**, *33*, 395–400. [CrossRef]
288. Mehrotra, S.; Moses, J.C.; Bandyopadhyay, A.; Mandal, B.B. 3D printing/bioprinting based tailoring of in vitro tissue models: Recent advances and challenges. *ACS Appl. Bio Mater.* **2019**, *2*, 1385–1405. [CrossRef]
289. Zhang, A.; Liu, Y.; Qin, D.; Sun, M.; Wang, T.; Chen, X. Research status of self-healing hydrogel for wound management: A review. *Int. J. Biol. Macromol.* **2020**, *164*, 2108–2123. [CrossRef]
290. Long, L.; Liu, W.; Hu, C.; Yang, L.; Wang, Y. Construction of multifunctional wound dressings with their application in chronic wound treatment. *Biomater. Sci.* **2022**, *10*, 4058–4076. [CrossRef]
291. Fang, H.; Xu, J.; Ma, H.; Liu, J.; Xing, E.; Cheng, Y.Y.; Wang, H.; Nie, Y.; Pan, B.; Song, K. Functional materials of 3D bioprinting for wound dressings and skin tissue engineering applications: A review. *Int. J. Bioprinting* **2023**, *9*, 757. [CrossRef]
292. Chen, D.; Heyer, S.; Ibbotson, S.; Saloniitis, K.; Steingrímsson, J.G.; Thiede, S. Direct digital manufacturing: Definition, evolution, and sustainability implications. *J. Clean. Prod.* **2015**, *107*, 615–625. [CrossRef]
293. Ruffo, M.; Tuck, C.; Hague, R. Make or buy analysis for rapid manufacturing. *Rapid Prototyp. J.* **2007**, *13*, 23–29. [CrossRef]
294. Eyers, D.R.; Potter, A.T. E-commerce channels for additive manufacturing: An exploratory study. *J. Manuf. Technol. Manag.* **2015**, *26*, 390–411. [CrossRef]
295. Sasson, A.; Johnson, J.C. The 3D printing order: Variability, supercenters and supply chain reconfigurations. *Int. J. Phys. Distrib. Logist. Manag.* **2016**, *46*, 82–94. [CrossRef]
296. Anderson, C. *Makers: The New Industrial Revolution*; Random House: Manhattan, NY, USA, 2012.
297. Holmström, J.; Partanen, J. Digital manufacturing-driven transformations of service supply chains for complex products. *Supply Chain. Manag. Int. J.* **2014**, *19*, 421–430. [CrossRef]
298. Kumar KP, A.; Pumera, M. 3D-Printing to Mitigate COVID-19 Pandemic. *Adv. Funct. Mater.* **2021**, *31*, 2100450. [CrossRef] [PubMed]
299. 3D Printing in Healthcare Market (By Component: System, Materials, Services; By Technology: Droplet Deposition, Photopolymerization, Laser Beam Melting, Electronic Beam Melting (EBM), Laminated Object Manufacturing, Others; By Application: External Wearable Devices, Clinical Study Devices, Implants, Tissue Engineering; By End User)-Global Industry Analysis, Size, Share, Growth, Trends, Regional Outlook, and Forecast 2023–2032. August 2023. Available online: <https://www.precedenceresearch.com/3d-printing-in-healthcare-market> (accessed on 7 September 2023).
300. Arif, U.Z.; Khalid, M.Y.; Noroozi, R.; Hossain, M.; Shi, H.H.; Tariq, A.; Ramakrishna, S.; Umer, R. Additive manufacturing of sustainable biomaterials for biomedical applications. *Asian J. Pharm. Sci.* **2023**, *18*, 100812. [CrossRef] [PubMed]

**Disclaimer/Publisher’s Note:** The statements, opinions and data contained in all publications are solely those of the individual author(s) and contributor(s) and not of MDPI and/or the editor(s). MDPI and/or the editor(s) disclaim responsibility for any injury to people or property resulting from any ideas, methods, instructions or products referred to in the content.